Study on Wave-induced Scour around Pile Groups

Ghazanfari Hashemi Samaneh

2014

STUDY ON WAVE-INDUCED SCOUR AROUND PILE GROUPS

Samaneh GHAZANFARI HASHEMI

Department of Civil and Earth Resources Engineering

Disaster Prevention Research Institute

Laboratory of Coastal Sedimentary Environment

Kyoto University

This dissertation is submitted for the degree of Doctor of Philosophy

2014

This dissertation is dedicated to

my Father, my Mother

and my Husband

ABSTRACT

Various arrangements of pile groups are widely being used as supports of marine structures. As piles are located on erodible beds of the sea, scouring is a threat to the stability of such structures and the determination of scour hole properties is one of the most important factors that should be considered well in their designs.

The scour properties around a single pile are affected by properties of sediment, wave, and pile geometry. In case of pile groups, the characteristics of the pile group as well as piles interactions between the piles in marine environment should be added to the controlling parameters and the complexity of study of wave-induced scour around pile groups is doubled consequently.

Though most of these supports are constructed in form of groups of piles, majority of studies has accumulated about scour around single piles and little has been gained regarding the scour at pile groups. Less findings and empirical formulas are also available for prediction of pile group scour. However, comparisons of the results provided by available empirical approaches show that they are not accurate enough to satisfy safe deigns. Thus following the lack of enough precisions and the complexity of the modelling of scouring phenomena, significant trials have been done to improve and modify available approaches or to find reliable alternatives for them.

On the other hand, soft computing models have been introduced as a robust method to model complex problems. Artificial neural networks (ANN) as a famous data-mining approach have been widely applied in current-induced predictions in addition to wave-induced scour estimations around single piles. Most of the results showed that ANN provides a better alternative to the statistical curve fitting. However, literature shows

that, in recent applications of ANN in predictions of scour around the piles, only a specific arrangement of pile groups was tested and the effects of geometrical parameters such as the distance between the piles and their numbers were not investigated yet.

Recently, a new soft computing approach named Support Vector Machines (SVM) also has been successfully applied in hydraulic and marine problems such as the prediction of wind speed, run-off modelling, prediction of storm surge, hourly reservoir inflow forecasting, effective forecasting of hourly typhoon rainfall and prediction of significant wave height. Nevertheless, applications of this model in pile groups scour due to waves has not been confirmed yet.

In this research, an in-depth experimental study of the effects of configuration on the scouring of a group of wave-induced piles is addressed. In addition, the applicability of data mining approaches of Support Vector Machines and Artificial Neural Networks for predictions of scour depth around pile groups is assessed using the large-scale experimental data.

In the laboratory experiments, series of large scale scouring tests were done for 3×3, 2×3, 2×2 and 1×2 arrangements of pile groups exposed to waves and equilibrium scour depth around them were surveyed in the wave basin of Ujigawa Open Laboratory of Kyoto University. In the large-scale laboratory tests, for the single-pile cases, it was mainly observed that by the increase of $KC = 3.9$ to $KC = 5.9$, the symmetrical bed profile along X-section was changed to an asymmetrical one showing the asymmetrical formation of vortices. In the two piles tests, it was noticed that for both KC numbers, the trends of scoured bed profile for front and back rows of piles were almost same along X section; however, the trends are reverse for smaller $KC\ number$, $KC = 3.9$. In both KC numbers, along X section the scoured bed profile of the pile that is located in

the backside was above the front-pile at all recorded points. Four-piles tests, showed that for both KC numbers, the scour depth remained constant in the gaps along the X-sections. In case of six piles, it was observed that along X-sections, the bed profiles have the same trends in all three rows of piles. In nine-piles experiments, same as the six-piles arrangement, in case of both KC numbers the first row of piles scoured more and the related graphs are located below other back-side rows consequently. Overall results of the bed survey indicate that in most of the experimental cases, bed profiles along the first row of the piles, facing to the wave directions have higher scour values. It was also observed that amounts of recorded scour holes are dependent on the configuration factors of pile groups, i.e, whereas the number of piles increases, considering the arrangement and the amount of KC number, the scour depth may increase . Moreover, maximum scour holes occurs around rows of piles front to the wave direction.

In the modelling part, two soft computing models of SVM and ANN were developed and the applicability of these models were assessed for scour predictions using the large-scale experimental results. To develop the ANN model, various topologies of neural networks were built and the optimum structure was determined. To develop the SVM model, optimum user-defined parameters were selected based on error-minimising process. The predicted amounts of scour depth by data mining models of SVM and ANN confirmed the applicability of data mining approaches as an alternative approach that provides better predictions of scour depths due to waves compared to current available empirical formulae. Results also indicated that SVM predicts scour depths with better statistical measures compared to ANN. Comparison of the required computation times of both models also showed that SVM is a more time-efficient model because of less computation time and less user-defined parameters to be selected by the user.

ACKNOWLEDGMENTS

Completion of this doctoral dissertation was possible with the support and help of several people to only some of whom it is possible to give particular mention here and express my sincere gratitude.

First and foremost, I would like to express my special appreciation and thanks to my supervisor, Professor Dr. Tetsuya Hiraishi, Professor of the Laboratory of Coastal Sedimentary Environment, Disaster Prevention Research Institute (DPRI), Kyoto University. I appreciate all his contributions of time and ideas to make my Ph.D experience productive. I would have never been able to accomplish as much without his expertise, encouragement, and unselfish support.

I would also like to thank my committee members, Professor Dr. Hajime Mase and Associate Professor Dr. Yasuyuki Baba for their brilliant comments and suggestions to refine my thesis.

I wish to express my thanks to Dr. Ryoukei Azuma, for being very encouraging and supportive and for valuable discussions and comments during my study.

I am indebted to my colleagues, Dr. Hiroshi Matsuhita, Mr. Osamu Kishimoto, Mr. Kawata, Mr. Hikaru Nakamura, Mr. Ando, Mr. Yusuke Tanaka, Mr. Yudai Furukawa, Mr. Shuhei Tanabe, and Mr. Shouta Okura who have all extended their supports and I gained a lot from them.

I acknowledge all the professors and staffs in Ujigawa Open Laboratory, DPRI, Kyoto University. I would like to thank Mr. Seiji Fujihara and Mr. Yoshinori Yoshida. I express my gratitude to Ms. Yuri Matsumoto for her kind support in administrative works.

I am most grateful to the Nikki Saneyoshi Foundation for the financial support during my PhD study.

I take the opportunity to express my thanks to my husband's family for their kind encouragements. Words cannot express my profound gratitude to my beloved parents, my father Seyed Hassan Ghazanfari Hashemi and my mother Parvin Samadi to whom I owe a lot, and to my sisters Ghazaleh, Reyhaneh, Rezvaneh, Maedeh and my brother Mohammad for their loving support. To my beloved husband Dr. Amir Reza Mansoori, I feel indebted and express my thanks. Not only for supporting me for everything, but also for encouraging me throughout this experience.

CONTENTS

1 INTRODUCTION TO WAVE-INDUCED SCOURING PHENOMENA AROUND PILE GROUPS 1

1.1 HORSESHOE VORTICES IN CURRENT 2

1.2 HORSESHOE VORTICES CHARACTERISTICS IN WAVES 4

1.3 LIFE SPANS OF THE HORSE-SHOE VORTICES 6

1.4 THE LEE-WAKE VORTICES 8

1.5 THE CONTRACTION OF STREAMLINES 10

1.6 CALCULATION OF SCOUR AROUND A SLENDER PILE IN WAVES 11

1.7 WAVE-INDUCED SCOUR AROUND A GROUP OF SLENDER PILES 12

1.8 LOCAL AND GLOBAL SCOUR AROUND PILE GROUPS 13

1.9 SIDE BY SIDE TWO PILE ARRANGEMENTS 15

1.10 LITERATURE REVIEW 15

1.11 OBJECTIVES OF THIS RESEARCH 16

1.12 OUTLINES OF THE DISSERTATION 17

2 EXPERIMENTAL STUDIES ON WAVE-INDUCED SCOUR AROUND A GROUP OF SLENDER PILES 19

2.1 EXPERIMENTAL SETUP 20

2.2 TIME DETERMINATION FOR THE EXPERIMENT 30

2.3 SINGLE PILE EXPERIMENT 30

2.4 TWO PILES EXPERIMENT 34

2.5 FOUR PILES EXPERIMENT 39

2.6 SIX PILES EXPERIMENT 42

2.7 NINE PILES EXPERIMENT 46
2.8 SUMMARY 49
3 DATA MINING APPROACHES IN PREDICTION OF SCOURING 52
3.1 ARTIFICIAL NEURAL NETWORKS (ANN) 53
3.2 SUPPORT VECTOR MACHINES (SVM) 60
3.2.1 Classification problems 60
3.2.2 Support vector regression 65
3.3 APPLICATION OF SVM AND ANN IN PREDICTION OF SCOUR PROBLEM AROUND SINGLE PILE 70
3.4 SUMMARY 74
4 PREDICTION OF SCOUR USING ANN AND SVM 76
4.1 DIMENSIONAL AND NO DIMENSIONAL PARAMETERS CONTROLLING SCOUR DEPTH 77
4.2 DATA SET USED 79
4.2.1 Small-scale experiments of Sumer and Fredsoe 79
4.2.2 Field data of Bayram and Larson 83
4.2.3 Large-scale experimental data of this study 86
4.3 DEVELOPMENT OF SVM AND ANN 88
4.3.1 ANN model 88
4.3.2 SVM model 95
4.4 RESULTS OF SVM AND ANN 97
4.4.1 Comparison of the results of data mining approaches 97
4.4.2 Verification by the experimental data presented in this study 100
4.4.3 Summary of the results 102
4.5 COMPARISONS OF THE COMPUTATION TIMES 102
4.6 SENSITIVITY ANALYSIS 103
4.7 COMPARISON OF ALL APPROACHES 104

4.8 SUMMARY 106

5 CONCLUSIONS AND RECOMMENDATIONS 108

5.1 CONCLUSIONS 108

5.2 RECOMMENDATIONS FOR FUTURE RESEARCHERS 111

REFERENCES 113

LIST OF FIGURES 117

LIST OF TABLES 122

CURRICULUM VITAE 124

1 Introduction to Wave-induced Scouring Phenomena around Pile Groups

When a pile is exposed to the flow, flow pattern around the pile will be changed significantly. The first substantial change is the formation of a three dimensional separation caused by the obstacle itself. In addition, the rotation of the incoming flow will form the horseshoe vortex that makes the gradient of shear stress distribution at the front and back of the pile.

Overall, the scouring phenomenon is based on two different flow regimes and two scour patterns should be studied consequently. When the pile size is small enough that the flow can be separated, the vortices will be formed and leads to the slender-pile regime. In the second type, the pile size is so large that the flow regime cannot be separated, hence the vortices will not be formed. However, observations do indicate the

presence of scouring in the large-pile regime as well but the mechanism of scouring phenomena is completely different in such regimes.

When the ratio of pile diameter (D) to wavelength (L), ($^{D}/_{L}$) is small, the body of the pile can affect the flow regime, otherwise the large-scale regime with quite different scouring mechanism will be present. It is generally accepted that the slender-pile regime will be formed when the ratio $^{D}/_{L}$ is less than 0.1 ($^{D}/_{L} < 0.1$) and Keulegan-Carpenter numbers (KC) become more than one ($KC > 1$) (Isaacson 1979, Sumer and Fredsøe 1997).

On the other hand, piles are mostly constructed on forms of groups as supports of marine structures, whereas interactions between piles will cause different mechanism of scouring around piles compared to single pile cases. Hence, the single pile regime will be discussed in the next sessions and it will be proceeded by the effect of the interactions of piles in case of pile group arrangement.

1.1 Horseshoe vortices in current

The flow pattern and scouring phenomena around a cylindrical pile has been studied by many researchers so far (e.g. Breusers and Raudkivi (1991) and Melville and Chiew (1999)).

Figure 1-1 shows the pattern of flow and induced scouring around a cylindrical pile. As it can be seen in the figure, when a pile exposed to flow, the horseshoe vortices will be formed in front of the pile primarily and their formation will be proceeded by the vortex flow pattern at the lee-side. Finally, streamlines will contract at the side edges of the pile and the front and back of the structure will face the pressure gradient. On the water surface, the velocity head ($(\rho U^2/2)$, where ρ is the fluid density and U is the flow velocity) reaches the maximum.

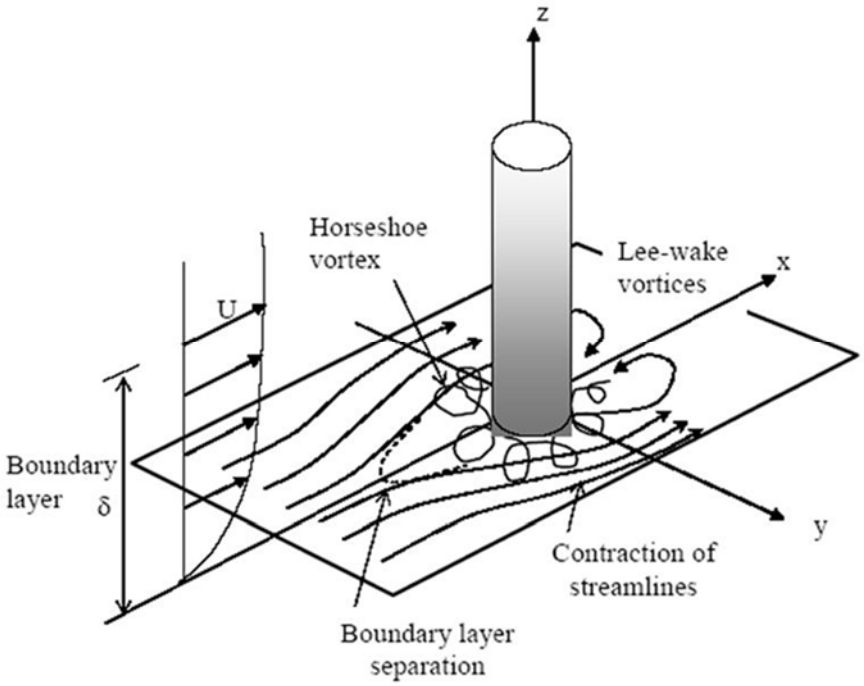

Figure 1-1. The change in the flow pattern and the boundary layer after being exposed to current (Sumer and Fredsøe 2002)

As the streamlines encounter the pile, the rotation of the incoming flow lines result in the formation of horseshoe vortex (Sumer, Fredsøe et al. 1992); moreover, because of the adverse pressure gradient in the pier, the boundary layer will make the three dimensional separation in the boundary layer along the S line of the Figure 1-1. The three dimensional separation is the reason of the formation of the spiral vortex around the pile as well. Overall, it can be concluded that parameters such as boundary layer thickness and diverse pressure gradient in front of the structure cause the separation of the flow. Studies of researchers such as Sumer and Fredsøe (2002) also showed that parameters such as Reynolds number ($Re = {Ud}/{\nu}$), boundary layer thickness (${\delta}/{D}$) and geometry of the pile strongly affect the formation of horseshoe vortices in steady currents.

All the processes mentioned will make the local scour around the piles and the sediments will be deposited and accumulated on the downstream where the powers of the vortices are decreased. In this case, the underflow condition acts as a jetty that hits the bed under the pile. When the related components of bed shear stress, particles weight and present turbulences reaches the equilibrium condition, the clear water scouring condition will start. Under clear water condition, sediment transport may not occur and just a slight motion of the bed particles might happen. In a live-bed, an excess shear stress should exist for the sediment transport due to scouring so that the bed particles can be moved from their place. The variations of bed shear stress in an erodible bed will create the mechanisms of sediment transport, bed scour and local scour of the pile.

1.2 Horseshoe vortices characteristics in waves

When a pile is affected by wave as well as current, in addition to parameters such as R_{e_D} , $\delta/_D$ and pile geometry that were mentioned previously, the Keulegan-Carpenter (KC) will be added to the controlling parameters of scouring. In this case, KC can be calculated as follows:

$$KC = \frac{U_m T}{D} \tag{1-1}$$

Where U_m is the maximum undisturbed orbital velocity at the sea bottom just above the wave boundary, D is the pile diameter and T is the wave period. The U_m can be calculated as follows:

$$U = U_m \ sin(\omega T_w) \tag{1-2}$$

Where U is the orbital velocity of water particles on the bed, ω is the angular frequency of the water particles near the bed surface and can be:

$$\omega = \frac{2\pi}{T} \tag{1-3}$$

The constant called the amplitude of the orbital motions of the water particles calculated as bellows:

$$a = \frac{U_m T_m}{2\pi} \tag{1-4}$$

Substituting Eq. (1-2**)** to Eq. (1-4**)** in Eq. (1-1**)**, KC number is expressed as bellows:

$$KC = \frac{2\pi a}{D} \tag{1-5}$$

As it can be seen in Eq. (1-1**)** to Eq.(1-4**)**, the KC formulae in general is proportional to $2a/D$ amount. In other words, in small KC numbers, the amplitude of the orbital motion of water particles (a) is smaller than pile diameters (D). Due to such conditions, as the boundary layer cannot be separated from the bed, the horseshoe vortices may not be formed as well.

In contrary, for large KC numbers, the amplitude of the water particles orbital motions may be larger than the pile diameter and each half period resembles a steady current condition and the horseshoe vortices will have the same role as of a steady current.

Figure 1-2 shows the study results of Sumer, Christiansen et al. (1997)about the time variations around the vortices formation spots in waves.

As it can be clearly seen in the wave sinus function, when the wave is uprising the amount of ωt is $0 < \omega t < 180$ and while the wave drops, this amount is $180 < \omega t < 360$. Figure 1-2 also displays that in $KC < 6$; the horseshoe vortices were not formed. Study results of other researchers indicate that in KC=1 the flow over the pile surface separates (Sumer and Fredsøe 2002), while considering Figure 1-2, $KC = 6$ is necessary for separation in front of the pile. This amount is much higher than the one needed for the flow separation at the pile surface.

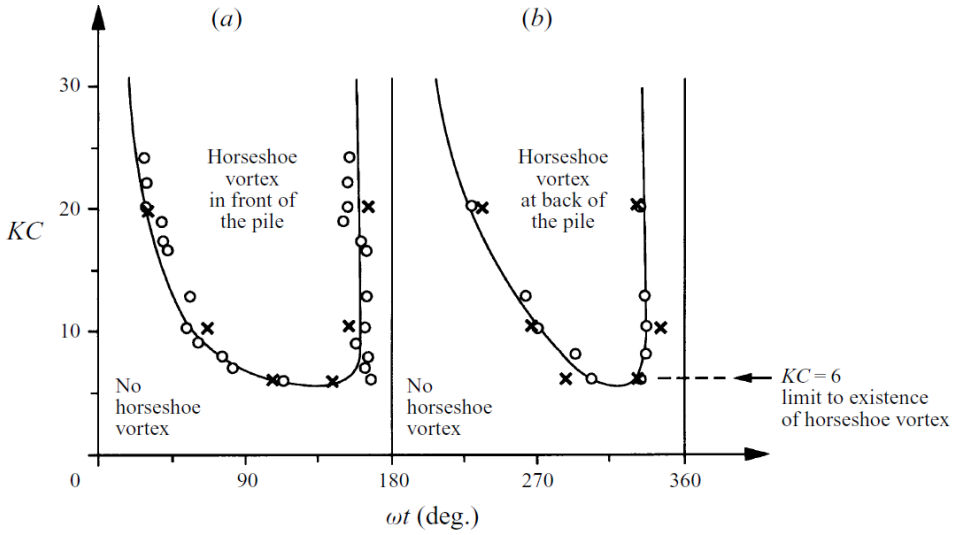

Figure 1-2. Presence of horseshoe vortices by KC and ωt variations (Sumer, Christiansen et al. 1997)

According to Sumer and Fredsøe (2002), the value of adverse pressure gradient is also important to investigate the separation around the pile. As the amount of adverse pressure gradient at the front of the pile is 5 times less than the one of the surface, the separations occur at large KC numbers on those points while the required KC for separation at the pile surface is KC=1.

1.3 Life spans of the horse-shoe vortices

Figure 1-3 displays the development and disappearance of the horseshoe vortices for different phases of ωt =0, 50, 90,123, 172 in KC =10.3. As it can be clearly seen in Figure 1-3 (1) to Figure 1-3 (5) the first appearance of the horseshoe vortices are in the flow reversal and their disappearances occur when the flow reverses again. The new horseshoe vortices will appear to emerge in the next half cycle of the motion at the other side. In addition, comparisons between Figure 1-3 (2) and Figure 1-3 (3) indicate

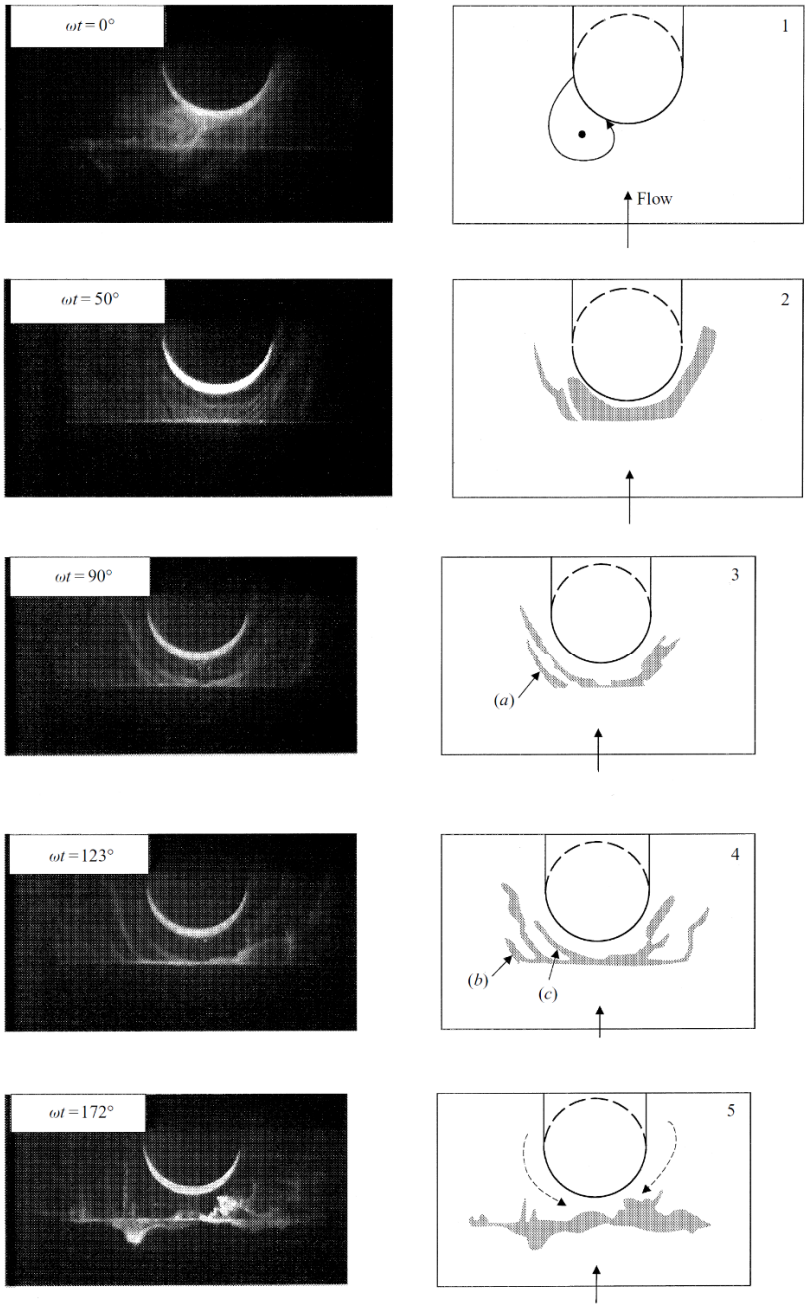

Figure 1-3. The development of horseshoe vortices in KC =10.3 (Sumer, Christiansen et al. 1997)

that the persistence of horseshoe vortices is longer in larger KC numbers. For instance, in $KC = 10$, the horseshoe vortices occur at $\omega t = 50°$ and disappears at $\omega t = 160°$ so the lifespan of such vortices will be $\Delta\omega t = 110°$ while for $KC = 25$ the appearance and

disappearance of horseshoe vortices occur at $\omega t = 23°$ and $\omega t = 160°$ consequently. In other words, the life span of horseshoe vortices at $KC = 25$ is 137° which is larger than those of KC =10. A longer persistence and life span as the KC increases is because of the formation of adverse pressure gradient, which is necessary for the formation of horseshoe vortices in addition toKC number.

1.4 The lee-wake vortices

The lee-wake vortices are mainly caused by the rotation in the boundary layer over the surface of the pile. In fact the boundary layer occurred around the pile rotates to form the lee-wake vortices. In case of steady current, the lee-wake flow mainly controlled by R_{e_D} and the pile geometry and in presence of waves in addition to steady currents, the KC number should be considered as well as two other parameters (R_{e_D}, Pile geometry). In case of a rough pile, the relative roughness K_s/D also emerges as an additional controlling parameter.

Over the past decades, an extensive knowledge has been gathered about the formation of vortex flow behind the pile (Sumer and Fredsøe 2002). Study results of Sumer, Christiansen et al. (1997), about the lee-wake vortex formation at different KC and ωt in case of a vertical cylinder is shown in Figure 1-4.

Results of their studies indicated that as long as $2.8 \leq KC \leq 4$, the symmetric separation occurs and the pair symmetric vortices are washed around the pile as the flow reverses (Figure 1-4 a). As the range of KC increases to$17 \leq KC \leq 23$, the vortices grow larger in each half period (Figure 1-4 d).

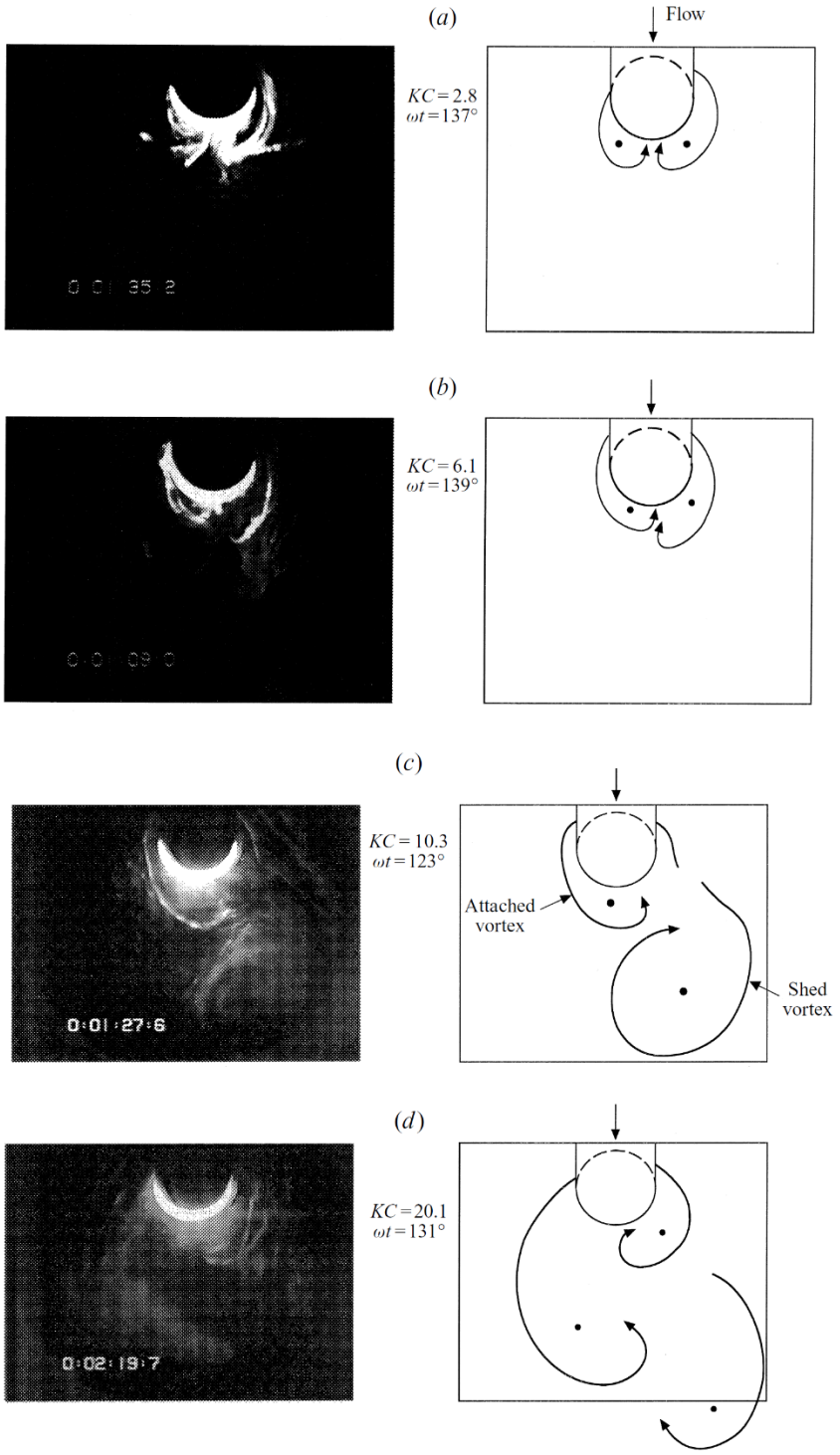

Figure 1-4. The formation of lee-wake vortex at various KC and ωt (Sumer, Christiansen et al. 1997)

1.5 The contraction of streamlines

The effect of streamline contraction was shown in the counters of bed shear stress in Figure 1-5.

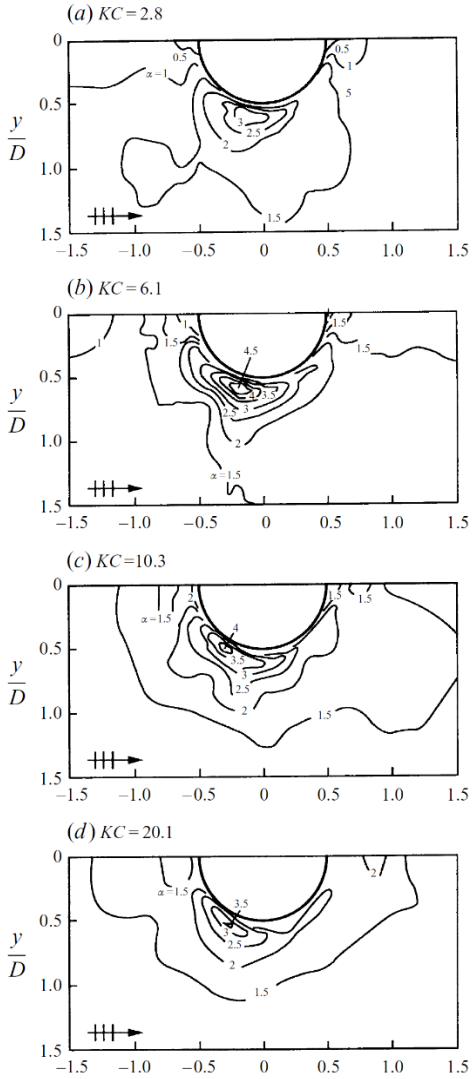

Figure 1-5. Display of bed shear stress counters (Sumer, Christiansen et al. 1997, Sumer and Fredsøe 2002)

As it can be clearly seen, the concentration of bed shear stress occurs at or near the side edges of the pile. Figure 1-5 also indicate that in some points the amount of bed shear

stress is 4.5 times the upstream bed shear stress that finally results in the increase in the sediment transport around the pile.

1.6 Calculation of scour around a slender pile in waves

As the KC increases, the length of lee-wake vortices will become larger and affects the wider area of the bed respectively. Moreover; as it was seen in Figure 1-3 and Figure 1-4, the increase in KC number result in the increase of life spans as well as the size of the horseshoe vortices so it will be expected that the influence of the horse-shoe vortices and lee-wake vortices on the scour to be increased. Study results of Sumer, Fredsøe et al. (1992) and Sumer, Christiansen et al. (1993) also confirm that by the rise in KC number amounts, the scour depth will increase.

Figure 1-6 displays the study results of Sumer, Fredsøe et al. (1992) done about the equilibrium scour depth around a circular pile.

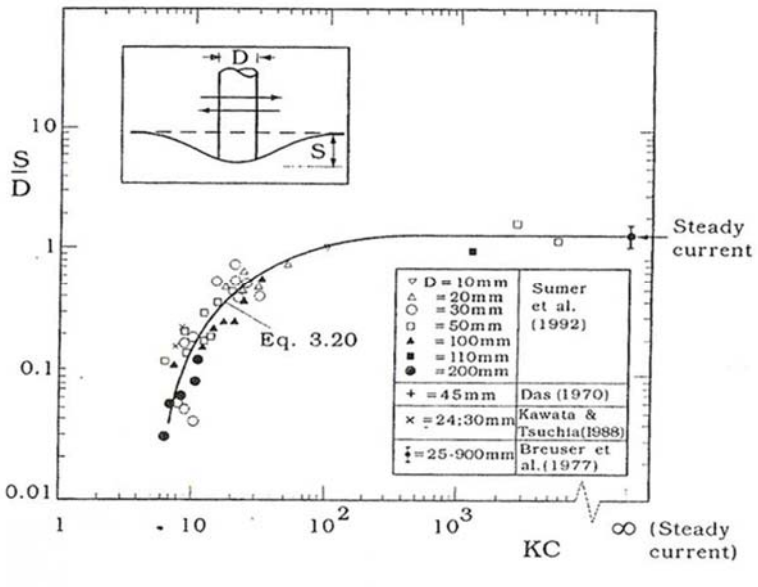

Figure 1-6. Variations of S/D against KC for a circular pile $\theta < \theta_{cr}$
(Sumer, Fredsøe et al. 1992)

Figure 1-6 indicates that as the $KC \rightarrow \infty$, the scour depth approaches a constant value. First reason is that considering the finite lifetime of the horseshoe vortices, the influence of lee-wake vortices approaches a constant value. Second, as the KC dependency of the horseshoe vortices in large KC numbers disappears the influence of the horseshoe vortices on the equilibrium scour depth should also approach a constant value. In addition, as it can be seen in Figure 1-6, the recorded scour amounts of large KC s are the same as those of steady currents. It can be concluded that as in the steady current condition the main controlling parameters of scouring is KC number, in wave-induced scour around a single pile in large KC numbers (KC >100), the scour depth is dependent to KC number.

In small KC numbers (KC <10), the scouring is directly related to lee-wake vortices which have shorter life spans than horseshoe vortices.

Sumer, Fredsøe et al. (1992) presented the empirical formulae for the experimental data of Figure 1-6 under live-bed condition.

$$\frac{S}{D} = 1.3\{1 - exp[-0.03(KC - 6)]\} \quad for\ KC \geq 6 \tag{1-6}$$

It should be noted that in Eq. (1-6) only the influence of KC number is seen and effects of other important parameters such as N_{RE} (Reynolds number) and N_s (sediment number) remain unconsidered. Nevertheless, the influence of cross-sectional shape on scour depth for square and diamond shapes has been investigated and presented in (Sumer, Christiansen et al. 1993).

1.7 Wave-induced scour around a group of slender piles

Unlike the scour around the single piles, few amount of knowledge has been accumulated about scour around a group of slender piles (Wang and Herbich 1983, Herbich, Schiller et al. 1984, Eadie and Herbich 1986, Sumer, Christiansen et al. 1993,

Kobayashi and Oda 1994, Sumer and Fredsøe 1998). The scour at pile groups may occur as local and global scour (Sumer, Fredsøe et al. 2005). In the followings, the local and global scour around a group of vertical piles due to waves are discussed.

1.8 Local and global scour around pile groups

Figure 1-7 and Figure 1-8 indicate the differences between local and global scours around pile groups.

Figure 1-7, clearly shows the global and local scour around a piles steeled platform in the field and Figure 1-8 shows the observed global and local scour phenomena in the experimental studies. In the related figures, two different types of scour: the local and a saucer shaped global scour can be clearly identified. As it was mentioned in the preceded sections, the formation of horseshoe vortices and the contraction of streamlines are the main controlling factor of local scour around the piles.

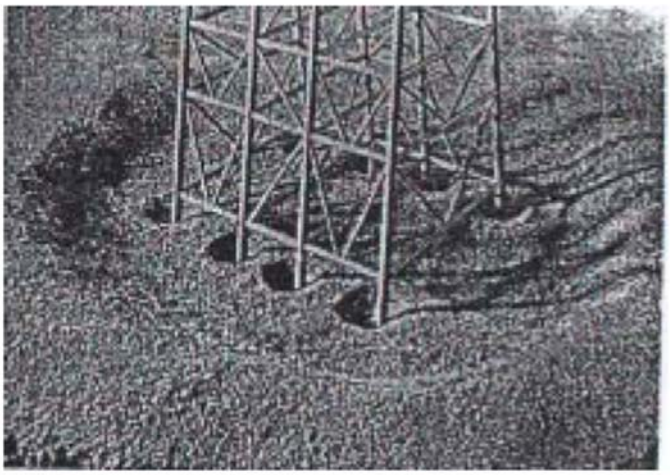

Figure 1-7. A conceptual display of local and global scour around a piled steel platform (Angus and Moore 1982)

Figure 1-8 Global and local scour around a 9 piles-arrangement at the experiment (Sumer, Fredsøe et al. 2005)

Based on experimental studies of Sumer and Fredsøe (2002), the local scour is mainly influenced by two parameters of gap between the piles and the turbulence induced by each pile. The followings summarize their achievements as bellows.

As mentioned in previous chapters scouring phenomena is strongly influenced by KC number.

$$\frac{S}{D} = f(KC) \tag{1-7}$$

As the number of piles increases and a single pile converts to the group piles, the gaps between the piles become important and it can be expressed as below:

$$\frac{S}{D} = f\left(KC, \frac{G}{D}\right) \tag{1-8}$$

Figure 1-9 displays the equilibrium scour depth against the G/D ratio for different 2-pile arrangements for $KC = 13$.

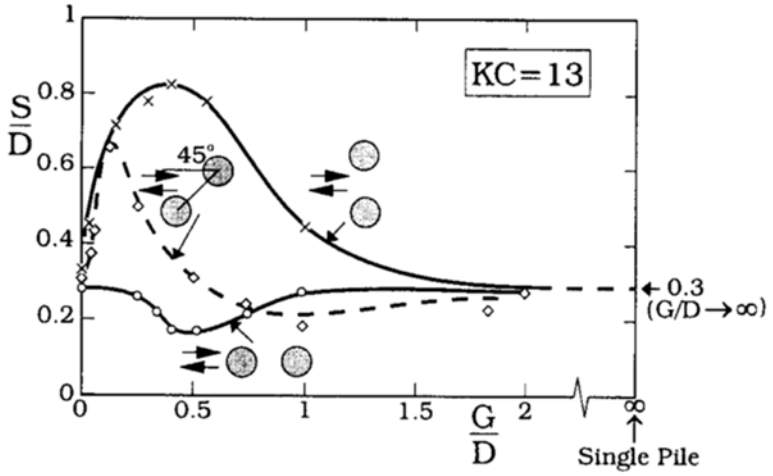

Figure 1-9. S/D against G/D for 2-pile arrangements (Sumer and Fredsøe 1998)

1.9 Side by side two pile arrangements

Experimental studies of Sumer & Fredsoe (1998) indicated that, except the small amounts of G/D ($G/D < 0.1$) and large amounts of G/D ($G/D > 2$) the maximum scour depth, occurs at the middle point of the gap between the piles. On the other hand for $G/D < 0.1$ and $G/D > 2$ the maximum scour occurs at the outside edges of the piles.

1.10 Literature review

The previously mentioned experimental studies of Sumer and Fredsøe (1998) have shown that the wave-induced scour depths of piles are influenced by properties of piles, bed and waves or currents. In addition, to study the scour depth around pile groups, the interactions between the piles make the mechanism of scouring different from those of single piles.

Scour around a single pile has been investigated quite extensively (for example, Eadie and Herbich (1986); Eadie and Herbich (1986); Kobayashi and Oda (1994); Palmer

(1969);Sumer, Fredsøe et al. (1992); Sumer, Christiansen et al. (1993); Wang and Herbich (1983)). On the contrary, limited amount of studies have been done about the wave-induced scour around pile groups.

Chow and Herbich (1978) studied pile groups made of three, four and six piles. They investigated the influence of gap to diameter ratio (G/D) where G is the space between piles and D is the pile diameter; however at the time of their studies the key role of KC number in scouring phenomena due to waves was unknown. The parameter that was shown by Sumer, Fredsøe et al. (1992) and Kobayashi and Oda (1994) to be the main controlling parameter to study pile scours some years after.

Bayram and Larson (2000) studied the scour depth around a 2×2 pile groups in the field. Their study also showed that the equilibrium scour depth is governed by KC number. They presented an empirical relationship for estimating the equilibrium scour depth using the KC number in the 2×2 pile arrangement. However, their formulae was given for a unique (2×2) arrangement of piles mainly based on KC number.

Results of their investigations indicated the effect of KC number in scour depths amounts around the pile groups. Their studies also showed the importance of other effective parameters of Reynolds number (N_{RE}) and sediment number (N_s).

Considering the complexity of modelling the scour process and scour hole properties around pile groups due to waves, the existing approaches are not capable of accurate estimation of the scour depth around pile groups with different arrangements. Hence, a robust model is very useful for the estimation of scour depth. One of the most common approaches as an alternative to empirical approaches is the soft computing method.

1.11 Objectives of this research

The literature shows that despite of the importance of the investigation of scouring phenomena around pile groups as supports of marine structures, studies around this topic is very scarce and most of the researches concentrated on single pile scour conditions. This study aims to extend the knowledge about pile group scour under waves by focusing on the effect of configuration parameters. To achieve these goals different arrangements of single, two, four, six and nine piles are exposed to waves and sets of large-scale scour experiments are done about them. Then the characteristics of scoured bed around them are surveyed and discussed focusing on the arrangement parameter.

On the other hand, regarding the complexity of the prediction of pile group scour due to waves and the lack of formulae with acceptable precision, this research also aims to assess the applicability of soft computing models of ANN and SVM and introduce them as a reliable alternative for semi-empirical formulae for estimating scour depth around pile groups. To achieve this goal, the ANN and SVM models are developed and their predictions of scour depths are compared with measurements. The better model has closer predictions to observed amounts of scour. Finally, it is concluded that SVM and ANN can provide better predictions of wave-induced scour compared to semi-empirical formulae in terms of accuracy.

1.12 Outlines of the dissertation

This research concerns the experimental investigation of scouring phenomena around various arrangements of pile groups as well as the assessment of the applicability of data mining models of SVM and ANN to predict the scour depth around pile groups.

This dissertation contains 5 chapters, from introduction in chapter 1 through conclusion in chapter 5 as described below:

Chapter 1 briefly presents the background of the study, an introduction about the scouring phenomena, objectives of the research and a brief review of previous literatures.

Chapter 2 presents the results of the large-scale experimental studies about different configurations of piles due to waves carried out in the laboratory and describes the results of the experiments. Results of the bed surveys are given in this chapter.

Chapter 3 presents an introduction about two data mining models (SVM and ANN) that are applied in this study. The controlling parameters as well as the mathematical descriptions of the models are discussed in this chapter. The introduction of SVM and ANN are also supported by estimation of wave-induced scour around single piles cases using them.

Chapter 4 presents the developments and the results of modelling by two data mining models of SVM and ANN. The proposed models are verified with the experimental results. The outputs of both models are compared with those of semi-empirical formulae in this chapter.

Chapter 5 summarises the conclusions based on the present study and gives some recommendations for future works.

2 EXPERIMENTAL STUDIES ON WAVE-INDUCED SCOUR AROUND A GROUP OF SLENDER PILES

As mentioned in Chapter 1, in addition to the evaluation of the applicability of soft computing models of SVM and ANN in scour predictions due to waves, this study also aims to present an in-depth experimental study about the effects of configuration in the scouring of pile groups. To achieve this goal, several sets of large-scale scour experiments were carried out in the wave basin of Ujigawa Open Laboratory for different arrangements of pile groups. Sumer and Fredsøe (1998) were of those few researchers who did some studies about scour around pile groups due to waves. In the studies of Sumer and Fredsøe (1998), the gap over diameter ratio (G/D), was among interpretative points of the experiment. In this research, the $G/D = 1$ was selected for all sets of experiments. It should be noted that, since the main goal is to compare the results of various arrangements of piles, a constant ratio of gap between the piles over

diameter (G/D), was kept as 1 for all cases. In all experimental cases both gap between the piles (G) and the diameter (D) of each piles were 10 cm.

Determination of the number of piles was also done by referring to the studies of Sumer and Fredsøe (1998). Since in the experimental study of Sumer and Fredsøe (1998), for $G/D = 1$ the tandem arrangement of 2 piles was not included, this arrangement was included in this research consequently. Furthermore, the 2×2 (4 piles), 2×3 (6 piles) and 3×3 (9 piles) arrangements also were not included in Sumer and Fredsøe (1998) and they have been considered in current experimental study.

On the other hand, since only KC numbers of 13, 37 for 91 percent of the experimental cases and KC numbers of 3 and 6.3 were considered for two experimental cases, KC numbers of 3.9 for $T = 1.2\ s$ and 5.9 for $T = 1.5\ s$ were selected for this research.

Both KC numbers and pile configurations of this study were selected according to what mentioned above so that the whole experimental data (Sumer and Fredsøe (1998) and current study) that are used in soft computing models (in Chapter 4) cover a wider range of wave and configuration characteristics. In other words, considering the nature of soft computing models (refer to Chapter 3), SVM and ANN models are developed based on a wide range of data of scouring of pile groups and provide more accurate predictions of scour.

To summarize, series of large-scale scouring experiments were carried out for various arrangements of 1, 2, 4, 6 and 9 piles exposed to waves with KC numbers of KC =3.9 and KC =5.9 and equilibrium scour depth around them were measured.

2.1 Experimental setup

The 45 m long, 30 m wide and 1m deep wave basin of Ujigawa Open Laboratory, Disaster Prevention Research Institute, Kyoto University was used for the experiments.

The basin is equipped with a piston wave generator with 20 paddles to produce regular waves. Figure 2-1 shows the wave basin and its dimensions.

Maximum wave height of 25 cm can be generated in water depth (d) of $d = 70\ cm$ and wave period (T) of $T = 1.5\ s$. The range of the wave periods that can be generated by the wave maker is between 0.4 s and 5 seconds.

Figure 2-1. Wave Basin of Coastal sedimentary Laboratory

The large-scale experimental model containing 9 piles the diameters and gaps of which were both 10 cm was designed according to Figure 2-2. All piles are made of Acrylic. All piles were removable and screwed on the base by bolts. The base was filled up to level of 15 cm by silica sand with the average diameter of 0.25 mm (sold in Japan as *No.6 Keisa*). At the beginning of each run of the experiment, the greatest possible effort was done to make the bed level as flat as possible.

Figure 2-3, Figure 2-5 and Figure 2-7 show the as-built photo of the pile group experimental model. As it can be seen in all figures, 16 small gauges ($D = 1\ cm$, total Height $= 23.3\ cm$, height from the erodible bed=9 cm) were installed at the perimeter

of each pile so that the scoured bed can be surveyed at 16 points around each pile. The precision of the scaling in the bars were 0.5 cm.

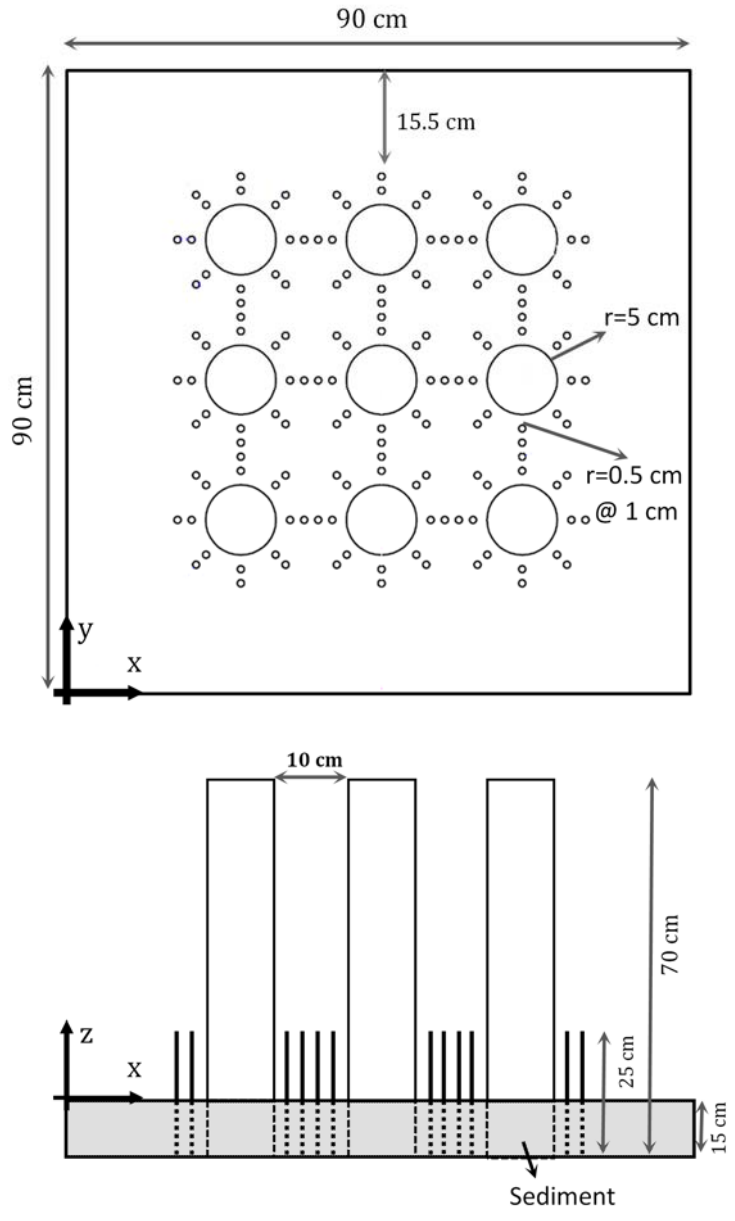

Figure 2-2. The primary design of the experimental model

It should be noted that small measuring bars might have some effects on the tests but because of two main points the interference of the gauges in scouring phenomena are negligible. First, since the diameter of the piles are among controlling parameters and the diameter of each gauge is 1 cm, the ratio of the diameter of the gauges to those of main piles are about 10 percent which results in the small interference of the gauges as pile element in the scouring process.

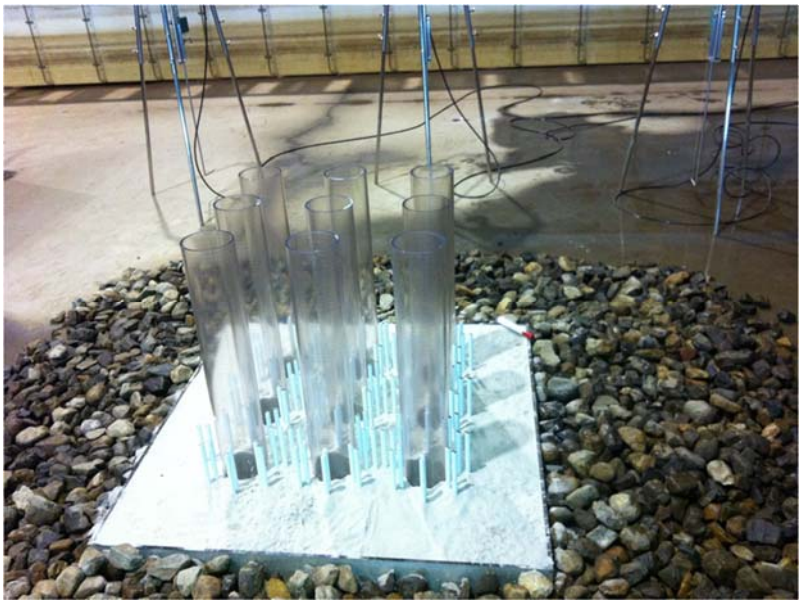

Figure 2-3. The as-built photo of the experimental model

On the other hand, the area of the conceptual donut shape effective scouring zone around each pile (shown in Figure 2-4) is calculated by deduction of the area of each main pile with the diameter of $D = 10\ cm$ ($A = \pi 5^2 = 78.5\ cm^2$) from the area of the conceptual circle with the diameter of $D = 15\ cm$ ($A = \pi 7.5^2 = 176.625\ cm^2$) which is equal to $176.625\ cm^2 - 78.5\ cm^2 = 98.15\ cm^2$. Moreover; the total area that is occupied by 16 piles around each mono-pile is $16 \times \pi 0.5^2\ cm^2 = 12.56\ cm^2$ which is equal to 12.8% of the total scoured area around each pile which does not cause

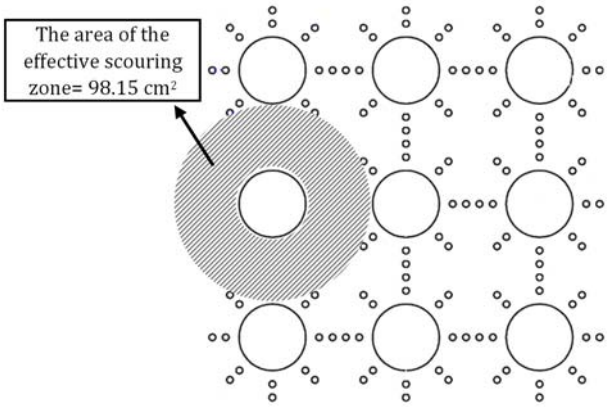

Figure 2-4. The illustration of the conceptual scouring zone around each pile

significant affect in the formation of the vortices and the scouring phenomena consequently.

The model was installed on the surface of the experimental base at the centre of the joining line of the first and last point of the wave generator and the boundary of the base was fixed and stabilized by rubble mound ($d_{50} = 30 - 35\ mm$) so that the model can resist against wave motions and cannot move during the experiments.

Figure 2-5. The plan view of the experimental model

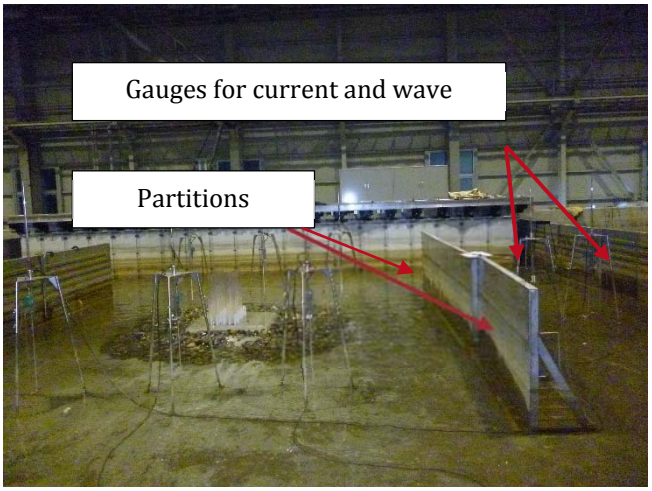

Figure 2-6. The installation of the experimental model in the wave basin

The length of the wave generator where paddles are installed, was divided into two spaces by two steel partitions according to Figure 2-6 to make two separate spaces, one for the scouring experiment and the other for undisturbed condition measurements consequently.

Six wave gauges were installed around the model (shown in Figure 2-7) and two gauges were installed at the separated space with undisturbed condition for velocity measurements.

In all experimental cases, water depth (d) was kept as 35 cm. To carry out each step it took about 35 $hours$ to fill in the basin up to required water depth of 35 cm

Sumer and Fredsøe (1998) carried out sets of two piles experiments in $KC = 13$. Figure 2-8 illustrates the result of their studies. In this figure, the amounts of S/D against G/D ; (where S is the scour depth, G is the gap between the piles and D is the diameter of the pile), were plotted for three types of 2-pile arrangements. As It can be clearly seen in Figure 2-8, by increasing the gap between the piles to large amounts ($G/D \rightarrow \infty$), scour depths around the piles reach the amounts of scour around a single

Figure 2-7 . The instalment of the experimental model in the wave basin

piles. This diagram denotes that if the ratio of the gap between the piles (G) to their diameters (D) , G/D is big enough, piles will not interact each other and will act as a single pile. Based on the findings of Sumer and Fredsøe (1998), to avoid individual behaviour of the piles, the gap over diameter ratio of $G/D = 1$ was selected to design the experimental model of this study.

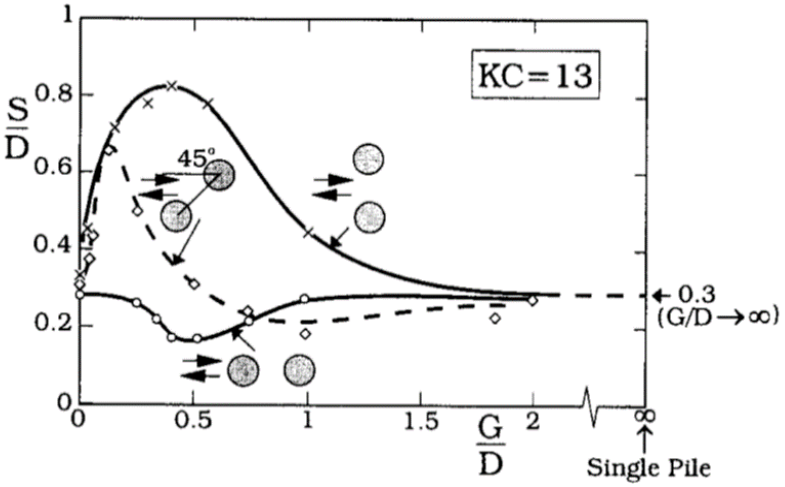

Figure 2-8.The amounts of S/D against G/D for 2-pile arrangements (Sumer and Fredsøe 1998)

Figure 2-9 shows the configurations studied by Sumer and Fredsøe (1998). In the experimental study of Sumer and Fredsøe (1998), for $G/D = 1$ the tandem arrangement (2×1 (Figure 2-9 (a)) were not included for KC numbers of $KC = 3.9$ and $KC = 5.9$ and the experimental cases for 2×1 arrangement were included in this research consequently.

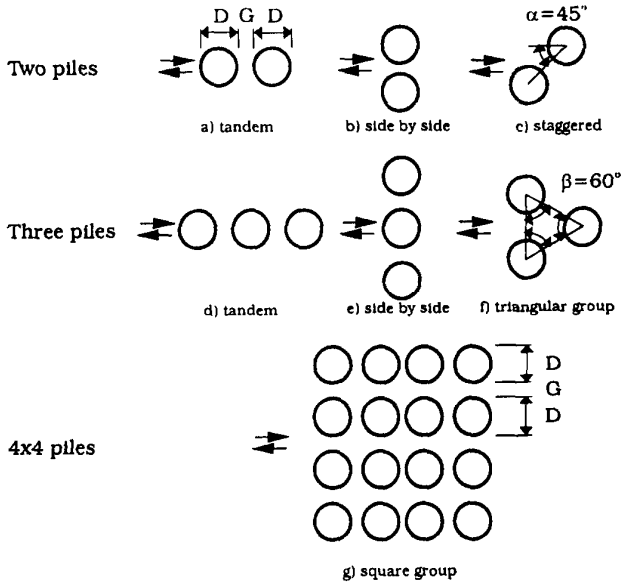

Figure 2-9. Pile group configurations studied by Sumer and Fredsøe (1998)

The two by two pile ($2 \times 2 = 4$ piles), two by three ($2 \times 3 = 6$ piles) and three by three $3 \times 3 = 9$ piles) arrangements also were not included in (Sumer and Fredsøe 1998) so they have been considered in current experimental study.

On the other hand, since in the experimental study of Sumer and Fredsøe (1998) , only KC numbers of $KC = 13$ and $KC = 37$ were used for 91 percent of the experimental cases and KC numbers of $KC = 3$ and $KC = 6.3$ were considered only for two experimental cases, for this study KC numbers of $KC = 3.9$ and KC=5.9 for $T = 1.2\ s$ and $T = 1.5\ s$ were selected respectively.

It should be highlighted that, for each experimental case, wave periods of $T = 1.2\ s$ and $T = 1.5\ s$ and wave height of $H_w = 12\ cm$ were adjusted as inputs of the wave maker to generate regular waves in water depth of $d = 35\ cm$.

In brief, both main experimental parameters: KC numbers ($KC = 3.9$and $KC = 5.9$) and pile arrangements (1×2, 2×3, 2×2, 3×3) that were considered in this study complete the previous studies of Sumer and Fredsøe (1998) and provide a wider entire arrange of pile group experimental data based on KC number and pile group configurations. Specifically , from the view of number of piles in the pile arrangements which is considered as one of the configuration parameters that affects scouring, the data provided by Sumer and Fredsøe (1998) includes 2,3,4 and16 piles in the arrangement and the data set that is addressed in this study includes 2,4,6 and9 piles in the arrangement. Figure 2-10 shows the scheme of the pile group arrangements, used in this study. In Chapter 4, the number of piles in the arrangement in addition to other

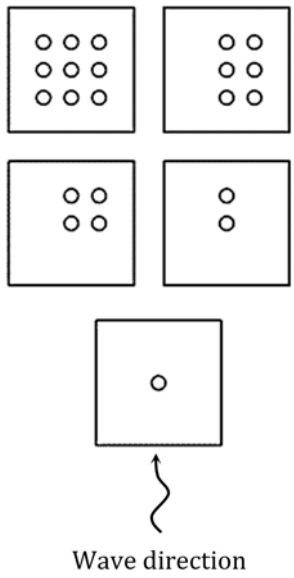

Figure 2-10. The arrangement of pile groups used in experiments

controlling parameters of scouring is used to estimate the wave-induced scour around pile groups.

Regarding the large scale of the experiment, a bed survey was done manually by recording the scoured bed at 16 points around each pile. Based on Figure 2-2, X-Y coordinates and sections were used to display amounts of scour depth at designated points. Figure 2-11 shows the coordinates as well as the horizontal and vertical sections along which the results of the bed survey were reported in this research.

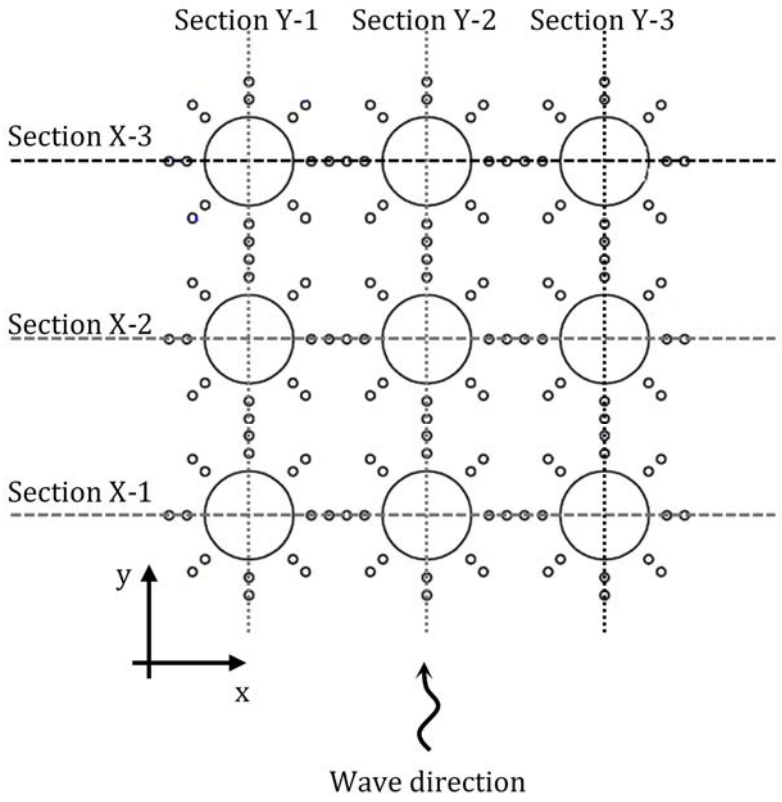

Figure 2-11. X-Y coordinates and sections used for bed survey

2.2 Time determination for the experiment

To determine the required time for occurrence of equilibrium scour depth, single pile experiment was done for time-determination and reference purposes. Figure 2-12 shows the experimental model related to single pile experiment.

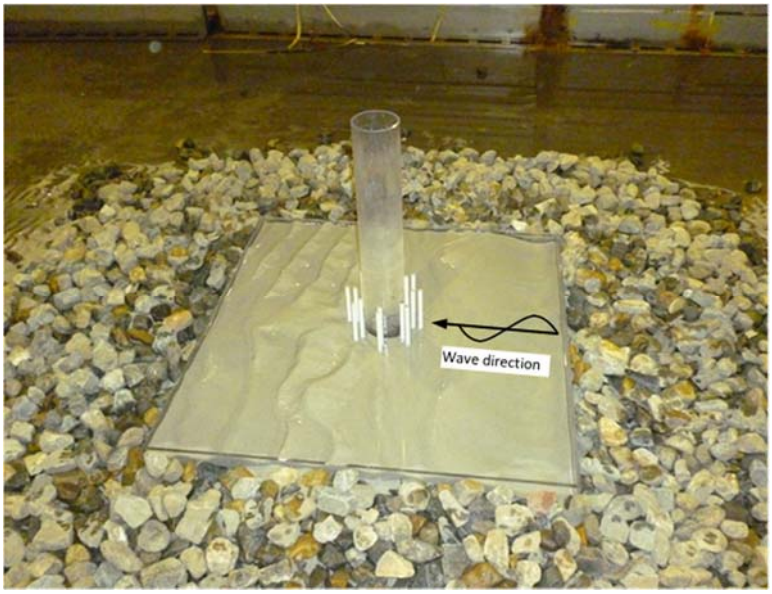

Figure 2-12. Photo of the single pile experimental model

The surveyed scour in case of single pile in 20 minutes intervals were shown in Figure 2-13. As it can be seen in Figure 2-13, having passed an hour, the depth of scour hole was not changed and the one-hour was determined as the experimental time for all sets of experiments consequently.

2.3 Single pile experiment

Having flatted the bed, adjusting the water level to $d = 35\ cm$, single pile was exposed to waves with periods of $T = 1.2\ s$ and $T = 1.5\ s$ and Height of $H = 12cm$. Table 2-1 illustrates the wave properties recorded by each sensor for wave periods of $T = 1.5\ s$. As the recorded significant wave heights ($H_{1/3}$) are almost equal to the average wave

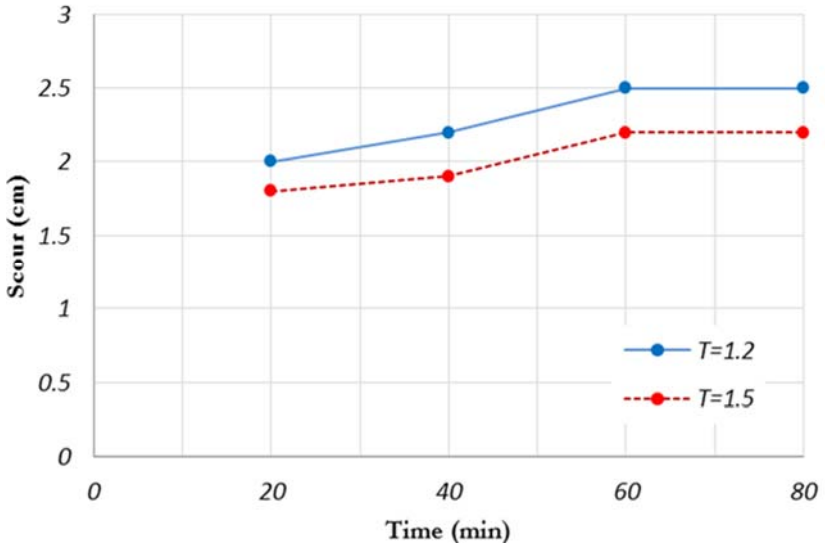

Figure 2-13. Scour development over time for single pile

heights (H_{bar}), it can be confirmed that generated waves by the generator are all regular waves and regular wave theories are applicable for this research and required wave properties to study scouring are calculated by using regular wave formulas in the proceeded sections.

Table 2-1. Wave properties in case of 4 piles for T=1.2s

Wave gauge number	H_{max}	$H_{1/10}$	$H_{1/3}$	H_{bar}	H_{rms}	T_{max}	$T_{1/10}$	$T_{1/3}$	T_{bar}
1	9.725	9.552	9.38	9.094	9.098	1.195	1.2	1.2	1.2
2	10.476	10.331	10.163	9.878	9.882	1.199	1.2	1.199	1.2
3	11.946	11.726	11.58	11.275	11.278	1.197	1.199	1.199	1.2
4	9.173	9.031	8.554	8	8.015	1.229	1.201	1.201	1.2
5	12.426	12.213	12.04	11.784	11.787	1.195	1.197	1.2	1.2
6	12.776	12.345	11.925	11.179	11.315	1.2	1.194	1.194	1.173
7	10.22	9.881	9.577	9.138	9.146	1.185	1.206	1.201	1.2

Results of the bed survey in case of single pile were plotted in Figure 2-14 to Figure 2-17. Scour depths were plotted along X-sections and Y-sections for both KC numbers ($KC = 3.9$ for $T = 1.2$ and $KC = 5.9$ for $= 1.5$) respectively.

In a single-pile experiment, the difference between maximum scour depths for both KC numbers is not so significant. As the KC number increases to $KC = 5.9$, the symmetrical bed profile along X section was changed to an asymmetrical one for $KC = 5.9$.

The symmetrical bed profile which is noticed for $KC = 3.9$, is in line with the observations of Sumer, Christiansen et al. (1997). As discussed in Chapter 1, according to their studies, as long as $2.8 \leq KC \leq 4$, the symmetric separation occurs and the pair symmetric vortices are washed around the pile as the flow reverses (Figure 1-4 a). It is concluded that, by increase in KC number to 5.9, the amount of KC is no longer $2.8 \leq KC \leq 4$ and the asymmetric formation of vortices results in the asymmetric scour around the pile.

Moreover, by the increase in KC number to $KC = 5.9$, the amounts of scour depth in front of the pile will be equal to the deposition amount, in front and back of the pile along Y-section. While in smaller KC number $KC = 3.9$, only scouring in front and back of the pile were recorded.

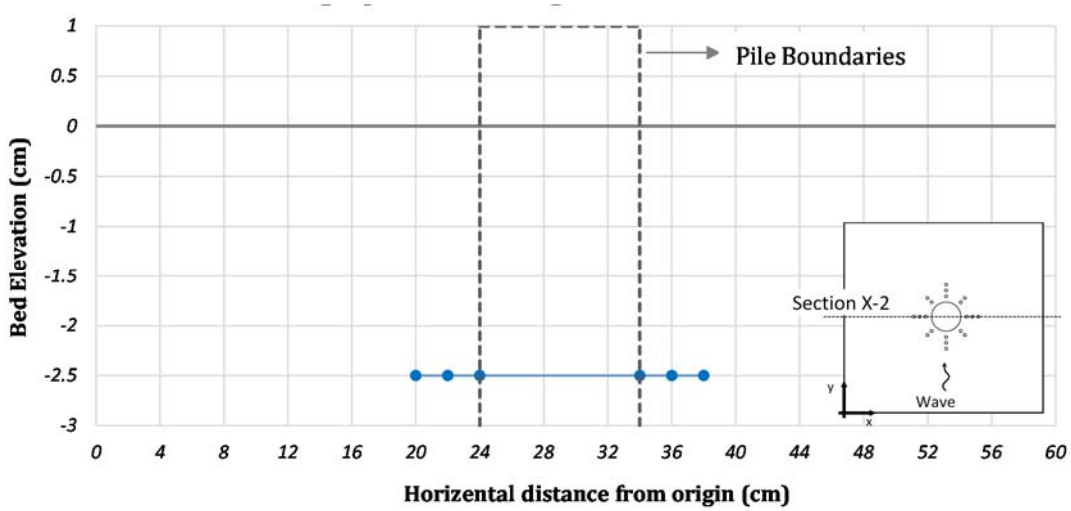

Figure 2-14. Bed profile of single pile along X section for $KC = 3.9$

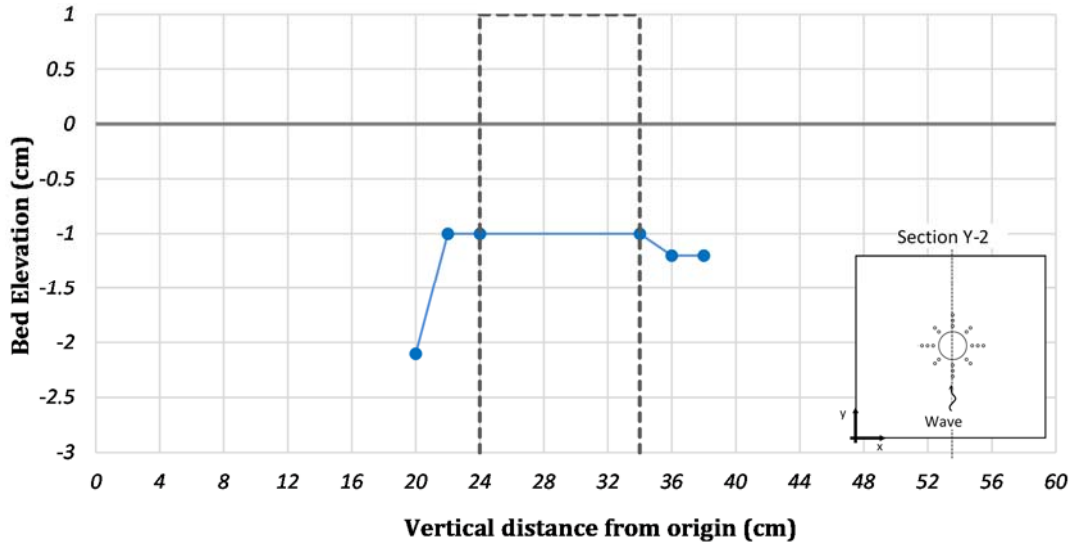

Figure 2-15. Bed profile of single pile along Y section for $KC = 3.9$

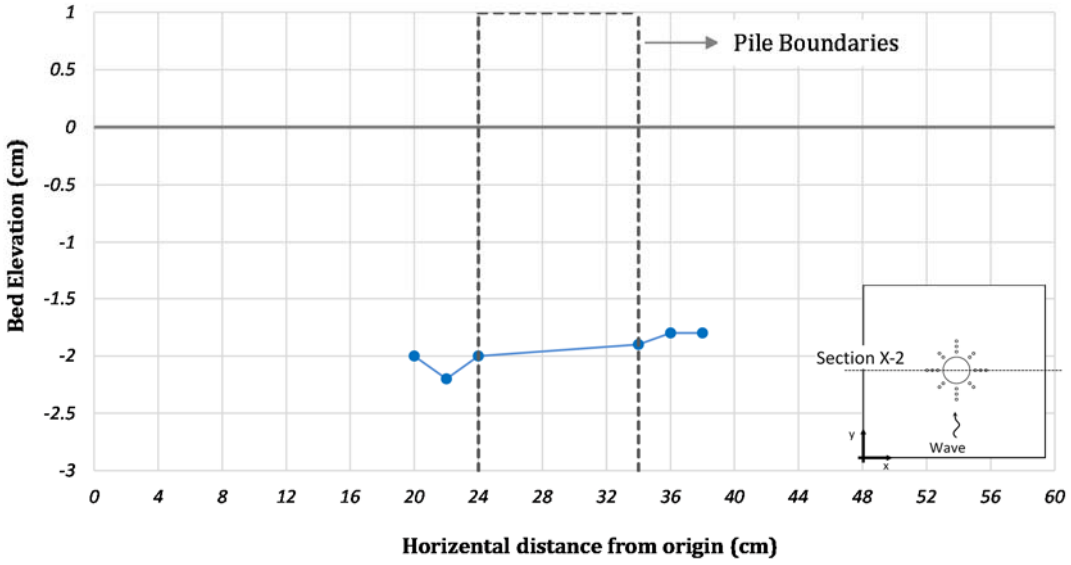

Figure 2-16. Bed profile of single pile along X section for $KC = 5.9$

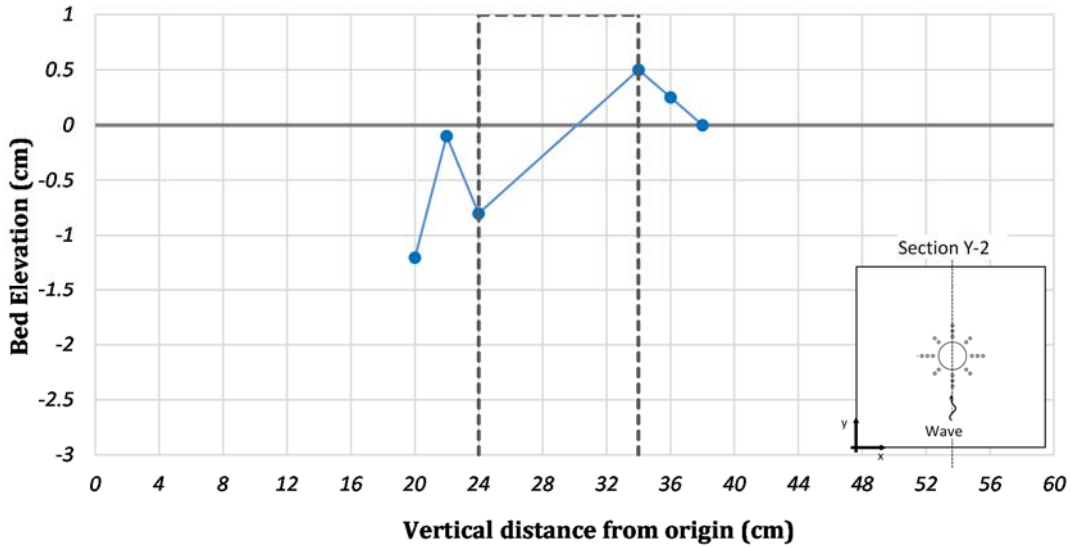

Figure 2-17. Bed profile of single pile along Y section for $KC = 5.9$

2.4 Two piles experiment

Figure 2-18 shows the experimental model related to 2-piles experiment. Two piles arrangement forms the 1×2 configuration or tandem arrangement named by Sumer and Fredsøe (1998) (also refer to Figure 2-9 (a)) wherein one row of piles is parallel to the wave direction and two rows are vertical to the wave directions consequently.

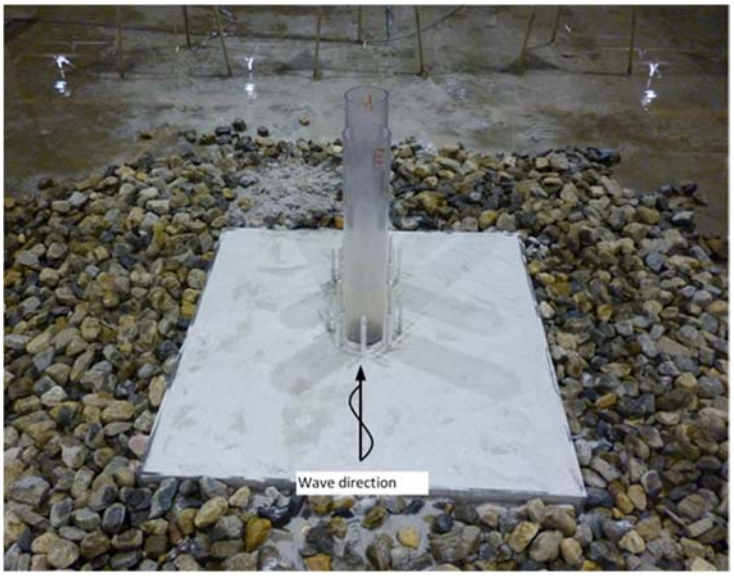

Figure 2-18. Photo of the two piles experimental model

Having exposed the piles to the waves with $T = 1.2\ s$ and $T = 1.5\ s$, the scour depths were plotted along the X and Y sections respectively. Results of the bed survey were displayed in Figure 2-19 to Figure 2-22. As it can be seen in Figure 2-21, in case of larger KC number, the scoured bed profile of the backside-pile, along X section is above the front-pile at all recorded points, which shows the higher scour depths at the front pile along X-2 sections. In addition, the trends of the scoured bed are almost same but reverse along X sections for $KC = 3.9$ representing the formation of reverse vortices along each X section.

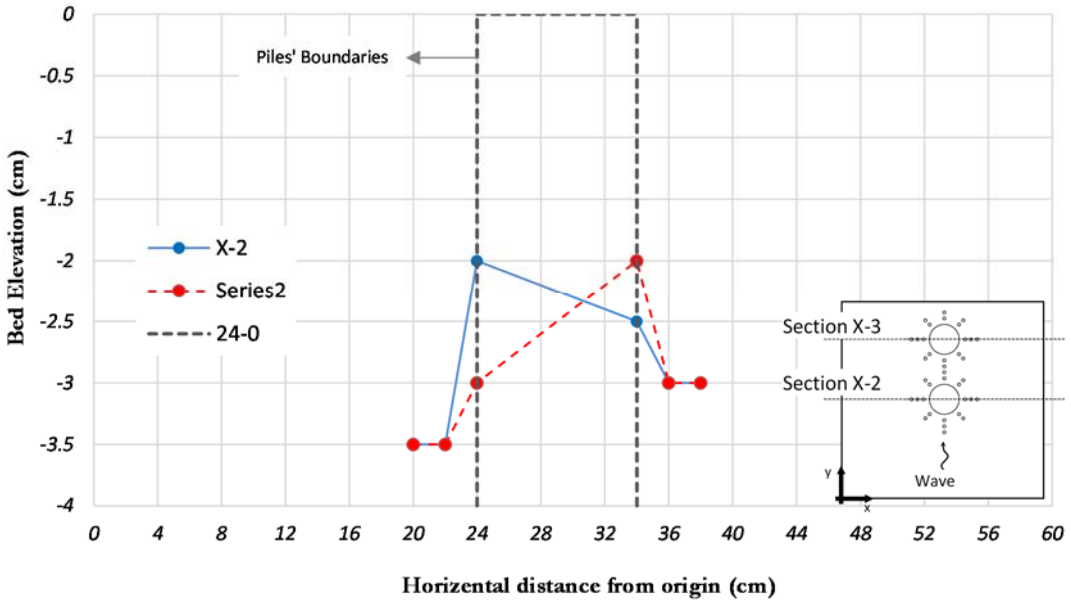

Figure 2-19. Bed profile of two piles along X section for $KC = 3.9$

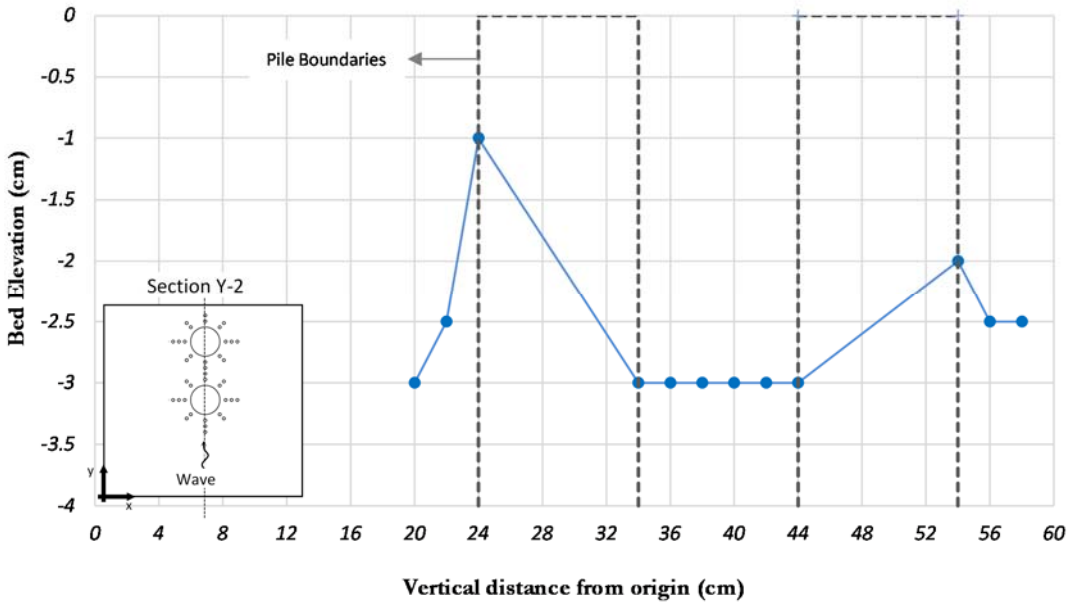

Figure 2-20. Bed profile of two piles along Y section for $KC = 3.9$

In smaller KC number $C = 3.9$, the scoured depth along Y section between the piles is a constant amount of 3 cm which is different from the diverse trend between the piles

with larger KC of $KC = 5.9$ that relies on more turbulent vortices between the piles in larger KC number.

According to Sumer and Fredsøe (1998), for side-by-side arrangements, as the KC number increases, for same ratios of G/D, the increase in scour depth is expected. In the present experimental case, which has the tandem arrangement according to the configuration definition of Sumer and Fredsøe (1998), by increasing the KC number, the scour depth decreases about 0.5 cm which is the 16.67% of the 3 cm scour recorded for larger KC number. It should be noted that Sumer and Fredsøe (1998) studied the tandem arrangements at constant KC numbers of $KC = 13$ for different spacing between the piles.

Though the difference between the recorded scour depths is not so large, the formerly reported difference in variation of S/D by KC was mainly caused because of the difference in the arrangement parameter. As in case of side- by-side arrangements the wave firstly faces two obstacles and the space between them and in case of tandem arrangement, the wave attacks one obstacle, which results in quite difference in formation of vortices and change of sediment transport consequently. It can be concluded that regardless of the number of piles in modelling, application of an appropriate arrangement parameter is necessary as well.

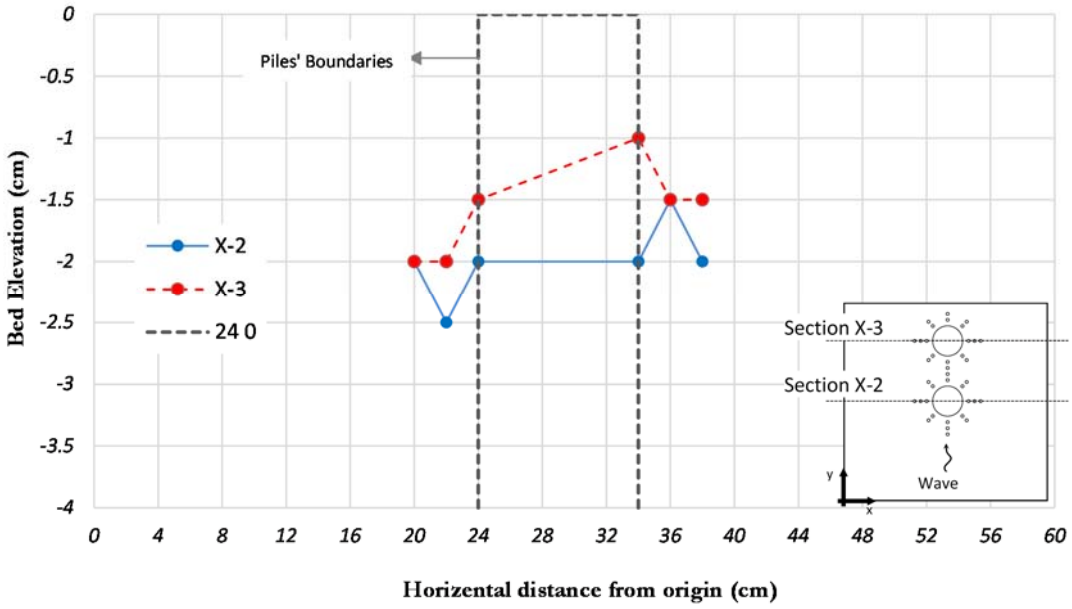

Figure 2-21. Bed profile of two piles along X section for $KC = 5.9$

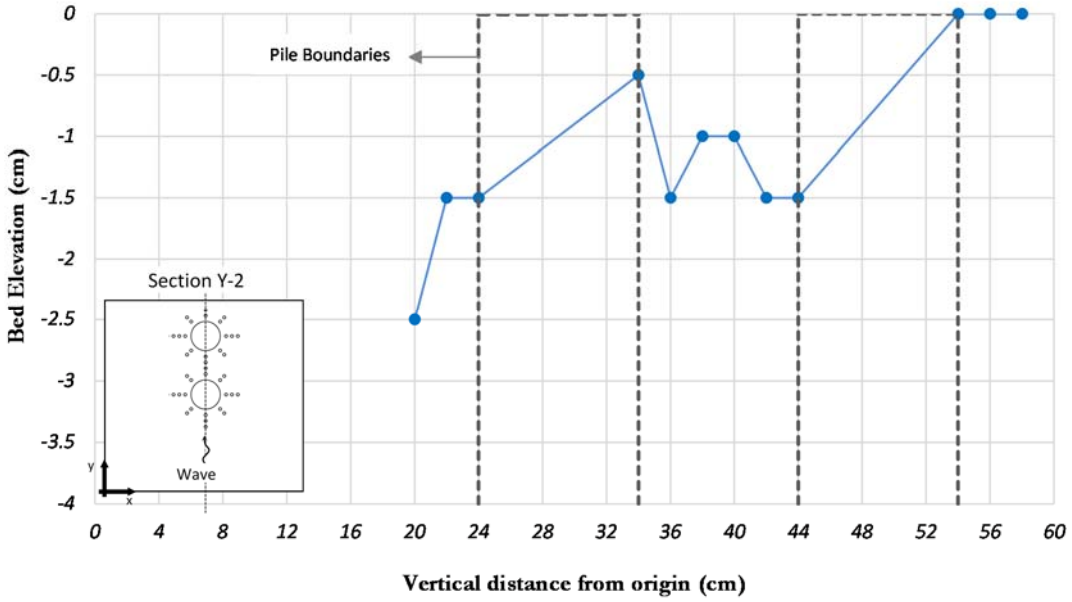

Figure 2-22. Bed profile of two piles along the Y-section for $KC = 5.9$

2.5 Four piles experiment

Figure 2-23 illustrates the experimental model used in 4 piles experiment. The numbers of piles, which are parallel to the wave direction as well as those vertical to it, are both two. These numbers are similar to the field survey conveyed by Bayram and Larson (2000) from the point of arrangements.

Piles were exposed to KC numbers of 3.9 and 5.9 in wave periods of $T = 1.2\ s$ and $T = 1.5\ s$. Having passed a one hour, scoured depths were surveyed at 24 point around each pile. Results of the bed survey were plotted for X and Y sections according to Figure 2-24 and Figure 2-27.

According to Figure 2-24, it can be seen that maximum recorded scour for both rows along X section is 4 cm at the piles front to the wave direction.

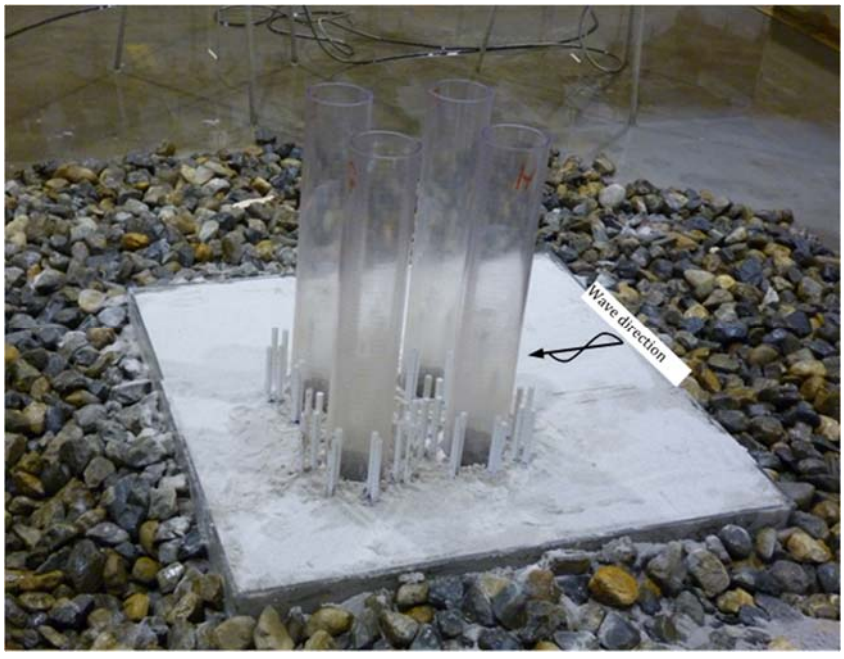

Figure 2-23. Photo of the four piles experimental model

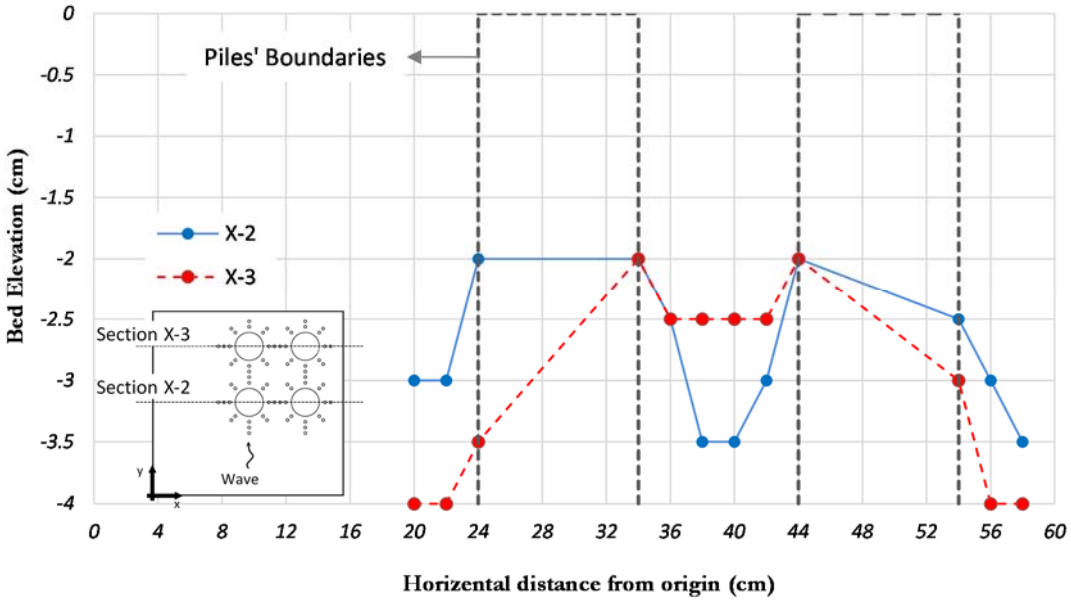

Figure 2-24. Bed profile of 4 piles along X section for $KC = 3.9$

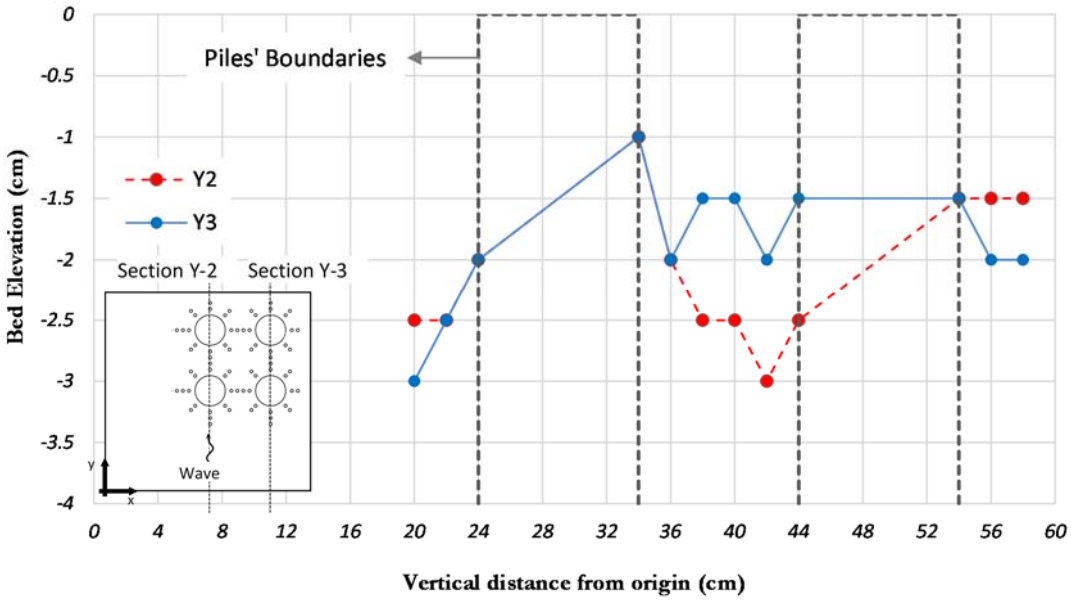

Figure 2-25. Bed profile of 4 piles along Y section for $KC = 3.9$

According to Figure 2-25 maximum scour depth for $KC = 3.9$, at the Y sections are 3 cm which increased about 25 percent compared to the scour amounts recorded for X sections.

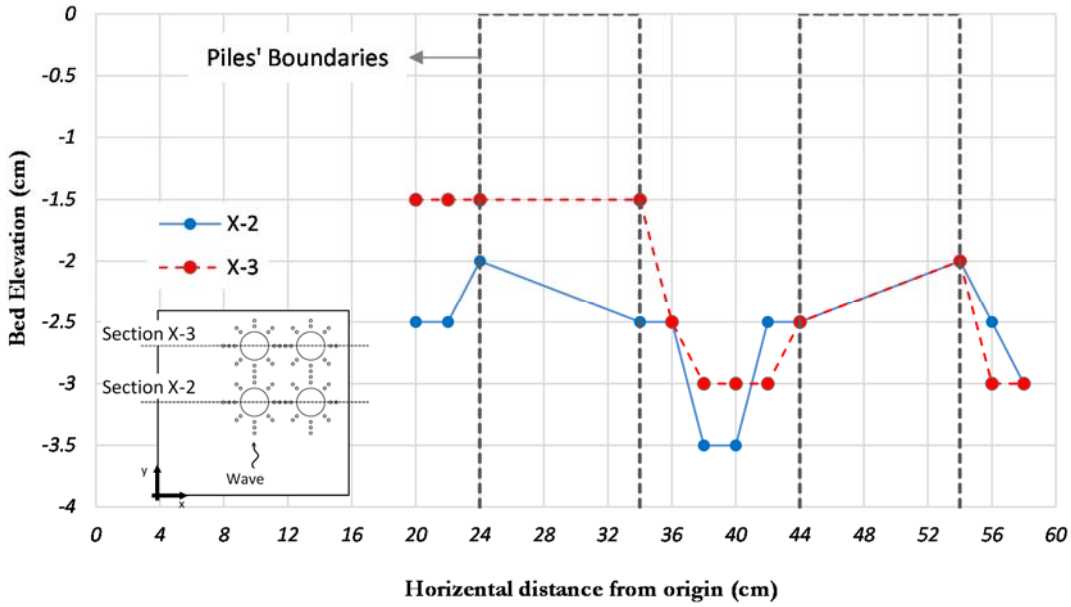

Figure 2-26. Bed profile of 4 piles along X section for $KC = 5.9$

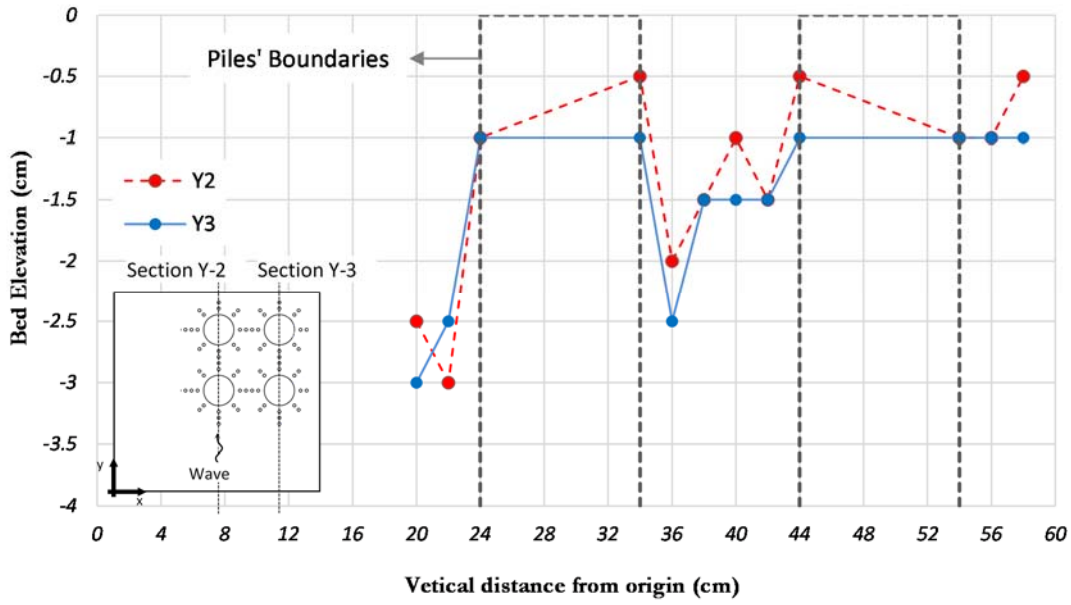

Figure 2-27. Bed profile of 4 piles along Y section for $KC = 5.9$

Figure 2-26 illustrates the scour depth of $T = 1.5\ s$ which is equivalent to KC numbers of $KC = 5.9$ in this study. It can be seen that the maximum of recorded scour depth is 3.5 cm at the front piles.

It can be also noticed that unlike the tandem arrangement of 2 piles, the scoured bed profiles are not above or below the other one for all points. For both KC numbers, the scour depth remained constant in the gap along the X section.

In addition, the trend of the scoured bed of both rows along Y sections for both KC numbers according to Figure 2-25 and Figure 2-27 are almost same. According to Figure 2-25, in smaller KC at some points the profiles are overlapped showing same scoured bed. The trends also indicate more scouring along the left row of piles.

In case of larger KC number, $KC = 5.9$ the trends of the graphs along Y sections in Figure 2-27 are almost same. Overall, the scoured bed of the left row is located above the right one, which means that in the vicinity of the right side row the bed was scoured more significantly.

2.6 Six piles experiment

Figure 2-28 illustrates the experimental model used in 6 piles experiment. The number of piles facing to the wave is 2 and three rows of piles are vertical to the wave direction. The configuration used in this set of experiment, represents the 2 by 3 (2×3) arrangement of pile group.

Six piles experimental model was exposed to KC numbers of 3.9 and 5.9 in wave periods of $T = 1.2\ s$ and$T = 1.5\ s$. Having passed a one hour, scoured depths were surveyed at 18 point around each pile. Figure 2-29 to Figure 2-32 illustrate the results

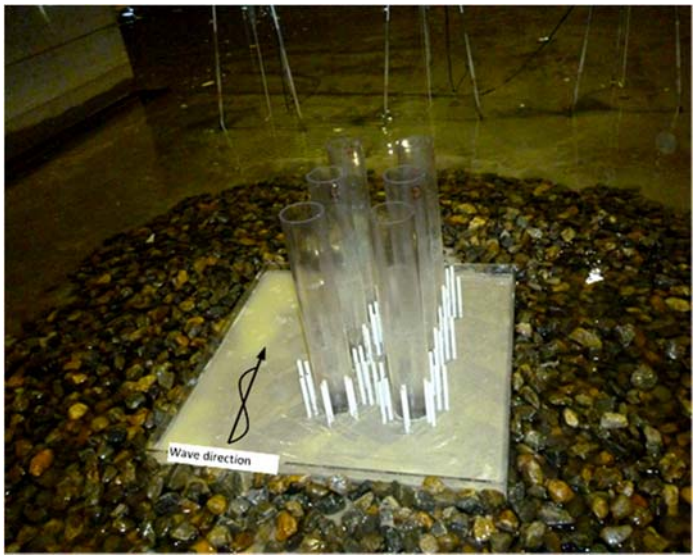

Figure 2-28. Photo of the six piles experimental model

of the bed survey for this set of experiment. It can be noticed that along X-sections, the scoured bed profiles have the same trends in all three rows of piles. On the other hand, the scoured profile of the first row is located below the other two profiles, which shows the deeper equilibrium scour depth along the first row facing the wave. Moreover, the bed profile along the gap between all three rows is a straight line demonstrating the constant scoured bed in the space between the piles.

The trends of the bed profile for both KC numbers along the Y-sections are almost same excluding few points and overlap to some extent, which represent the approximate symmetrical eroded profile along that section.

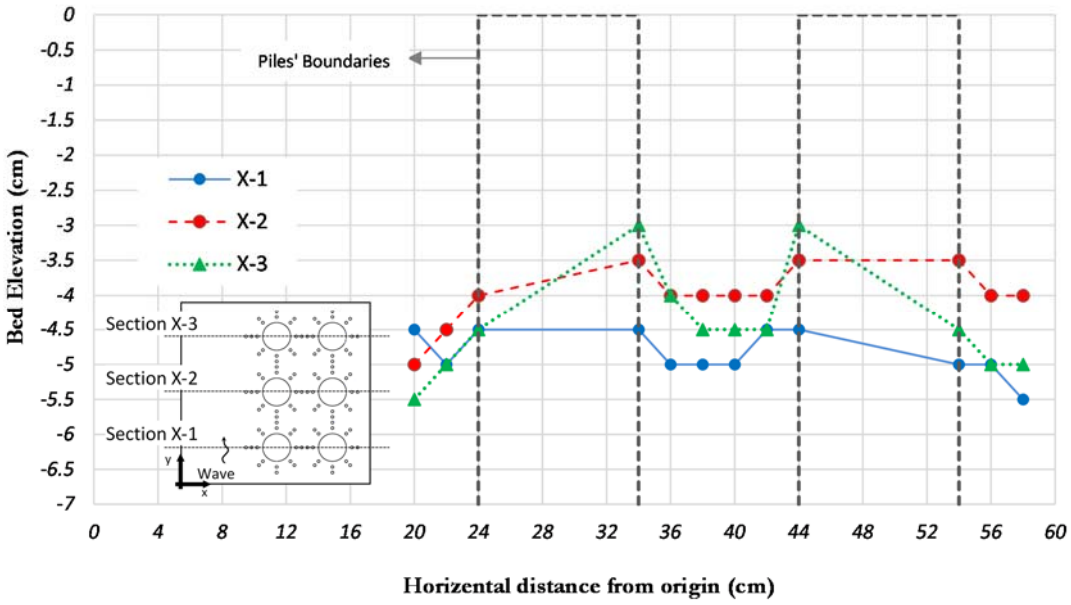

Figure 2-29. Bed profile of 6 piles along X section for $KC = 3.9$

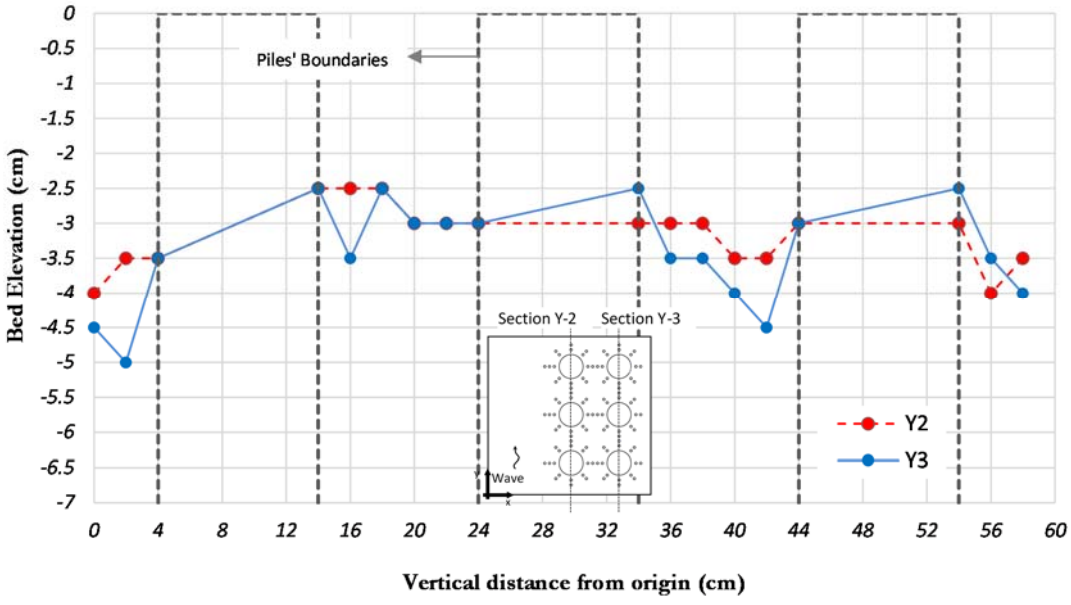

Figure 2-30. Bed profile of 6 piles along Y section for $KC = 3.9$

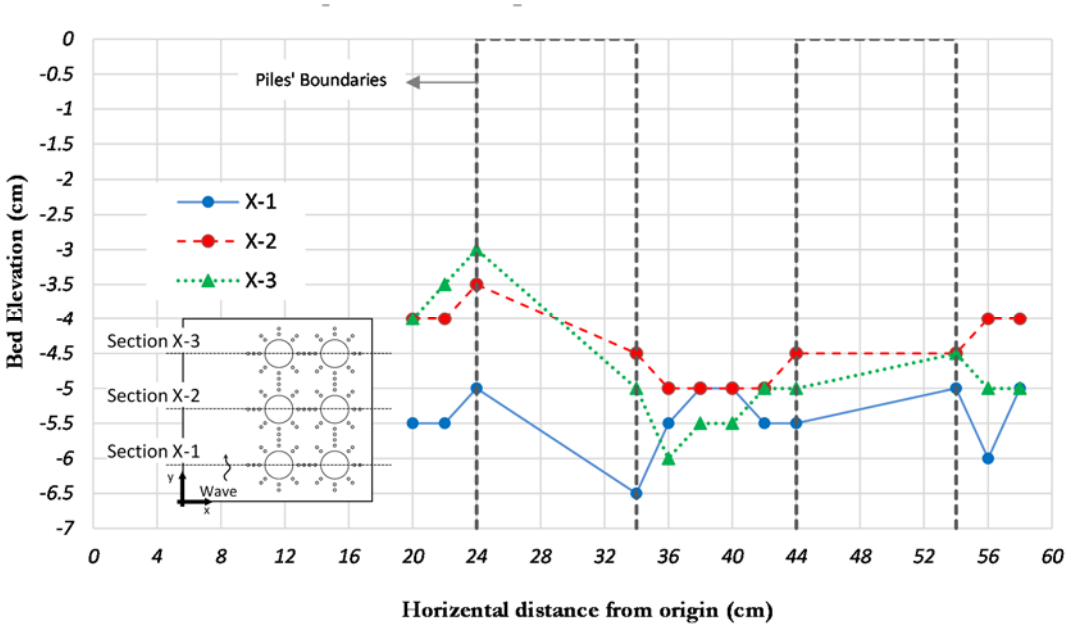

Figure 2-31. Bed profile of 6 piles along X section for KC = 5.9

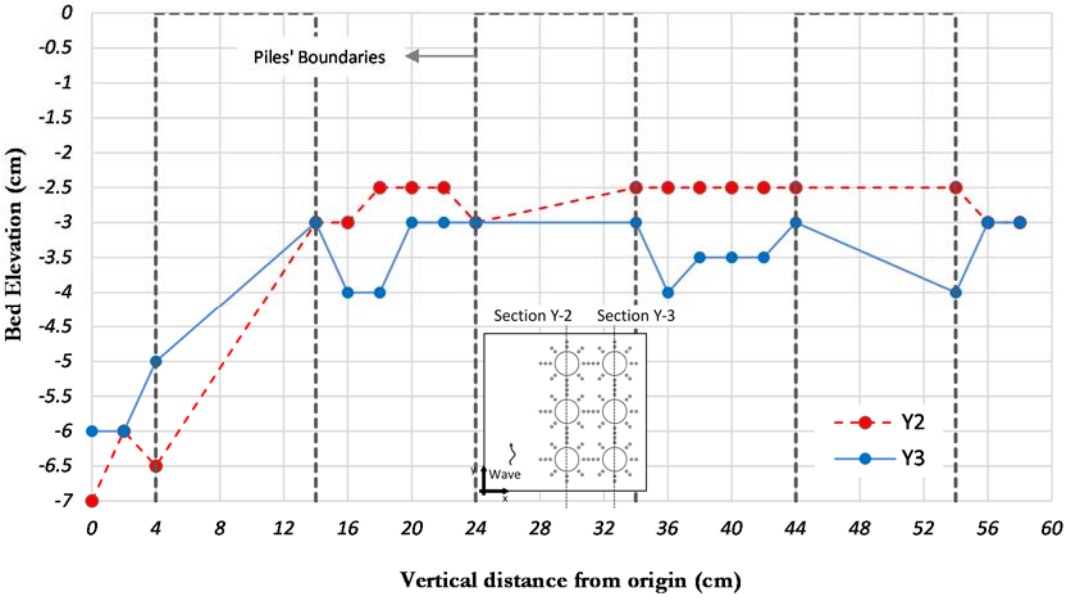

Figure 2-32. Bed profile of 6 piles along Y section for KC = 5.9

Overall, the amounts of observed scours are 75% larger compared to those of 4 piles with less number of mono-piles in the arrangement. Considering same gap over

diameter ratios ($G/D = 1$) and same KC numbers for both 4 and 6 piles configurations, the effect of arrangement of piles in the scouring problem is strongly highlighted consequently.

2.7 Nine piles experiment

Figure 2-33 illustrates the experimental model used in 9 piles experiment. The number of piles facing to the wave is 3 and 3 rows of piles are vertical to the direction of the wave. The arrangement of piles of the experimental model represents the 3 by 3 (3×3) configuration of pile groups. Nine piles experimental model was exposed to KC numbers of 3.9 and 5.9 in wave periods of $T = 1.2\ s$ and $T = 1.5\ s$.

Having passed a one hour, scoured depths were surveyed at 24 points around each pile. Results of the bed survey were plotted for X and Y sections according to Figure 2-34 to Figure 2-37.

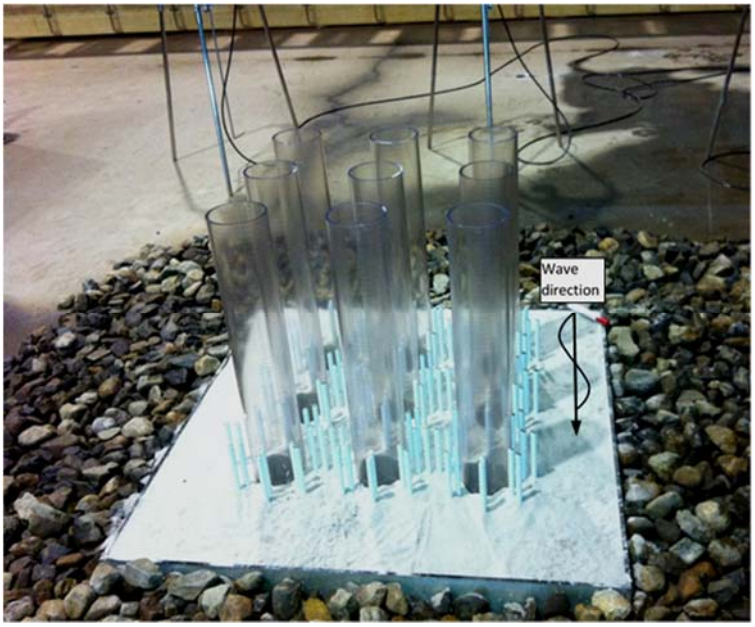

Figure 2-33. Photo of the 9 piles experimental model

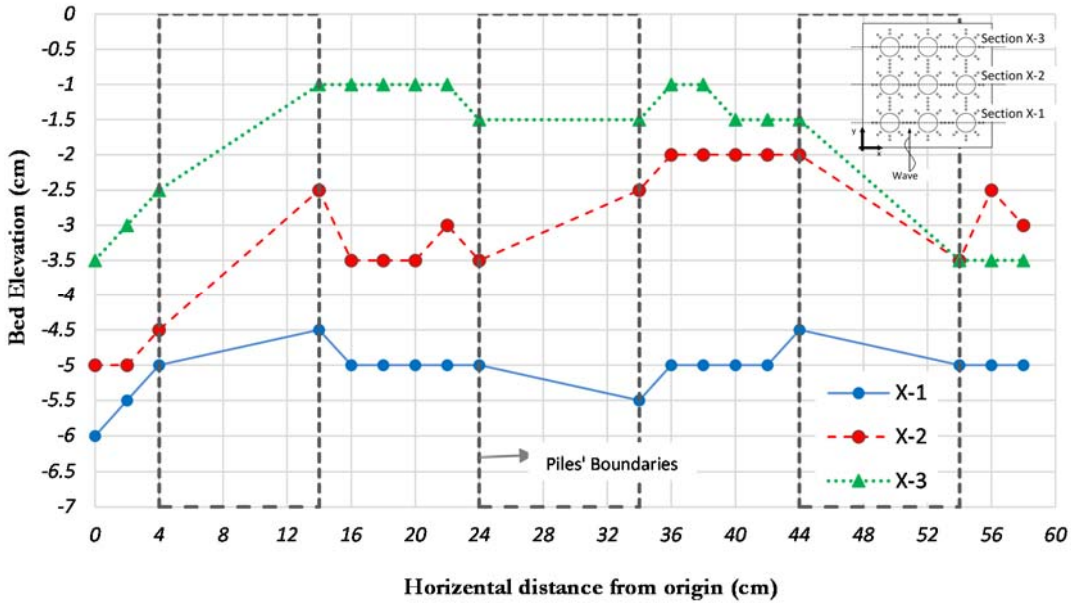

Figure 2-34. Bed profile of 9 piles along X section for $KC = 3.9$

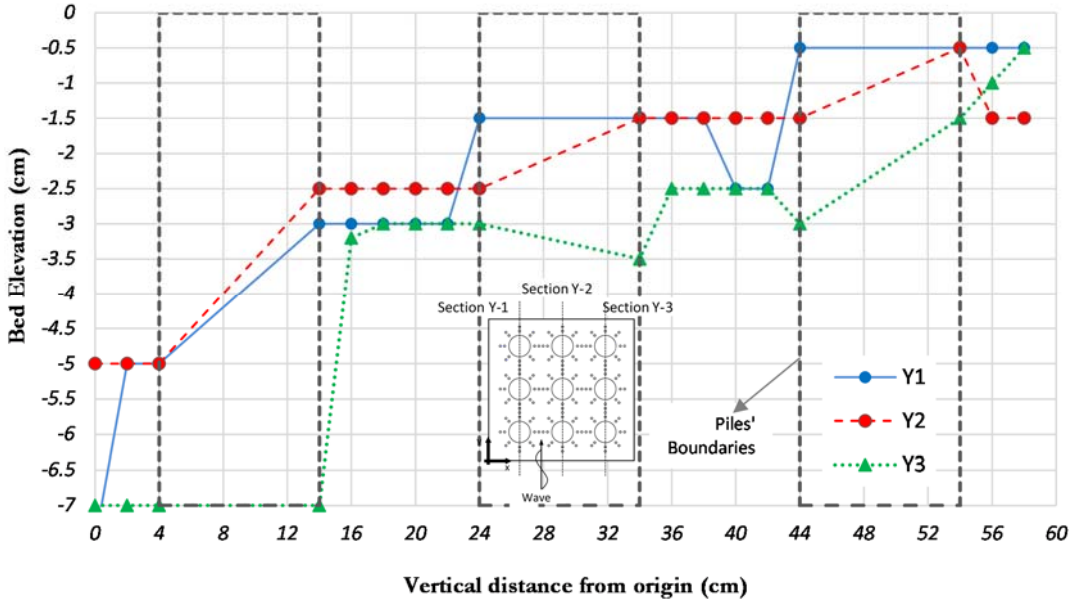

Figure 2-35. Bed profile of 9 piles along Y section for $KC = 3.9$

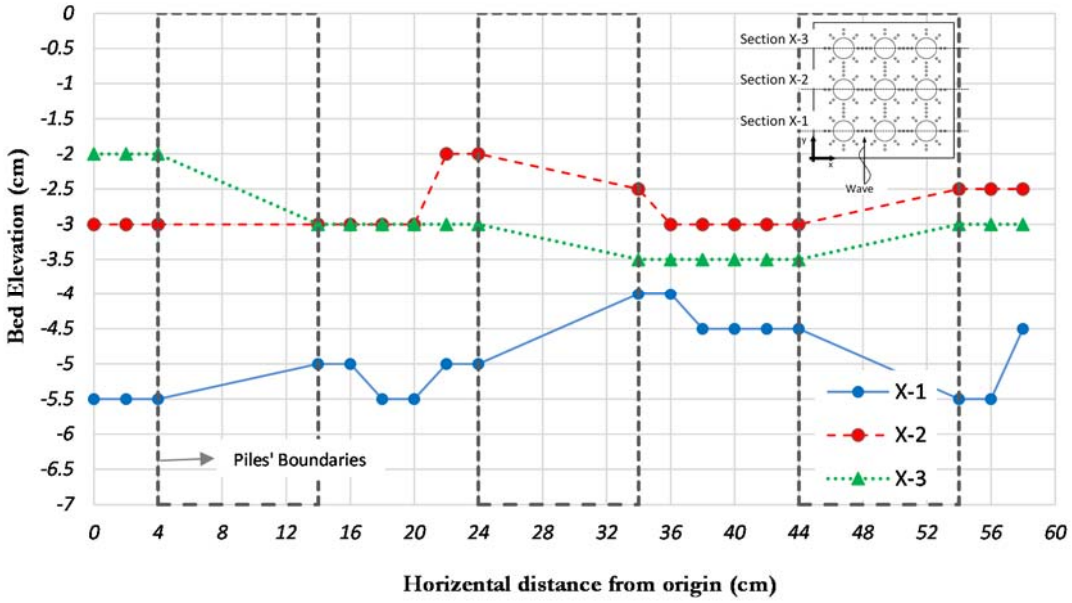

Figure 2-36. Bed profile of 9 piles along X section for $KC = 5.9$

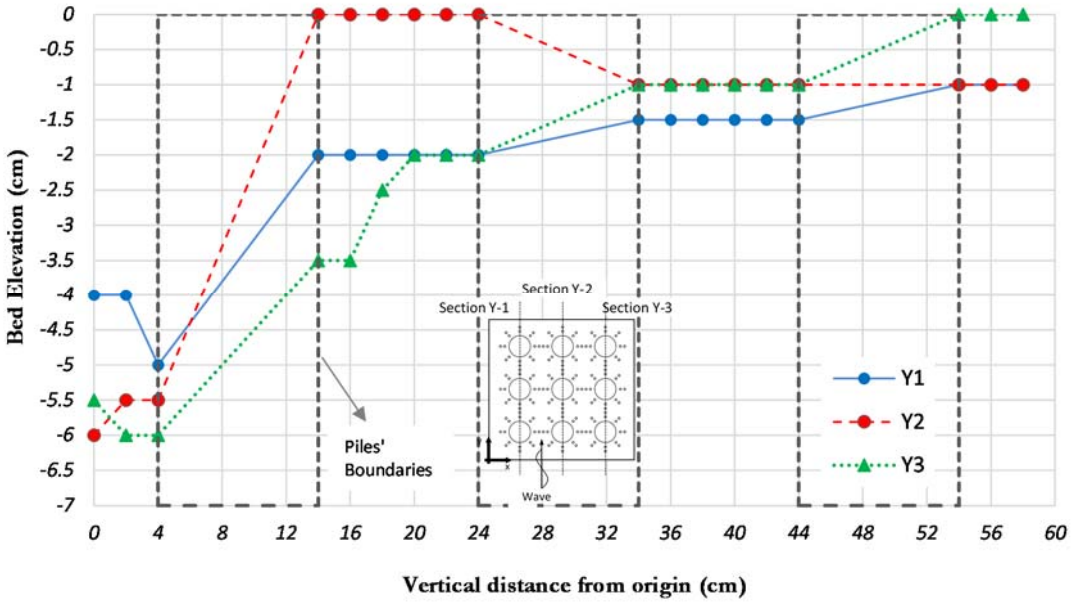

Figure 2-37. Bed profile of 9 piles along Y section for $KC = 5.9$

Similar to the 6 piles arrangement, in case of both KC numbers along the X sections, the first row of piles front to the wave scoured more and the related graphs are located

below other back-side rows consequently. Comparison of Figure 2-34 and Figure 2-36 shows that the 1st and 3rd row of piles along X-1 and X-3 sections, have the most and least amount of scour respectively and the scoured bed profile of the 2nd row is located between them. However, by increase in KC number, the scour amounts of the 2nd and 3rd rows of piles along X-2 and X-3 sections get closer.

In addition, the rises and drops of all graphs follow same trends except in the vicinity of the middle row of piles along the wave direction. The amounts of scour along the gaps remain constant along most of the sections either parallel or vertical to the wave direction.

The maximum equilibrium scour depth in case of smaller KC of KC=3.9 is larger than its maximum amount for larger KC number, denoting the importance of the configuration factor in addition to KC number in scouring of pile groups.

2.8 Summary

Series of large-scale scouring experiments were done for various arrangements of 3×3, 2×3, 2×2, 1×2 and single pile arrangements of piles representing 9, 6, 4, 2 and 1 piles cases respectively. The time-determination experiments were carried out and one hour was selected to reach the equilibrium scour depth.

Piles were exposed to waves with KC numbers of $KC = 3.9$ and $KC = 5.9$ for one hour and equilibrium scour depth around them were measured. Regarding the large scale of the experiment, survey of the scoured bed was carried out at 24 points around each pile for all cases. Results of the measurement at designated points around each pile were plotted on profiles of scoured bed along sections parallel and vertical to the wave direction for each experimental case.

In the single-pile experiment, as the KC number increased to $KC = 5.9$, the symmetrical bed profile along X section was changed to an asymmetrical one. Results of the single pile cases were in line with the findings of other researchers Sumer, Christiansen et al. (1997) about wave-induced scour around single piles based on the characteristics of the vortices at different KC numbers.

In the two piles tests with the 1×2 arrangement, it was observed that in larger KC number along X section, the scoured bed profile of the back pile was above the front pile at all recorded points. The scour trends were almost same along X section for $KC = 3.9$. For smaller KC number, $KC = 3.9$, the trends of the scoured bed were almost same but reverse along X section, showing the formation of reverse vortices along that section. On the other hand, comparison of the results of this set of experiment with the findings of Sumer and Fredsøe (1998) about the tandem arrangement of pile groups, confirmed the importance of considering the configuration parameter in addition to KC number in the study of scouring around pile groups.

In case of four-piles with 2×2 configuration, it was seen that for smaller KC number, the maximum scour depth recorded for both rows along X section was 4 cm and occurred at the piles front to the wave direction. In case of larger KCnumber, the maximum sour depth was 3.5 cm and similar to the case with smaller KC number was observed at the front piles. The trends of the scoured bed profiles for both KC numbers were almost same in this arrangement.

For six piles experiment representing 2×3 arrangements of piles, it was mainly noticed that for both KC numbers along X sections, the scoured bed profiles have the same trends in all three rows of piles. The bed profiles of the third row was located above two others demonstrating the least scour along that row of piles and the first row of piles facing to the wave had the lowest bed profile showing the most scour along

front piles. It was also noticed that profiles follow the approximately symmetrical slope along the Y sections. Furthermore, the maximum recorded scour was 75% larger than the maximum recorded scour for 2×2 arrangements with less number of piles in the pile group which considering same gap over diameter ratios (G/D) as well as same KC numbers for the experimental cases, highlights the effect of arrangement of the piles in the researches about the wave-induced scour of pile groups.

In nine piles tests, same as the 6 piles cases, for both KC numbers along X sections the first row of piles front to the wave direction had larger scour and related graphs were located below two other back rows. First and third row of piles had the most and least amounts of scour along X sections in this set of experiment. Moreover, the amounts of scour along the gaps remained constant for most of the sections either vertical or parallel to the wave direction. The maximum scour depth that was recorded for smaller KC number was less than this amount for larger one, denoting the effect of both KC number and configuration parameter factor for experimental studies and modelling of scouring phenomena around groups of piles.

Overall, the comparison of the bed profiles along each section for each arrangement indicates that in most of the cases sections along the first row of piles, facing to the wave directions have higher scour values compared to other sections and directions. It is concluded that using an arrangement parameter, which is defined based on the wave direction to consider the configuration of the pile group, is an important controlling factor. On the other hand, variations of observed scour values by the number of piles as well as the type of their arrangements in a pile group also highlights the importance of considering the configuration parameter in addition to the fundamentally considered parameter of KC number.

3 DATA MINING APPROACHES IN PREDICTION OF SCOURING

As mentioned earlier, the scour properties around a pile group is influenced by several parameters including sediment characteristics, properties of wave, pile geometry and piles interactions in marine environment which leads to making a complicated problem to be solved.

Regarding the complexity of scouring phenomena and the lack of reliable approaches, significant trails have been done to improve the current approaches or introduce satisfying alternatives for available methods.

Data mining approaches is one alternative to conventional empirical equations to estimate scour depth. Two robust data mining approaches named Artificial Neural Networks (ANN) and Support Vector Machines are introduce in this chapter to be used for scour predictions around pile groups.

Artificial Neural Networks (ANN) as a famous data-mining method have been widely applied in scour estimations (e.g. Liriano and Day (2001), Kambekar and Deo (2003), Bateni and Jeng (2007), Zounemat-Kermani, Beheshti et al. (2009), Kazeminezhad and

Etemad-Shahidi (2010)). Kambekar and Deo (2003) developed various artificial neural networks with different input variables to predict scour hole properties around a specific arrangement of pile group (2×2) due to waves. Most of the results of their study showed that ANN provides a better alternative to the statistical curve fitting.

Another soft computing approach, named Support Vector Machines (SVM), has been successfully applied in problems such as the prediction of wind speed (Mohandes, Halawani et al. 2004), runoff modelling (Bray and Han 2004), prediction of storm surge (Rajasekaran, Gayathri et al. 2008), hourly reservoir inflow forecasting (Lin, Chen et al. 2009), effective forecasting of hourly typhoon rainfall (Lin, Chen et al. 2009) and prediction of significant wave height (Mahjoobi and Adeli Mosabbeb 2009).

In current study, in addition to study of scouring phenomena by laboratory experiments, in order to reach a better alternative of conventional empirical equations, assessing the performance of ANN and SVM in pile group scour predictions due to waves for the large- scale experimental data is addressed.

In this chapter, the development criteria of the alternative models of ANN and SVM, the required parameters to define the SVM and ANN model and the mathematical definitions of them are discussed. The introductions are supported by application of ANN and SVM regression to predict scour depth around single piles with different diameters due to various waves and bed characteristics.

3.1 Artificial neural networks (ANN)

An artificial neural network (ANN) simply means an interconnected network of computational elements or neurons that resemble biological neurons of human brain. Human brain has the ability to learn from examples, recognize the various pattern of

input data and to process information promptly. Natural neurons receive signals through synapses located on the dendrites or membrane of the neuron. When the signals received are strong enough, the neuron is activated and emits a signal though the axon; this signal might be sent to another synapse and might activate other neurons. Figure 3-1 illustrates the scheme of a conceptual biological neuron.

A mathematical neural network tries to imitate the human brain in data processing. This imitation involves combining the weighted input data, adding bias term to it and passing the sum as transfer function that determines the strength of such transformed input before sending it to the next neurons.

The complexity of real neurons is highly abstracted when modelling artificial neurons. These neurons consist of inputs (like synapses), which are multiplied by weights (strength of the respective signals), and then computed by a mathematical function which determines the activation of the neuron. Another function (which may be the identity) computes the output of the artificial neuron (sometimes in dependence of a certain threshold). ANNs combine artificial neurons in order to process information.

A typical Artificial Neural Network (ANN) consists of nodes that are organized according to particular arrangement. These nodes are generally arranged in layers, starting from the first input layer and ending at the final output layer. There can be several hidden layers, each having one or more nodes (Khosronejad, Montazer et al. 2003, Jain and Deo 2006).

Three types of the most commonly used ANNs are normal feed-forward neural network, recurrent neural network, and competitive neural network (Islam and Kothari 2000, Khosronejad, Montazer et al. 2003). In this study, a feed-forward neural network with a back propagation training algorithm is used. The basic element of a back propagation network is the processing node. Each processing node behaves like a

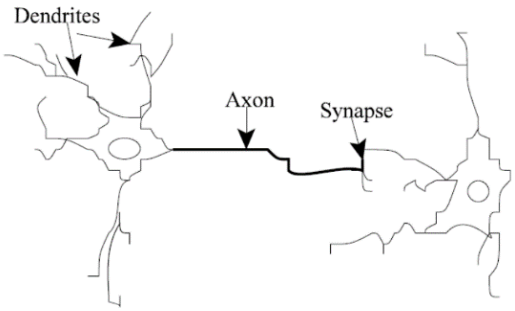

Figure 3-1. Conceptual biological neuron (Gershenson 2003)

biological neuron. The neurons are arranged in layered structure. Information passes from the input to the output layer. The neurons of each layer are connected to each other. Thus, the output of each neuron is only dependent to the data it receives from the previous layer and the connection weights. Figure 3-2 illustrates a back propagation neural network, with the interconnecting weighted links. Considering Figure 3-2, each node sums the value of its input data multiplied by the weight

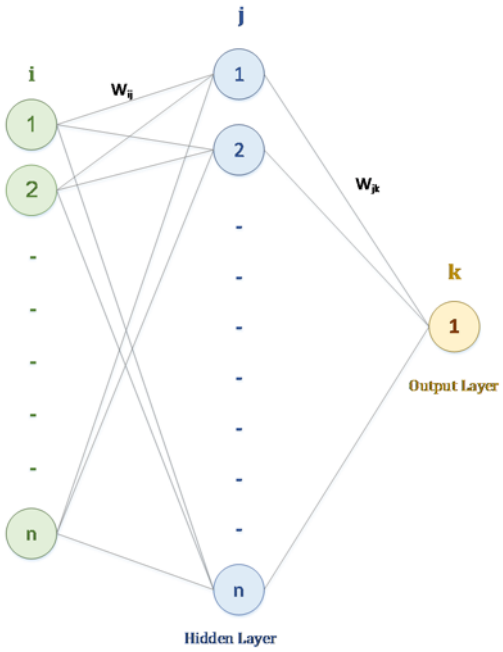

Figure 3-2. A back propagation neural network (Singh, Pal et al. 2008)

associated with each link. The sum then activated when it passes through an activation function f to generate the output. There is no interconnection between the nodes of the same layer.

In a back propagation neural network, generally an input layer acts as a distribution structure for the data presented to the network. After this layer, there are one or more processing layers, called hidden layers. The final processing layer is called the output layer. All the links between each node have an interconnecting weight. When a value is passed from the input layer, the values are multiplied by the interconnecting weight and summed up to derive the net output (y_i) to the unit.

$$y_i = \sum_i W_{ij} x_i \tag{3-1}$$

where W_{ij} is the interconnecting weight from unit i to unit j and x_i is the input at the input layer. The net output is derived net output y_i is then transformed by the activation function $f(y_{i)}$ to produce an output for unit j.

$$y_i = Activation\ Function \sum_{J=1}^{n} W_{ij} x_i \tag{3-2}$$

The inputs are computed by a mathematical function, which determines the activation of the neuron. Another function (which may be the identity) computes the output of the artificial neuron. ANNs combine artificial neurons in order to process information. Figure 3-3 describes the role of Activation function in a back-propagation network.

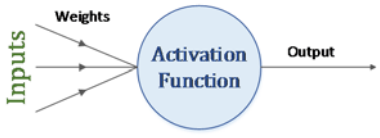

Figure 3-3. Role of an activation function in a Back propagation network (Gershenson 2003)

An activation function commonly used in back propagation algorithm is the sigmoid (Sigma S_{ij}) function.

$$S_{ij} = \sum_{j=1}^{n} w_{ij} \ a_{ij} \quad where \ a_{ij} = \frac{1}{\left(1 + e^{-\sum_{j=1}^{n} x_i w_{ij}}\right)^n} \tag{3-3}$$

$$y_i = \frac{1}{\left(1 + e^{-\sum_{j=1}^{n} x_i w_{ij}}\right)^n} \tag{3-4}$$

Some of other most commonly used activation functions are presented in Table 3-1. The values of the interconnecting weights are adjusted by the network during the training process to achieve the desired input/output relation of the network with the minimal overall training error in multi-layer networks. The back propagation method is one of algorithm is one of the most commonly used methods. This method uses a supervised iterative process to minimize an error function for the network output and a set of target outputs.

The difference between the actual output of the network and the desired output is used to adjust the weights so that in the next stage that the same data is given to the network

Table 3-1. Some commonly used activation functions

Function	**Formula**
Identity function	$g(x) = \mathrm{x}$
Binary step function	$g(x) = \begin{cases} 1 \ if \ (X \geq \theta) \\ 0 \ if \ (X \geq \theta) \end{cases}$
Bipolar sigmoid function	$g(x) = \frac{1}{1 + e^{-x}}$

the actual output will get closer to the desired one. The goal of training stage is to minimize the global difference called error of the network, between the desired output and the actual output of the network:

$$E = \frac{1}{p}\sum_{p=1}^{p} E_p \tag{3-5}$$

where p is total number of training patterns and E_p is error for training pattern p given by:

$$E_p = \frac{1}{2}\sum_{k=0}^{N}(y_k - t_k)^2 \tag{3-6}$$

In Eq. (3-6**)** N is the total number of output neurons; y_k is network output at the $k$thoutput neuron and t_k is target output at the kth output neuron.

As this error is computed in each stage, it is then fed backward through the network towards the input layer with the weights connecting the units being changed in relation to the magnitude of the error. This process is repeated until the error rate is minimised or reaches an acceptable level, or until a specified number of iterations has been accomplished.

A geometric interpretation (adopted and modified from Lippmann (1987)) which is shown in Figure 3-4 can help explicate the role of hidden units (with the threshold activation function)(Jain, Mao et al. 1996).

Each unit in the first hidden layer forms a hyper-plane in the pattern space; boundaries between pattern classes can be approximated by hyper-planes. A unit in the second hidden layer forms a hyper-region from the outputs of the first-layer units; a decision region is obtained by performing an AND operation on the hyper-planes. The output-layer units combine the decision regions made by the units in the second hidden layer by performing logical OR operations.

Remember that this scenario is depicted only to explain the role of hidden units. Their actual behaviour, after the network is trained, could differ. A two-layer network can form more complex decision boundaries than those shown in Figure 3-2.

Although multilayer feed-forward networks using back-propagation have been widely employed for classification and function approximation, many design parameters still must be determined by trial and error.

If more layers are added, same error calculations should be done, however, calculating the error depends on the inputs and weights of the first layer. For practical reasons, ANNs implementing the back propagation algorithm do not have too many layers, since the time for training the networks grows exponentially. In addition, there are refinements to the back-propagation algorithm that allow a faster learning.

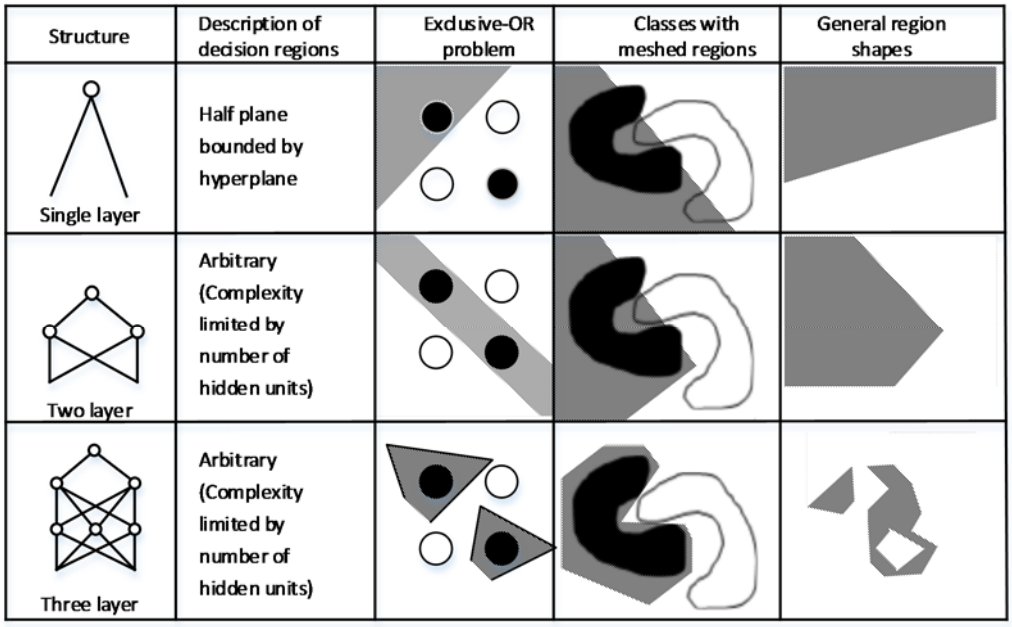

Figure 3-4. A geometric interpretation of the role of the hidden unit in a two-dimensional input space (Jain, Mao et al. 1996)

3.2 Support Vector Machines (SVM)

Support vector machines, like artificial neural networks, are a kind of data-mining approach. SVM has been successfully applied to a number of applications ranging from particle identification, facial identification and text categorization to engine knock detection, bioinformatics and database marketing. The classification problem is used to investigate the basic concepts behind SVM and to examine their strengths and weaknesses from a data-mining perspective (Campbell 2000). Regression algorithms of support vector machines are achieved by some modification to the classification algorithms of SVM.

3.2.1 Classification problems

In a classification problem, it is aimed to carry out the optimum classification of the mixed data. To simplify the explanation, let us consider a binary classification problem and assume that the two sets of data are linearly separable, where a plane exists to classify the data into two sets consequently. Figure 3-5 shows two planes of many infinite separating planes. Intuitively one prefers the solid plane since small perturbations of any point would not introduce misclassification errors. Without any additional information, the solid plane is more likely to generalize better on future data. Geometrically we can characterize the solid plane as being “furthest” from both classes.

The main point in classification problem, is to identify the optimum discriminant plane and one class will be allocated to one group the value of which is +1 and the other group would be assigned to the other side of the plane the value of which are -1.

Assignments of the value to each class are done by the classification function. In the example of binary classification, the range of the function is limited to binary values of +1 and -1. Under this condition, the classification function can be considered as:

$$f(x_i) = y_i = \pm 1 \qquad (3\text{-}7)$$

where x_i are input data points and y_i are output data. Considering x_i as input data, if the $f(x_i)$value is -1 it belongs to one class and if its value is +1 it belongs to another class and the classification task will be done respectively.

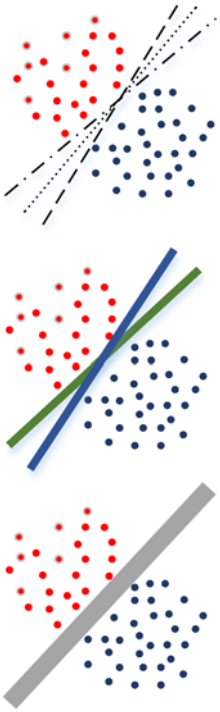

Figure 3-5. Two possible linear discriminant planes (Bennett and Campbell 2000)

The mathematical definition of the above-mentioned function is the Sign function. So the Eq. (3-7) is modified as below:

$$f(x_i) = Sign(w\vec{x} - b) \qquad (3\text{-}8)$$

where w, is the weight vector and, x_i, b denotes the distance of each data point from the discriminant plane. To find the plane furthest from both sets, we can simply

maximize the distance or margin between the support planes for each class. The distance or margin between these supporting planes can be illustrated as:

$$\gamma = \frac{|-1-1|}{|w|^2} \tag{3-9}$$

Thus maximizing the margin is equivalent to minimizing $\frac{|w|^2}{2}$ in the following quadratic optimization program:

$$\begin{cases} minimize\ g(w) = \dfrac{|w|^2}{2} \\ subject\ to\ y_i\ (w_i x_i + b) \geq 1 \end{cases} \tag{3-10}$$

Now, the classification problem can be written as a Lagrange function as below:

$$L = \frac{1}{2}(\overrightarrow{w}.\overrightarrow{w}) - \sum_{i=1}^{m} \alpha_i\ (y_i(\overrightarrow{w}.\vec{x} + b) - 1)\ ;\ \alpha_i \geq 0 \tag{3-11}$$

where L, is the Lagrangian function and α_i is the Lagrangian multiplier. By taking the derivatives with respect to b and w and resubstituing in the primal function, the Wolfe dual lagrangian will be acquired as below (Campbell 2000):

$$\begin{aligned} w(\alpha) &= \sum_{i=1}^{m} \alpha_i - \frac{1}{2}\sum_{i,j=1}^{m} \alpha_i \alpha_j y_i y_i (\vec{x}_i.\vec{x}_j) \\ subjectto: \alpha_i \geq 0 &\sum_{i=1}^{m} \alpha_i y_i \end{aligned} \tag{3-12}$$

w is calculated by Eq. (3-13) and b is calculated by the support vectors for which the $\alpha_i > 0$.

$$w = \sum_{i=1}^{m} y_i \alpha_i x_i \tag{3-13}$$

Ideally, we would like no points to be misclassified and no points to fall in the margin. However, we must relax the constraints that insure that each point is on the appropriate side of its supporting plane. Any point falling on the wrong side of its supporting plane is considered as an error. We want to simultaneously maximize the

margin and minimize the error. This can also be considering a nonnegative slack or error variable is added to each constraint and then added as a weighted penalty term in the objective as follows:

$$\begin{cases} Minimize\ \mathrm{w}(\alpha) \\ \text{subject to: } \sum \alpha_i y_i = 0,\ \ 0 \le \alpha_i < C \end{cases} \tag{3-14}$$

In many cases the linear discriminants are not appropriate for the data set, resulting in high training set errors, SVM methods will not perform well. In those cases, one has to examine the SVM approaches that have been generalized to construct highly nonlinear classification functions.

Considering the classification problems as Figure 3-6, simple linear discriminant functions will not work well and result in high training set errors. In such cases quadratic functions like the circle pictured is needed. A classic method for solving such problems is simply add additional attributes to the data that are nonlinear functions of the original data. Existing linear classification algorithms can be then applied to the expanded dataset in feature space producing nonlinear functions in the original input space.

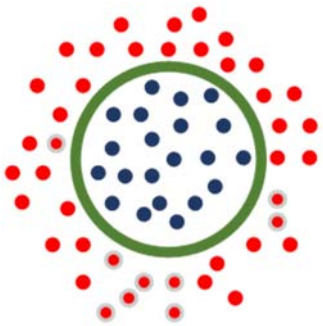

Figure 3-6. Example of non-separable cases by simple linear discriminant functions (Campbell 2000)

To get a better representation of the data, we can map the data points into an alternative higher dimensional space, called feature space by using a kernel function as below.

$$K: \vec{x}_{ij}: \vec{x}_j \rightarrow \phi(x_i).\phi(x_j) \tag{3-15}$$

In Eq. (3-15), K is the Kernel function and $\phi(x_i)$and $\phi(x_j)$are functions of x_i and x_j variables. With a suitable choice of kernel according to Eq. (3-16) the non-separable data in the original input space can become separable in the feature space and the examples like Figure 3-6 will be solvable.

$$k(x_i, x_j) = \phi(x_i).\phi(x_j) \tag{3-16}$$

In Table 3-2 some of the more popular kernels are given.

Table 3-2. Examples of some kernel functions

$\boldsymbol{k(u,v)}$	$\boldsymbol{\theta(u)}$
$k(x_i, x_j) = e^{-(x_i - x_j)^2/2\sigma^2}$	RBF
$k(x_i, x_j) = (x_i.x_j + 1)^d$	$Polynominal$
$k(x_i, x_j) = \tanh(\beta x_i.x_j + b)$	$FFNNC$

Finally, the binary classification function in the featured space can be written as below:

$$\begin{aligned} &Max: w(\alpha) = \sum_{i=1}^{m} \alpha_i - \frac{1}{2}\sum_{i,j=1}^{m} \alpha_i \alpha_j y_i\, y_j k(x_i, x_j) \\ &subject\ to: \alpha_i \geq 0 \sum_{i=1}^{m} \alpha_i y_i = 0 \end{aligned} \tag{3-17}$$

where the objective function for variable z is:

$$f(\vec{z}) = \sum_{i=1}^{m} y_i \alpha_i k(\vec{z}, x_i) + b \tag{3-18}$$

and variable b is calculated by Eq. (3-19) formulae:

$$b = -\frac{1}{2}\left[\max_{\{i|y_i=-1\}}\left(\sum_{j\in\{SV\}}^{m} y_i\alpha_j K(X_i, X_j)\right) + \min_{\{i|y_i=+1\}}\left(\sum_{j\in\{SV\}}^{m} y_i\alpha_j K(X_i, X_j)\right)\right] \qquad (3\text{-}19)$$

As the maximal margin hyper plane is being sought in the feature space, only the data points which lie closest to the hyperplane have $\alpha > 0$ and those points are support vectors. In that case other points will definitely have $\alpha = 0$ which means that the representation of the hypothesis is mainly given by those $\alpha > 0$ points which are not only "closest" to the hyper plane but the most "informative" parameters among the whole data points which are called "Support vectors".

Most datasets contain noise and the SVM may fit this noise leading to poor generalization. The effect of the noise can be reduced by applying a "soft margin and allowing for training errors" concepts in classification. Two main schemes are currently used to apply soft margins. In the first, for the learning task, the box constraint (C) is also considered:

$$0 < \alpha_i < C \qquad (3\text{-}20)$$

and in the second, small positive constant is added to the leading diagonal of the kernel matrix:

$$k(x_i, x_j) \rightarrow k(x_i, x_j) + \lambda \qquad (3\text{-}21)$$

C and λ control the trade-off between the training errors and the generalization ability and re chosen by means of validation test.

3.2.2 Support vector regression

The classification problem is used to investigate the basic concepts behind SVM and to examine their strengths and weaknesses from a data-mining perspective (Campbell 2000). Regression algorithms of support vector machines are achieved by some modification to the classification algorithms of SVM.

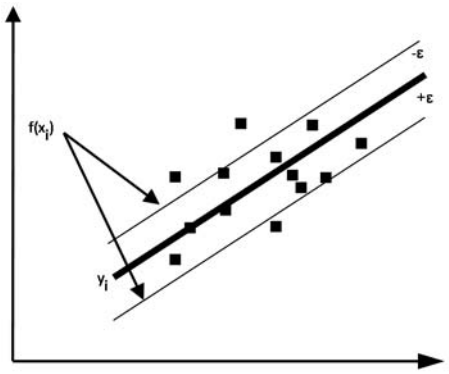

Figure 3-7. Scheme of the Support Vector Regression by standard deviation of ε

The idea of Support vector regression e-SVR and e-sensitive function was first introduced by Vapnik (1995). In support vector regression the objective is to find a function $f(x)$ which has at most e- deviation from the actually obtained targets $y_i$for all the training data $\{(x_1, y_1), .., (x_i, y_i)\}$ and at the same time is as flat as possible. In other words, errors are negligible as long as they are less than ε and any deviation larger than this is not accepted. Figure 3-7 depicts the idea of SVR graphically.

The regression function of $f(x)$ can be expressed as:

$$f(x) = (w, x) + b, w \in X, b \in \mathbb{R} \tag{3-22}$$

where w is a weight vector ($w \in R^n$), b is additive noise (b $\in R$) and (w, x) denote dot points in X. Flatness of the regression function $f(x)$ can be achieved by smaller values of w. The minimization problem can be written as a convex optimization problem (Singh, Pal et al. 2008):

$$\begin{cases} minimize \dfrac{1}{2}\|w\|^2 \\ subject\ to \begin{cases} y_i - (w, x_i) - b \le \varepsilon \\ (w, x_i) + b - y_i \le \varepsilon \end{cases} \end{cases} \tag{3-23}$$

On the other hand, the following restrict had been derived for the classification problem:

$$f(x) = sign(\vec{w}x + b) = y_i$$

$$\begin{aligned} &minimize\ \ g(\vec{w}) = \frac{1}{2}\|w\|^2 \\ &subject\ to\ y_i(\vec{w}.x_i + b) \geq 1; \forall_i \end{aligned} \tag{3-24}$$

and the $f(x_i)$ can be modelled as below:

$$f(x_i) = w.x_i + b \tag{3-25}$$

Finally, the optimization problem can be feasible if the error on any training data is less than ε. Sometimes, it is allowed to have some more induced errors. Hence slack variables ξ_i and ξ_i^* are introduced and the minimization formula Eq. (3-24**)** is written as follows (Vapnik 1995):

$$\begin{aligned} &minimize \frac{1}{2}\|w\|^2 + C\sum_{i=1}^{m}(\xi_i + \xi_i^*) \\ &subject\ \text{to} \begin{cases} y_i - (w_i, x_i) - b \leq \varepsilon + \xi_i \\ (w_i, x_i) + b - y_i \leq \varepsilon + \xi_i^* \\ \xi_i, \xi_i^* \geq 0 \end{cases} \end{aligned} \tag{3-26}$$

where the constant $C > 0$ determines the trade-off between the flatness of $f(x)$ and the tolerable amount larger than ε which is defined by the user. Under such condition, the sensitivity function is introduced as:

$$|\xi|_\varepsilon = \begin{cases} 0 if\ |\xi| \leq \varepsilon \\ |\xi| - \varepsilon \quad otherwise \end{cases} \tag{3-27}$$

Figure 3-8 illustrates the performance of slack variables. As clearly seen in Figure 3-8, only the points outside the shaded region contribute to the problem solving, as the deviations are penalized in a linear trend.

The standard dualization method utilizing Lagrange multipliers is used for regression problems. A Lagrange function from the objective and the corresponding constraints, by introducing a dual set of variables can be written as below:

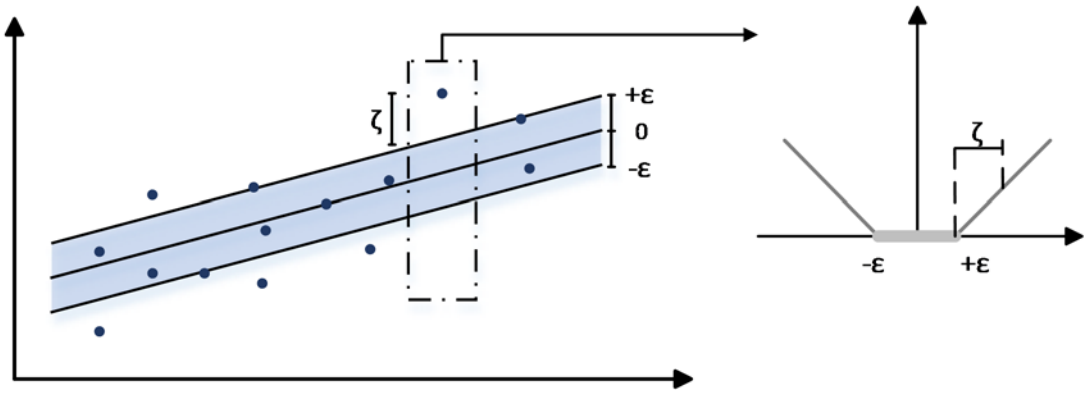

Figure 3-8. The soft margin loss setting for a linear SVM (Smola and Schölkopf 2004)

$$L = \frac{1}{2}\|w\|^2 + C\sum_{i=1}^{m}(\xi_i + \xi_i^*) - \sum_{i=1}^{m}(\eta_i\xi_i + \eta_i^*\,\xi_i^*)$$
$$-\sum_{i=1}^{m}\alpha_i(\varepsilon_i + \xi_i \;\; - y_i + (w, x_i) + b)$$
$$-\sum_{i=1}^{m}\alpha_i^*(\varepsilon_i + \xi_i^* - y_i + (w, x_i) + b) \qquad (3\text{-}28)$$
$$subject\ \ to: \begin{cases}\alpha_i, \eta_i \geq 0\\ \alpha_i^*, \eta_i^* \geq 0\end{cases}$$

where L is the Lagrange function and α_i , α_i^*, $\eta_i$and η_i^* are Lagrange multipliers. To find the optimum amounts of b , w and ξ_i^* by taking the derivatives of L with respect to these parameters and resubstituing in the primal function, the optimization function will be written as below:

$$\frac{\partial L}{\partial b} = 0 \Rightarrow \sum_{i=1}^{m}(\alpha_i^* - \alpha_i\ ) = 0 \qquad (3\text{-}29)$$

$$\frac{\partial L}{\partial w} = 0 \Rightarrow w - \sum_{i=1}^{m}(\alpha_i^* - \alpha_i\ )x_i = 0 \qquad (3\text{-}30)$$

$$\frac{\partial L}{\partial \xi_i^*} = 0 \Rightarrow C - \alpha_i^* - \eta_i^* = 0 \qquad (3\text{-}31)$$

Substituting Eq. (3-29) and Eq. (3-30) into Eq. (3-31) yields the final maximization problem.

$$maximize \begin{cases} -\frac{1}{2}\sum_{i=1}^{m}(\alpha_i - \alpha_i^*)(\alpha_j - \alpha_j^*)(x_i, x_j) \\ -\varepsilon\sum_{i=1}^{m}(\alpha_i + \alpha_i^*) + \sum_{i=1}^{m} y_i(\alpha_i - \alpha_i^*) \end{cases} \quad (3\text{-}32)$$

$$subject\ to \sum_{i=1}^{m}(\alpha_i - \alpha_i^*) = 0\ and\ \alpha_i, \alpha_i^* \in [0, C]$$

and the prediction function can be derived as below:

$$\eta_i^* = C - \alpha_i^* \quad (3\text{-}33)$$

$$w = \sum_{i=1}^{m}(\alpha_i - \alpha_i^*)x_i \Rightarrow \quad (3\text{-}34)$$

$$f(x) = \sum_{i=1}^{m}(\alpha_i - \alpha_i^*)(x_i, x) + b \quad (3\text{-}35)$$

As seen in Eq. (3-35), w is not present in the formulae. In other words, it is quite independent of parameter w and in final $f(x)$, calculation of w is not necessary consequently.

As mentioned earlier, nonlinear Support Vector Regressions can be used in complex and nonlinear problems by introducing kernel functions. Solving nonlinear problems can be achieved by mapping the data into a higher-dimensional feature space with the help of kernel functions as below:

$$K(x, x') = (\Phi(x), \Phi(x')) \quad (3\text{-}36)$$

The problem of support vector regression in the feature space can be written by substituting x_i, x_j in Eq. (3-32) by $K(x_i, x_j)$:

$$Maximize\begin{cases}-\frac{1}{2}\sum_{i,j=1}^{m}(\alpha_i - \alpha_i^*)(\alpha_j - \alpha_j^*)K(x_i, x_j)\\ -\varepsilon\sum_{i=1}^{m}(\alpha_i + \alpha_i^*) + \sum_{j=1}^{m} y_i(\alpha_i - \alpha_i^*)\end{cases} \quad (3\text{-}37)$$

$$subjectto \sum_{i=1}^{m}(\alpha_i - \alpha_i^*) = 0 and \alpha_i, \alpha_i^* \in [0, C]$$

and the final Kernel included $f(x)$ is written according Eq. (3-38**)**.

$$f(x) = \sum_{i=1}^{m}(\alpha_i - \alpha_i^*)K(x_i, x) + b \quad (3\text{-}38)$$

3.3 Application of SVM and ANN in prediction of scour problem around single pile

To have a practical introduction about ANN and SVM in scouring problems, ANN and SVM models are developed to solve a regression-type problem about calculation of wave-induced scour depth around single piles cases.

As noted in Chapter 1, Sumer and Fredsøe (2002) gave an empirical formulae (see Eq. (1-6)) to estimate scour depth around a single pile due to waves based on the laboratory data of Figure 1-6.

Regarding the introduction about scouring phenomena given in Chapter 1, to solve the scouring problem around single pile, N_{RE}, N_s, θ, KC are the controlling parameters of scouring around single piles and they are selected as the inputs of ANN and SVM (For more details about the parameters, refer to Sections 1.6 and 4.1) and the non-dimensional amounts of scour, S/D parameter is calculated as the outputs of the models.

For training and testing phase of both models, laboratory data of Dey, Sumer et al. (2006) and Sumer, Fredsøe et al. (1992) are used. The whole data is divided into two subsets for training and testing phases. The total number of single pile data is 88 cases. 80% of the data (71 data points) is used for training phase and 20% (17 data points) is used in validation.

A Multi-Layer Perceptron (MLP) with Back Propagation (BP) learning algorithm is used to train the network structure of the single pile scouring prediction. The number of neurons for input, hidden and output layers is determined as 4, 5 and 1 based on error minimizing process.

The performances of models are assessed quantitatively using the following statistical parameters: coefficient of correlation (CC), root mean square error ($RMSE$) and mean absolute error (MAE) which are defined as the following relationships:

$$CC = \frac{\sum(T_i - \overline{T_i})(O_i - \overline{O_i})}{\sqrt{\sum(T_i - \overline{T_i})^2 \sum(O_i - \overline{O_i})^2}} \quad (3\text{-}39)$$

$$RMSE = \sqrt{\frac{\sum_{i=1}^{N}(O_i - T_i)^2}{N}} \quad (3\text{-}40)$$

$$MAE = \frac{1}{N}\sum_{i=1}^{N}|O_i - T_i| \quad (3\text{-}41)$$

In the above formulae, T_i and O_i represent target and network outputs for the i th output, respectively; $\overline{T_i}$ and $\overline{O_i}$ are the average of target and network outputs and N is the total number of data points. A higher value of CC and smaller values of $RMSE$ and MAE mean a better model performance.

For development of the SVM model, as previously mentioned in the introduction of SVM, the regularization parameter C and the size of error in sensitive zone, control the

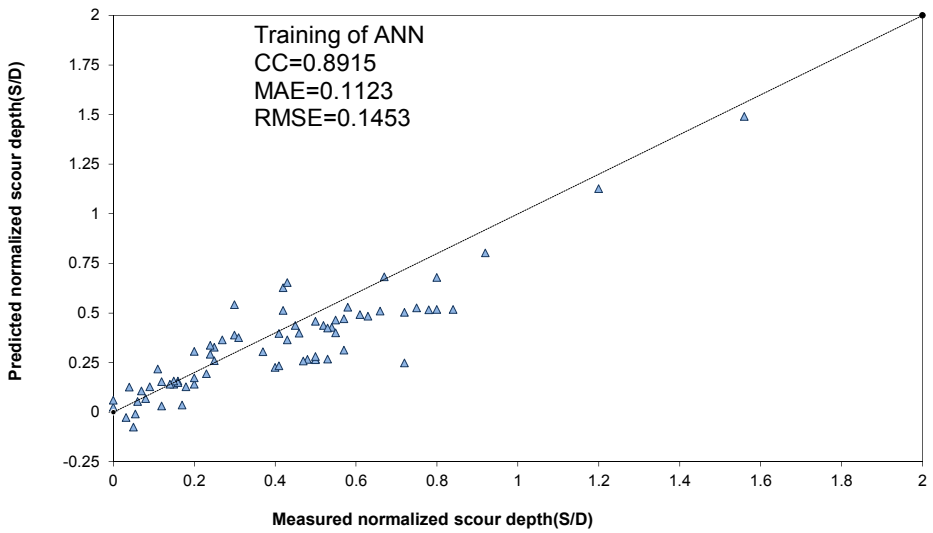

Figure 3-9. Comparison between the observed and predicted S/D by ANN for the training phase

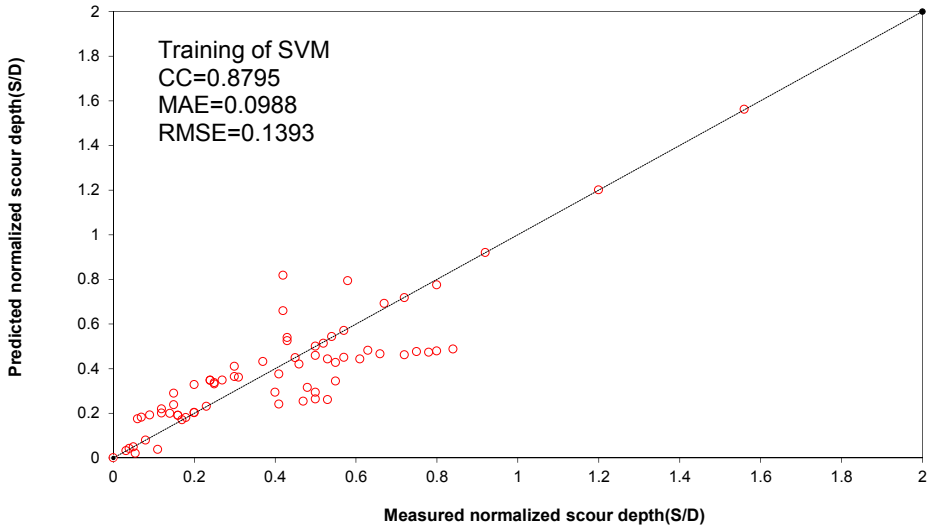

Figure 3-10. Comparison between the observed and predicted S/D by SVM for the training phase

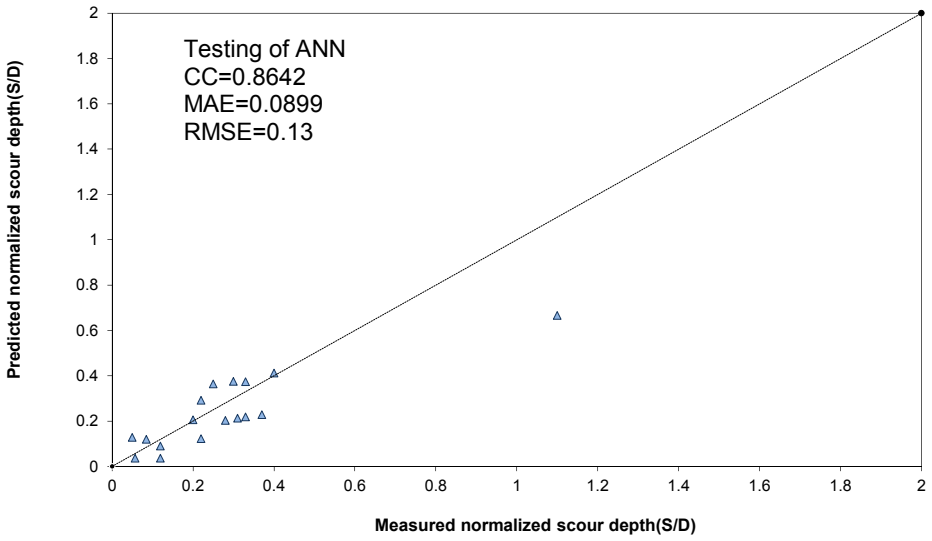

Figure 3-11. Comparison between the observed and predicted S/D by ANN for the testing phase

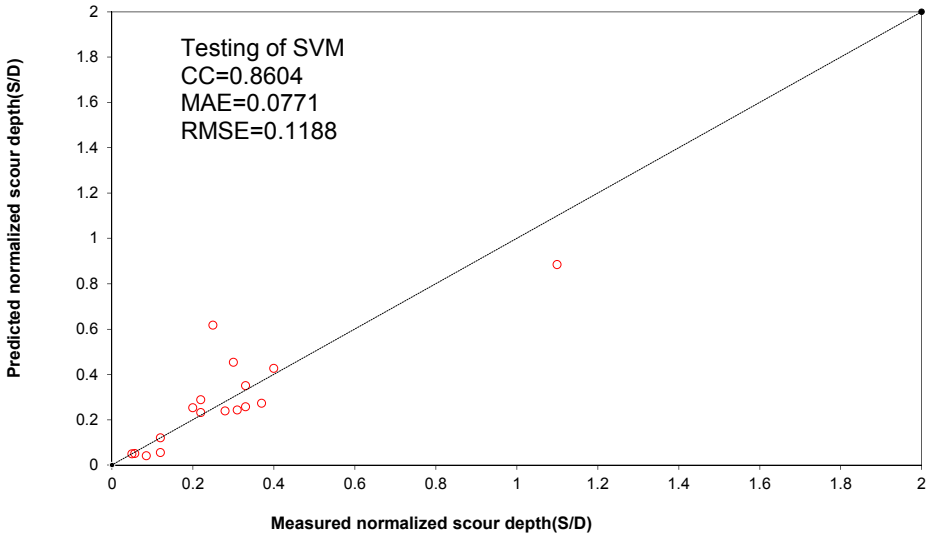

Figure 3-12. Comparison between the observed and predicted S/D by SVM for the testing phase

complexity of prediction. A value of $C = 12$ and $\varepsilon = 0.0010$ were selected based on the process of error minimizing.

In Figure 3-9, Figure 3-10, Figure 3-11and Figure 3-12 the predicted amounts of S/D by ANN and SVM are plotted against its observed amounts for the training and testing phases respectively. Error measures were also shown on the figures.

ANN model was trained by the $CC = 0.8915$ and $RMSE = 0.1435$. The Correlation Coefficient (CC) of the results predicted by SVM is $CC = 0.8795$ which is about 1% less than the correlation coefficient of the results of ANN, however the other error measure $RMSE$ of the predictions by SVM model is also about 1% less than the $RMSE$ of ANN model. Comparison of both error measures of CC and $RMSE$ indicate same predictions in terms of accuracy in the training phase for ANN and SVM models.

The correlation coefficient of the estimated amounts for S/D of the testing phase of both models are almost equal which are about 0.86 and for the assessment of the performance of the models, amounts of $RMSE$ are compared consequently. The $RMSE$ of the calculated amounts of wave-induced scour over diameter ratio S/D around single piles by SVM is 2% less than those of ANN and it can be concluded that SVM calculated amount of scour with better precision.

Same research criteria is followed in Chapter 4 to assess the applicability of SVM and ANN approaches in predictions of scour around pile groups due to wave.

3.4 Summary

The introduction about two data miming models of Artificial Neural Networks (ANN) and Support Vector Machines (SVM) were given in this chapter. Fundamentals, the governing rules and mathematical modelling of both soft computing models were also presented.

In case of the application of a typical back propagation training algorithm which is also used in this research, number of hidden neurons, number of iterations, acceptable error and the activation functions were expressed as factors to be determined for development of ANN. In case of modelling by Support Vector Machines (SVM), the amount of the trade-off of the plane, the tolerable error and the kernel functions are governing factors that should be considered for modelling by SVM.

The application of the introduced data mining models of ANN and SVM in scouring problems were also discussed in this section. ANN and SVM models were developed to solve a regression-type problem about calculation of wave-induced scour depth around single piles. The accuracy of the predicted amounts of scour by both models for training and testing phases were compared by statistical measures. Comparison of the results indicated that both models were trained with similar statistical error measures. However, the outputs of SVM in the testing phase can provide better results in terms of accuracy. Hence, it is concluded that SVM is a more reliable data-mining model than ANN.

4 PREDICTION OF SCOUR USING ANN AND SVM

As previously noted in Chapter 1 of this dissertation, regarding the complexity of the modelling of wave-induced scouring phenomena around pile groups as well as the lack of reliable alternatives for conventional models and empirical formulas of scouring with dissatisfying results, finding reliable alternatives for currently available methods seems necessary. On the other hand, following the reliable results of soft computing models in hydraulic and marine problems (refer to Chapter 3), applicability of Support Vector Machines and Artificial Neural Networks for wave-induced scour predictions around pile groups are studied in this chapter.

In this section, two soft computing models of SVM and ANN are developed and according to what is typically done for such methods, the majority of the data is used for training of the networks and then the results are validated through testing phase. In addition, experimental data including wave, bed and pile conditions presented in chapter 2, are used as inputs of SVM and ANN and the results of the models for scour depth will be compared to those of the experiments. Finally, the performance of the

models are assessed using error measures and will be discussed in the discussion section.

4.1 Dimensional and no dimensional parameters controlling scour depth

As discussed in Chapter 1 and Chapter 3, wave-induced scour around a single pile depends on several groups of variables such as the characteristics of the wave and the sediment properties and geometry of the pile. Thus, the following functional relationship can be used to describe the equilibrium scour depth for a single pile (Sumer et al. 1992b):

$$S = f(T, d_{50}, U_m, U_{fm}, D, s, \upsilon) \quad (4\text{-}1)$$

Where S is the equilibrium scour depth, T is the wave period, d_{50} is the medium sediment diameter, U_m is the maximum undisturbed orbital velocity at the sea bottom just above the wave boundary, U_{fm} is the shear velocity at the undisturbed bed given by $U_{fm} = (0.5f)^{0.5}U_m$ in which f is the wave friction factor, D is the pile diameter, s is the specific gravity of sediments and υ is the kinematics viscosity. Parameter f can be calculated by Eq. (4-2) (Dey, Sumer et al. 2006).

$$f = 0.04\left(\frac{a}{\varepsilon}\right)^{-0.25} \quad for \;\; a/\varepsilon > 50$$
$$f = 0.4\left(\frac{a}{\varepsilon}\right)^{-0.75} \quad for \;\; a/\varepsilon \leq 50 \quad (4\text{-}2)$$

where a is the amplitude of wave, ε is the equivalent roughness height of Nikuradse, assumed as $2d_{50}$.

Using the dimensional analysis, the above relationship can be presented in non-dimensional form as follows (Sumer, Fredsøe et al. 1992):

$$\frac{S}{D} = f(N_{RE}, N_s, \theta, KC) \quad (4\text{-}3)$$

where N_{RE} is the pile Reynolds number, N_s is the sediment number, θ is the Shield's parameter and KC is the Keulegan– Carpenter number defined as follows:

$$N_{RE} = \frac{U_m D}{\nu} \tag{4-4}$$

$$N_s = \frac{U_m}{\sqrt{g(s-1)d_{50}}} \tag{4-5}$$

$$\theta = \frac{U_{fm}^2 D}{(s-1)g d_{50}} \tag{4-6}$$

$$KC = \frac{U_m T}{D} \tag{4-7}$$

The non-dimensional parameters should include the effect of various physical processes occurring during the scour, i.e. flow–seabed interaction, flow–structure interaction and sediment transport. In Eq. (4-3), the Reynolds number and Keulegan–Carpenter number describe the flow pattern around piles, whereas the Shield's parameter and sediment number represent the mutual effects of flow on the seabed. Note that regarding the results and findings of the large-scale experimental studies addressed in Chapter 2 of this dissertation, in addition to the typically considered parameter of KC number defining a configuration parameter based on the position of the piles relative to the wave direction is also necessary. Hence, for a group of vertical piles, in addition to the above parameters, spacing between the piles (G), number of piles normal to the flow (n) and number of piles parallel to the flow (m) are defined to be used in the estimation of scour depth around pile groups. Considering these new parameters, the maximum scour depth S normalized by pile diameter D can be best expressed as follows (see also Ghazanfari-Hashemi, Etemad-Shahidi et al. (2011)) :

$$\frac{S}{D} = f(N_{RE}, N_s, \theta, KC, \frac{G}{D}, \frac{m}{n}) \tag{4-8}$$

Furthermore, in the large-scale experimental studies of this dissertation, the number of piles in the arrangement was also notified as an important parameter in modelling of scouring of pile groups. In this study, in addition to m/n, the $m \times n$ parameter is also used to model the number of piles as an additional arrangement parameter of the pile groups and the fundamental formulae of modelling can be written as below:

$$\frac{S}{D} = f(N_{RE}, N_s, \theta, KC, \frac{G}{D}, \frac{m}{n}, m \times n) \quad (4\text{-}9)$$

By using the $m \times n$ parameter in addition to m/n, different arrangements with similar amounts of m/n ratios can be distinguished.

4.2 Data set used

To develop the fundamental model, three groups of data sets including prototype, small-scale and large scale data, i.e. datasets collected by Bayram and Larson (2000) in the field and by Sumer and Fredsøe (1998) in the laboratory in addition to the large-scale experimental data presented in this study, were used for modelling.

4.2.1 Small-scale experiments of Sumer and Fredsoe

Small-scale experiments of Sumer and Fredsøe (1998) were conducted in a wave flume of 4 m in width, 1 m in depth and 28 m in length. The medium sediment diameter d_{50} was 0.2 mm and the water depth was maintained at 40 cm. The development of scour was monitored using an underwater mini-video camera and undisturbed-flow velocity measurements were done at a distance of 5 cm away from the bed. From this study, 44

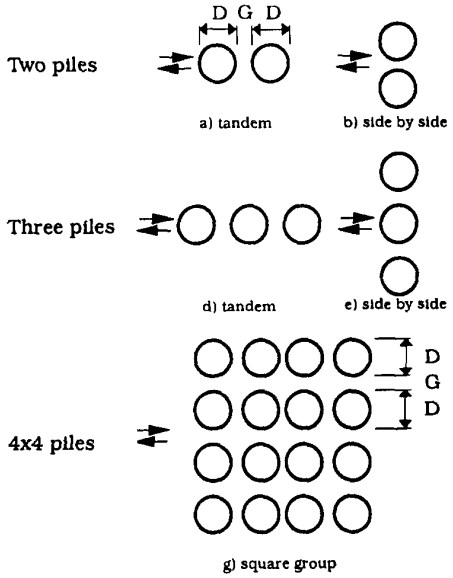

Figure 4-1. Configurations of the used pile groups in the laboratory (Sumer and Fredsøe 1998)

datasets of side-by-side, tandem and 4×4 arrangements were selected. These arrangements of pile groups are shown in Figure 4-1.

Table 4-1 shows the selected data of Sumer and Fredsøe (1998) applied in this study. The ranges of different parameters also are given in Table 4-2. As shown in Table 4-2, the configurations selected from this study covers a wide range of G/D from 0 to 2, KC numbers ranging from 3 to 37, and arrangement parameters m/n and $m \times n$ which vary from 0.33 to 3.0 and 2 to 16 respectively.

Table 4-1. Selected data of Sumer and Fredsøe (1998) applied in this study

Arrangement	$T(s)$	$d_{50}(m)$	$U_m(m/s)$	$U_{fm}(m/s)$	m	n	$G(m)$	$D(m)$	$S(m)$
tandem2pile	4.5	0.0002	0.26	0.018	1	2	0.0009	0.09	0.0252
tandem2pile	4.5	0.0002	0.26	0.018	1	2	0.0009	0.09	0.0252
tandem2pile	4.5	0.0002	0.26	0.018	1	2	0.0234	0.09	0.0252
tandem2pile	4.5	0.0002	0.26	0.018	1	2	0.036	0.09	0.0153
tandem2pile	4.5	0.0002	0.26	0.018	1	2	0.0468	0.09	0.0153
tandem2pile	4.5	0.0002	0.26	0.018	1	2	0.0675	0.09	0.0198
tandem2pile	4.5	0.0002	0.26	0.018	1	2	0.0882	0.09	0.0252
sidebyside2pile	4.5	0.0002	0.26	0.018	2	1	0	0.09	0.0297
sidebyside2pile	4.5	0.0002	0.26	0.018	2	1	0.0009	0.09	0.0396
sidebyside2pile	4.5	0.0002	0.26	0.018	2	1	0.0126	0.09	0.0648
sidebyside2pile	4.5	0.0002	0.26	0.018	2	1	0.0252	0.09	0.0702
sidebyside2pile	4.5	0.0002	0.26	0.018	2	1	0.0351	0.09	0.0747
sidebyside2pile	4.5	0.0002	0.26	0.018	2	1	0.0504	0.09	0.0702
sidebyside2pile	4.5	0.0002	0.26	0.018	2	1	0.09	0.09	0.0396
sidebyside2pile	4.5	0.0002	0.26	0.018	2	1	0.18	0.09	0.0252
tandem3pile	4.5	0.0002	0.26	0.018	1	3	0.0009	0.09	0.0198
tandem3pile	4.5	0.0002	0.26	0.018	1	3	0.018	0.09	0.0153
tandem3pile	4.5	0.0002	0.26	0.018	1	3	0.0225	0.09	0.0153
tandem3pile	4.5	0.0002	0.26	0.018	1	3	0.027	0.09	0.0153
tandem3pile	4.5	0.0002	0.26	0.018	1	3	0.045	0.09	0.0252
tandem3pile	4.5	0.0002	0.26	0.018	1	3	0.09	0.09	0.0252
tandem3pile	4.5	0.0002	0.26	0.018	1	3	0.18	0.09	0.0252
sidebyside3pile	4.5	0.0002	0.26	0.018	3	1	0	0.09	0.0549
sidebyside3pile	4.5	0.0002	0.26	0.018	3	1	0.0018	0.09	0.0747
sidebyside3pile	4.5	0.0002	0.26	0.018	3	1	0.009	0.09	0.0801
sidebyside3pile	4.5	0.0002	0.26	0.018	3	1	0.018	0.09	0.0954
sidebyside3pile	4.5	0.0002	0.26	0.018	3	1	0.0225	0.09	0.09
sidebyside3pile	4.5	0.0002	0.26	0.018	3	1	0.045	0.09	0.0747
sidebyside3pile	4.5	0.0002	0.26	0.018	3	1	0.09	0.09	0.045
sidebyside3pile	4.5	0.0002	0.26	0.018	3	1	0.18	0.09	0.0252

Table 4-1. Selected data of Sumer and Fredsøe (1998) applied in this study

Arrangement	$T(s)$	$d_{50}(m)$	$U_m(m/s)$	$U_{fm}(m/s)$	m	n	$G(m)$	$D(m)$	$S(m)$
4pile	4.5	0.0002	0.26	0.018	4	4	0	0.032	0.02496
4pile	4.5	0.0002	0.26	0.018	4	4	0.0013	0.032	0.01856
4pile	4.5	0.0002	0.26	0.018	4	4	0.0048	0.032	0.02496
4pile	4.5	0.0002	0.26	0.018	4	4	0.0048	0.032	0.03008
4pile	4.5	0.0002	0.26	0.018	4	4	0.0128	0.032	0.0624
4pile	4.5	0.0002	0.26	0.018	4	4	0.016	0.032	0.056
4pile	4.5	0.0002	0.26	0.018	4	4	0.032	0.032	0.01856
4pile	4.5	0.0002	0.26	0.018	4	4	0.064	0.032	0.02144
4pile	4	0.0002	0.11	0.008	4	4	0	0.032	0.02496
4pile	4	0.0002	0.11	0.008	4	4	0.0048	0.032	0.00352
4pile	4	0.0002	0.11	0.008	4	4	0.0128	0.032	0.0032
sidebyside2pile	1.8	0.0002	0.15	0.012	2	1	0.036	0.09	0.0099
sidebyside2pile	3	0.0002	0.19	0.014	2	1	0.036	0.09	0.0603
sidebyside2pile	4.5	0.0002	0.37	0.024	2	1	0.036	0.09	0.0846

Table 4-2. Ranges of the experimental data presented by Sumer and Fredsøe (1998)

Parameters	Range	Mean	Std. Dev.
θ	0.02-0.18	0.086	0.024
N_s	1.94-6.54	4.16	0.749
KC	3-37	17.12	9.695
N_{RE}	3000-30000	16659	6339
G/D	0-2	0.492	0.568
m/n	0.33-3	1.428	0.963
$m \times n$	2-16	5.93	5.99
S/D	0.1-1.95	0.559	0.406

4.2.2 Field data of Bayram and Larson

Bayram and Larson (2000) investigated the scour around a group of vertical piles with arrangement of 2×2 (Figure 4-2). They collected the field data of a pile group located in Ajigaura Beach in Japan. The measurements of that survey started from 1975 and ended in 1996. Each single pile had 0.6 m diameter and was installed 2.67 m apart from the other ones in a 2×2 arrangement. Weekly surveys were made of 9 groups of vertical pile which were located 30 m apart from each other from 80 stations with spacing of 3.0 m.

Table 4-3 shows the data of the field survey published by Bayram and Larson (2000). The ranges of governing parameters are also given in Table 4-4. It should be noted that the ranges of S/D are much wider than those of laboratory data of Sumer and Fredsøe (1998).

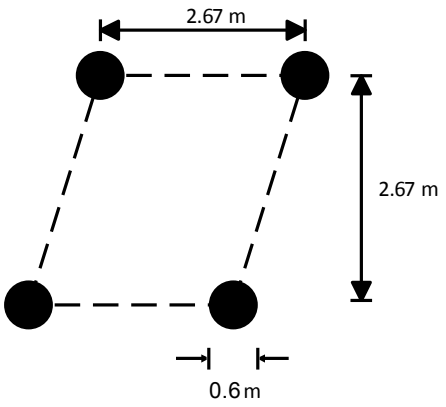

Figure 4-2. Configuration of the pile group in the field (Bayram and Larson 2000)

Table 4-3. Data of the filed survey published by (Bayram and Larson)

$T(s)$	$d_{50}(m)$	$U_m(m/s)$	$U_{fm}(m/s)$	m	n	$G(m)$	$D(m)$	$S(m)$
6.77	0.0002	0.76	0.07	2	2	2.67	0.6	1.18E+00
6.77	0.0002	0.86	0.08	2	2	2.67	0.6	1.00E+00
8.75	0.0002	1.54	0.12	2	2	2.67	0.6	1.90E+00
8.75	0.0002	0.91	0.08	2	2	2.67	0.6	2.10E+00
7.01	0.0002	0.91	0.08	2	2	2.67	0.6	1.11E+00
7.01	0.0002	0.93	0.08	2	2	2.67	0.6	9.60E-01
7.27	0.0002	0.78	0.07	2	2	2.67	0.6	6.48E-01
7.27	0.0002	0.85	0.07	2	2	2.67	0.6	7.08E-01
7.71	0.0002	0.75	0.07	2	2	2.67	0.6	9.60E-01
7.71	0.0002	0.76	0.07	2	2	2.67	0.6	8.82E-01
7.86	0.0002	1.09	0.09	2	2	2.67	0.6	6.72E-01
7.86	0.0002	1.24	0.1	2	2	2.67	0.6	7.32E-01
7.29	0.0002	1.18	0.1	2	2	2.67	0.6	1.15E+00
7.29	0.0002	1.22	0.1	2	2	2.67	0.6	1.10E+00
7.9	0.0002	1.23	0.1	2	2	2.67	0.6	7.68E-01
7.9	0.0002	1.48	0.12	2	2	2.67	0.6	1.00E+00
6.2	0.0002	0.97	0.08	2	2	2.67	0.6	4.20E-01
6.2	0.0002	1.14	0.1	2	2	2.67	0.6	6.72E-01
6	0.0002	1.13	0.1	2	2	2.67	0.6	1.25E+00
6	0.0002	1.17	0.1	2	2	2.67	0.6	1.19E+00
7.74	0.0002	0.92	0.08	2	2	2.67	0.6	9.00E-01
7.74	0.0002	0.98	0.08	2	2	2.67	0.6	7.50E-01
7.23	0.0002	0.69	0.06	2	2	2.67	0.6	1.23E+00
7.23	0.0002	0.74	0.07	2	2	2.67	0.6	1.15E+00
7.84	0.0002	1.1	0.09	2	2	2.67	0.6	1.22E+00
7.84	0.0002	1.18	0.1	2	2	2.67	0.6	1.16E+00
7.1	0.0002	1.28	0.11	2	2	2.67	0.6	9.00E-01
7.1	0.0002	1.36	0.11	2	2	2.67	0.6	1.40E+00
7.25	0.0002	1.25	0.1	2	2	2.67	0.6	1.35E+00
7.25	0.0002	1.27	0.1	2	2	2.67	0.6	1.00E+00
7.37	0.0002	1.06	0.09	2	2	2.67	0.6	1.26E+00
7.37	0.0002	1.14	0.09	2	2	2.67	0.6	1.42E+00

Table 4-3. Data of the filed survey published by (Bayram and Larson)

$T(s)$	$d_{50}(m)$	$U_m(m/s)$	$U_{fm}(m/s)$	m	n	$G(m)$	$D(m)$	$S(m)$
7	0.0002	0.91	0.08	2	2	2.67	0.6	1.26E+00
7	0.0002	1.01	0.09	2	2	2.67	0.6	1.42E+00
7.27	0.0002	0.68	0.06	2	2	2.67	0.6	8.58E-01
7.27	0.0002	0.83	0.07	2	2	2.67	0.6	9.00E-01
9.8	0.0002	0.57	0.05	2	2	2.67	0.6	9.00E-01
9.8	0.0002	0.62	0.05	2	2	2.67	0.6	7.98E-01
7.42	0.0002	0.76	0.07	2	2	2.67	0.6	1.10E+00
7.42	0.0002	0.85	0.07	2	2	2.67	0.6	1.05E+00
7	0.0002	1.17	0.1	2	2	2.67	0.6	1.30E+00
7	0.0002	1.27	0.1	2	2	2.67	0.6	1.23E+00
6.46	0.0002	0.71	0.06	2	2	2.67	0.6	1.00E+00
6.46	0.0002	0.79	0.07	2	2	2.67	0.6	7.32E-01
6.49	0.0002	1.23	0.1	2	2	2.67	0.6	1.27E+00
6.49	0.0002	1.47	0.12	2	2	2.67	0.6	1.13E+00
8.14	0.0002	1.06	0.09	2	2	2.67	0.6	1.00E+00
8.14	0.0002	1.22	0.1	2	2	2.67	0.6	1.14E+00
7.15	0.0002	0.95	0.08	2	2	2.67	0.6	6.48E-01
7.15	0.0002	1.06	0.09	2	2	2.67	0.6	6.48E-01
7.69	0.0002	1.29	0.1	2	2	2.67	0.6	1.46E+00
7.69	0.0002	1.34	0.11	2	2	2.67	0.6	1.45E+00
7.16	0.0002	1.73	0.13	2	2	2.67	0.6	1.25E+00
7.16	0.0002	1.87	0.14	2	2	2.67	0.6	1.51E+00
7.98	0.0002	1.23	0.1	2	2	2.67	0.6	1.48E+00
7.98	0.0002	1.37	0.11	2	2	2.67	0.6	1.05E+00
7.88	0.0002	0.65	0.06	2	2	2.67	0.6	1.00E+00
7.88	0.0002	0.81	0.07	2	2	2.67	0.6	9.48E-01

Table 4-4. Ranges of the field data presented by (Bayram and Larson)

Parameters	**Range**	**Mean**	**Std. Dev.**
θ	0.08–0.64	0.259	0.113
N_s	3.22–10.69	5.949	1.562
KC	7.6–22.5	13.136	3.754
N_{RE}	340 000–1100 000	64 9137	162 116
G/D	3.45	3.45	0
m/n	1	1	0
$m \times n$	4	4	0
S/D	0.7–3.5	1.801	0.511

4.2.3 Large-scale experimental data of this study

Experimental setup and results of the bed survey of this study were all expressed in detail in Chapter 2 of this dissertation and here just the summary of the data based on the required parameters for modelling are summarized in Table 4-5. The ranges of this group of data are also given in Table 4-6. As noted in the experimental setup, the ranges of G/D are the constant amount of 1 and KC numbers used in the large-scle experimental studies were $KC = 3.9$ and $KC = 5.9$. As it can be seen in Table 4-6, the amounts of S/D varies from 0.22 to 0.75 for wide range of arrangement parameters m/n and $m \times n$ with the range of 0.5 to 1 and 1 to 9 respectively.

Table 4-5. Data of the bed survey presented in this study

Arrangement	$T(s)$	$d_{50}(m)$	$U_m(\frac{m}{s})$	$U_{fm}(\frac{m}{s})$	m	n	$G(m)$	$D(m)$	$S(m)$
single pile	1.2	0.00025	0.32	0.025	1	1	0	0.1	0.025
single pile	1.5	0.00025	0.39	0.03	1	1	0	0.1	0.022
tandem2pile	1.2	0.00025	0.31	0.024	1	2	0.1	0.1	0.03
tandem2pile	1.5	0.00025	0.38	0.029	1	2	0.1	0.1	0.025
4pile	1.2	0.00025	0.31	0.024	2	2	0.1	0.1	0.04
4pile	1.5	0.00025	0.39	0.03	2	2	0.1	0.1	0.035
6pile	1.2	0.00025	0.32	0.025	2	3	0.1	0.1	0.055
6pile	1.5	0.00025	0.39	0.03	2	3	0.1	0.1	0.075
9pile	1.2	0.00025	0.32	0.025	3	3	0.1	0.1	0.07
9pile	1.5	0.00025	0.36	0.028	3	3	0.1	0.1	0.06
9pile	1.2	0.00025	0.33	0.025	3	3	0.1	0.1	0.05

Table 4-6. Ranges of the experimental data presented in this study

Parameters	**Range**	**Mean**	**Std. Dev.**
θ	0.014-0.022	0.017	0.004
N_s	5.43-6.9	6.105	0.592
KC	3.709-5.892	4.686	0.994
N_{RE}	30911-39282	34725	3368
G/D	1	1	0
m/n	0.5-1	0.849	0.216
$m \times n$	1-9	4.818	3.188
S/D	0.22-0.75	0.434	0.193

4.3 Development of SVM and ANN

The ANN and SVM models were developed using the previously discussed (in section 4.1) seven non- dimensional numbers as input parameters and the measured non-dimensional scour depths were used as outputs. The whole dataset (data of Sumer and Fredsøe (1998), Bayram and Larson (2000), and current study) consisting of 113 data points was divided into two parts randomly for training and testing purposes. About 40% of the test data were collected in the laboratory and the remaining were collected in the field. KC numbers varied from 3 to 37 and 8.3 to 37 in training and testing datasets G/D ranges were from 0 to 3.45 and 0.01 to 3.45 in training and testing sets, respectively. The arrangement parameter m/n varied from 0.33 to 3.0 in both training and testing sets. The number of 4×4 arrangements in training and testing were 90 and 2, 2×2 were 45 and 13, 2×1 were 10 and 1, 1×2 were 6 and 4, 3×1 were 7 and 1 , the number of 1×3 were 4 and 3, 2×3 were 1 and 1, 3×3 arrangements in training and testing were 2 and 1, respectively.

Same as what mentioned in Chapter 3, the performances of models are assessed quantitatively using the three statistical parameters: coefficient of correlation (CC), root mean square error ($RMSE$) and mean absolute error (MAE). A higher value of CC and smaller values of $RMSE$ and MAE mean a better model performance.

4.3.1 ANN model

In this study, a multi-layer perceptron neural network (MLP with a 7-1-1 architecture) with one hidden layer and back-propagation training algorithm was used. 7, is equal to the number of controlling parameters of scouring ($N_{RE}, N_s, \theta, KC, G/D, m/n, m \times n$ in Eq. (4-6**)** that are given to the network as inputs and 1, represents the number of parameters being estimated by the network as outputs and represents the normalized

scour depth (S/D)in the constructed artificial neural network of the present study. Referred to Figure 3-2, the scheme of the multi-layer perceptron of the maximum wave-induced scour estimation around pile groups is illustrated as Figure 4-3.

As also noted in Chapter 3, the optimized number of hidden neuron in a multi-layer perceptron neural network is determined by the process of error minimizing. For choosing the optimal number of hidden neurons, different numbers of hidden neurons in addition to the number of iterations, are tested and results are compared consequently. The optimum number of hidden neurons has the least errors.

To determine the best topology of the network for wave-induced scour estimation around pile groups, multi-layer perceptrons with various numbers of hidden neurons were constructed. Results of the networks with 1, 2, 3, 4, 5, 6, 7 and 8 hidden neurons representing 7-1-1, 7-2-1, 7-3-1, 7-4-1, 7-5-1, 7-6-1, 7-7-1, 7-8-1 topologies for varied numbers of iterations were reported in Table 4-7,

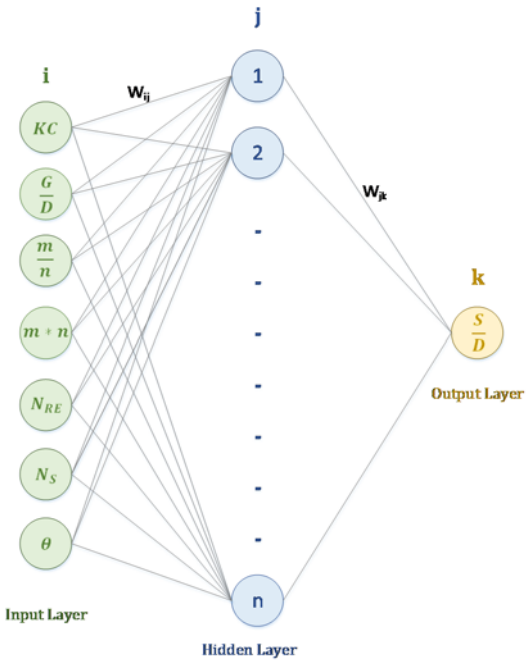

Figure 4-3. Scheme of the MLP network used in current study

Note that the "over fitting problem" might occur during neural network training. When this problem occurs the error on the training set is driven to a very small value, but when new data is presented to the network the error is large. The network has memorized the training examples, but it has not learned to generalize to new situations. One suggested way to avoid this condition, especially when the data set is small is to train multiple neural networks and average their outputs (Mathworks). This technique called n-fold cross validation. 10-fold-cross validation was used for this work and the results of the tables below are based on 10-fold cross validation testing.

Comparison of the results of Table 4-8 to Table 4-14 show that multi-layer perceptrons with 5, 6, 7 and 8 hidden layers are quite poor in terms of accuracy compared to those of 1, 2, 3 and 4. More reliable results based on both error measures (CC and $RMSE$) were highlighted for multi-layer perceptrons with 1, 2, 3 and 4 hidden layers.

Table 4-7. Results of the network with one hidden layer for different numbers of iteration

Number of iterations	$\boldsymbol{CC}$	$\boldsymbol{RMSE}$
10000	0.7791	0.4916
5000	0.7792	0.4914
3000	0.7798	0.4911
2000	0.7798	0.4907
1500	0.7802	0.4901
1000	0.7811	0.4891
500	0.7836	0.4864
400	0.7845	0.7854
300	0.7857	0.4839
200	0.7884	0.4807
100	0.4956	0.4718
50	0.8014	0.4648

For final selection of the neural network structure, results of the training and testing phase of the networks in addition to those of 10-fold cross validation testing displayed in table is considered. Table 4-15 summarizes the results of the networks with 7-1-1, 7-2-1, 7-3-1 and 7-4-1 topologies.

Table 4-8. Results of the network with 2 hidden layers for different numbers of iteration

Number of iterations	CC	$RMSE$
20000	0.7811	0.4963
10000	0.7898	0.4813
8000	0.7875	0.4836
5000	0.7816	0.4897
2000	0.7892	0.4739
1000	0.7797	0.4902
500	0.7799	0.4909
100	0.7997	0.4674

Table 4-9. Results of the network with 3 hidden layers for different numbers of iteration

Number of iterations	CC	$RMSE$
10000	0.6794	0.6421
8000	0.69	0.6187
5000	0.7138	0.5764
3000	0.7263	0.5575
1500	0.6742	0.6168
1000	0.7155	0.3928
800	0.7855	0.4813
500	0.7706	0.4969

Table 4-10. Results of the network with 4 hidden layers for different numbers of iteration

Number of iterations	CC	$RMSE$
10000	0.3857	1.32
5000	0.3845	1.3075
2000	0.6734	0.6513
1500	0.7709	0.5033
1000	0.7453	0.5439
800	0.7779	0.4927
700	0.7791	0.4908
650	0.7779	0.4923
600	0.7754	0.4954
500	0.7662	0.5059
400	0.7564	0.517

Table 4-11. Results of the network with 5 hidden layers for different numbers of iteration

Number of iterations	CC	$RMSE$
20000	0.4688	1.234
10000	0.4274	1.305
8000	0.4568	1.1877
5000	0.4533	1.1697
4000	0.4487	1.16
3000	0.4614	1.113
1000	0.5218	0.8893
500	0.5213	0.8865
100	0.7932	0.4777
50	0.7973	0.7732

Table 4-12. Results of the network with 6 hidden layers for different numbers of iteration

Number of iterations	CC	$RMSE$
50000	0.4009	1.79
11000	0.5783	0.9012
10000	0.5915	0.8526
9000	0.5796	0.8671
8000	0.5913	0.8286
7000	0.5983	0.8053
6500	0.5852	0.8172
6000	0.593	0.831
5000	0.564	0.8595
1000	0.455	1.0329
500	0.5702	0.7912
100	0.793	0.4917
50	0.7972	0.4734

Table 4-13. Results of the network with 7 hidden for different numbers of iteration

Number of iterations	CC	$RMSE$
20000	0.5029	1.149
10000	0.4176	1.2054
5000	0.3588	1.4679
1000	0.5276	0.8753
500	0.5471	0.8683
200	0.763	0.5188
100	0.7891	0.4842
50	0.7933	0.478

Table 4-14. Results of the network with 8 hidden for different numbers of iteration

Number of iterations	CC	$RMSE$
10000	0.3628	1.55
8000	0.3195	1.7412
5000	0.3648	1.2912
1000	0.5264	0.8954
500	0.5145	0.8874
100	0.7807	0.4947
50	0.7902	0.4813

Table 4-15. Results of the networks with different topologies

Number of hidden layers	**Number of iterations**	**10-fold cross validation**		**Results of training**		**Results of testing**	
		CC	$RMSE$	CC	$RMSE$	CC	$RMSE$
1	1500	0.7802	0.4901	0.8513	0.4494	0.9452	0.284
2	10000	0.7898	0.4813	0.8861	0.4162	0.7545	0.4009
3	800	0.7855	0.4813	0.8944	0.4554	0.8211	0.351
4	800	0.7779	0.4927	0.8722	0.5036	0.8924	0.3838

As Table 4-15 illustrates, the multi-layer perceptron with one hidden neuron has better results in the testing phase and the 7-1-1 structure with 1500 iterations is selected for the further assessments of the artificial neural network of scour-prediction in current work. Results of CC and $RMSE$ of 10-fold cross validation for all structures are almost same.

The learning rate of the 7-1-1 perceptron was assumed 0.3 and the training of the ANN models was stopped either when the acceptable level of error of about 0.08 per epoch was achieved or when the number of iterations exceeded a prescribed maximum of 1500.

Increasing the number of hidden neurons above 20 is suggested by Mathworks (as one of the probable way of improving the result of the ANN. Larger numbers of neurons in the hidden layer give the network more flexibility because the network has more parameters it can optimize. For confirmation of the selected number of hidden layers and checking this probable scenario as well, large numbers of hidden layers were assessed and related error measures were calculated. Results are shown in Table 4-16. Table 4-16 indicate that though the larger number of hidden neurons may provide better results, the results of the 10-fold cross validations of large number of hidden neurons are not satisfying because of the possibility of over fitting problem in final

Table 4-16. Results of the networks with large numbers of hidden layers

Number of hidden layers	$\boldsymbol{CC}$	$\boldsymbol{RMSE}$
10	0.5333	0.8859
15	0.4722	1.000
20	0.5233	0.8556
25	0.5338	0.8967
30	0.5218	0.4722

results. It can be concluded that the selected 7-1-1 structure is the optimum topology for the network of this study.

4.3.2 SVM model

The use of SVM requires setting of a few user-defined parameters. As discussed in Chapter 3, parameters such as the regularization parameter (C) and the type of kernel (polynominal or RBF) are described by the user. Previous investigators such as Singh, Pal et al. (2008) have shown that the polynominal kernel can be used successfully and we used the same type. The regularization parameter C and the size of error in

sensitive zone parameters ε control the complexity of prediction. A value of $C = 1$ and $\varepsilon = 0.0001$ were selected based on the process of error minimizing. For choosing the optimal C and ε, first ε was kept constant and C was varied according to Table 4-17. This was also tested vice versa and the results did not change significantly. The error minimizing of this process was shown in Table 4-18.

Table 4-17. Error variation as a function of C

C	Error statistics of training phase		Error statistics of testing phase	
	CC	$RMSE$	CC	$RMSE$
1	0.893	0.3526	0.9513	0.2576
2	0.8975	0.3499	0.9415	0.2667
3	0.9	0.3471	0.9322	0.277
4	0.9004	0.3485	0.9283	0.2809
5	0.9007	0.3478	0.9284	0.2808
10	0.9083	0.3305	0.8999	0.3274
20	0.9153	0.3157	0.8252	0.4277
50	0.9181	0.3096	0.819	0.4316
100	0.9207	0.3038	0.8225	0.4276

Table 4-18. Error variation as a function of ε

ε	Error statistics of training phase		Error statistics of testing phase	
	CC	$RMSE$	CC	$RMSE$
0.1	0.8886	0.3565	0.9297	0.3059
0.01	0.8936	0.3549	0.9492	0.2536
0.001	0.8929	0.3532	0.951	0.2582
0.0001	0.893	0.3526	0.9513	0.2567
0.00001	0.893	0.3525	0.9512	0.2577
0.000001	0.893	0.3525	0.9512	0.2579
0.0000001	0.8931	0.3524	0.9512	0.2579

Comparison of the results of the error statistics of the testing phase represent that the SVM model which is trained and tested based on regularization parameter ($C = 1$) provides better predictions.

Results of Table 4-18 indicate that, by selecting the size of error (ε=0.0001) on the training data and adjusting the trade-off of the plane to ($C = 1$) more accurate predictions for testing data is gained from the SVM.

4.4 Results of SVM and ANN

As described in previous section (4.3), a multilayer perceptron (MLP) neural network with and a polynominal SVM model were developed to predict the equilibrium scour depth around pile groups due t waves. In the following sections, the results of the developed models are discussed. Results of both data-mining approaches are also compared with those of empirical formulae.

4.4.1 Comparison of the results of data mining approaches

To assess the performance of the models, observed normalized equilibrium scour depth values (S/D) were plotted against the predicted ones for the training and testing data sets. Figure 4-4 and Figure 4-5 display the observed and predicted values for the training data using the developed ANN and SVM models.

These figures illustrate that the SVM model provides better results compared to the ANN model at the training phase.

The statistical measures of predictions were also shown on the plotted area. It can be seen that Correlation Coefficient of the trend line of SVM model is 4.5 percent higher than the one of ANN showing that SVM can provide lower estimation errors compared to ANN.

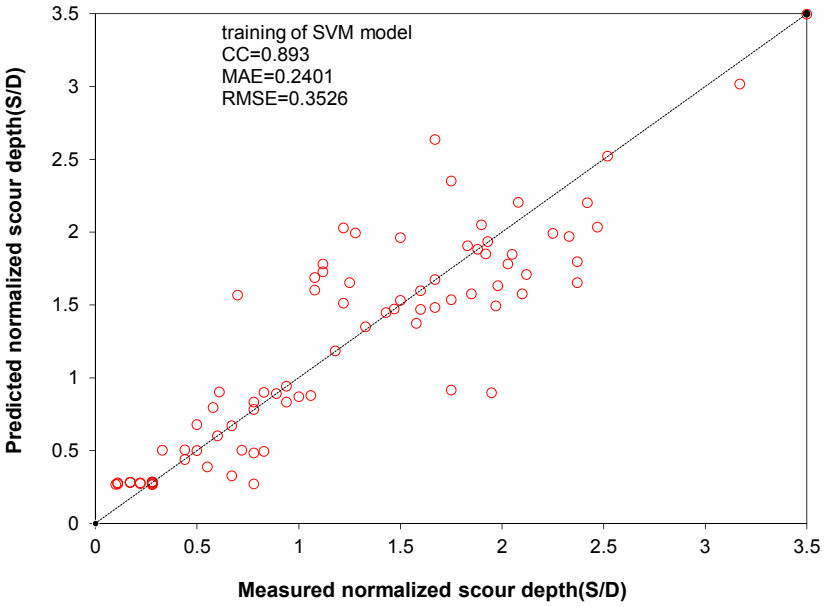

Figure 4-4. Comparison between the observed and predicted normalized scour depths by SVM for the training phase

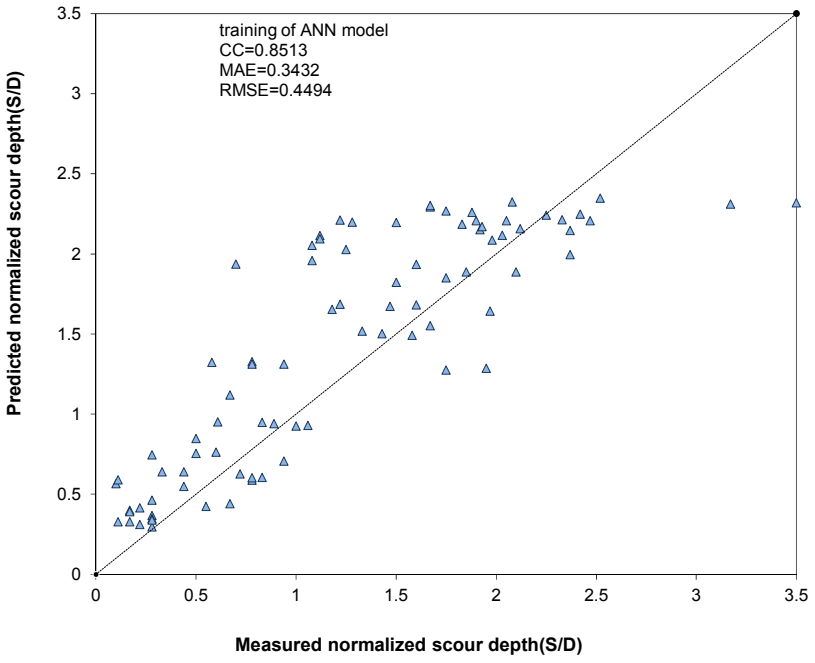

Figure 4-5. Comparison between the observed and predicted normalized scour depths by ANN for the training phase

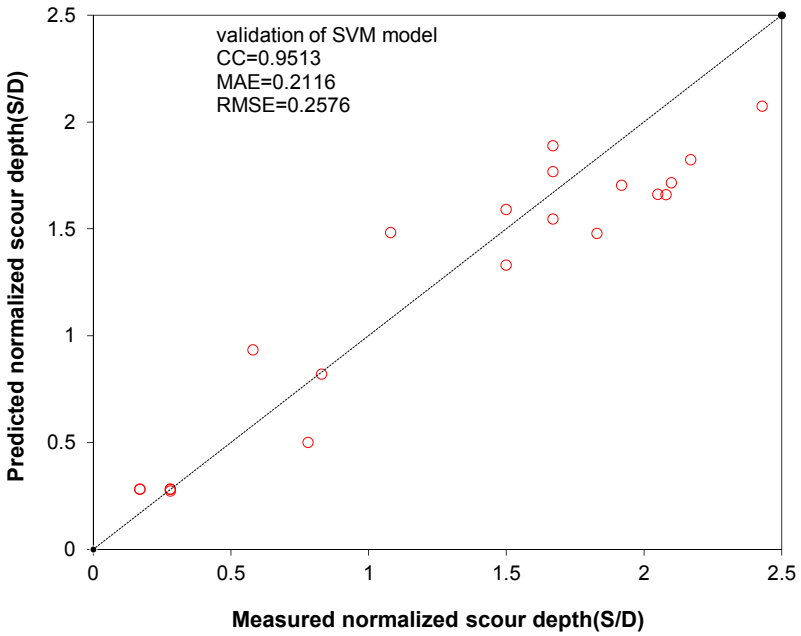

Figure 4-6. Comparison between the observed and predicted normalized scour depths by SVM for the testing phase

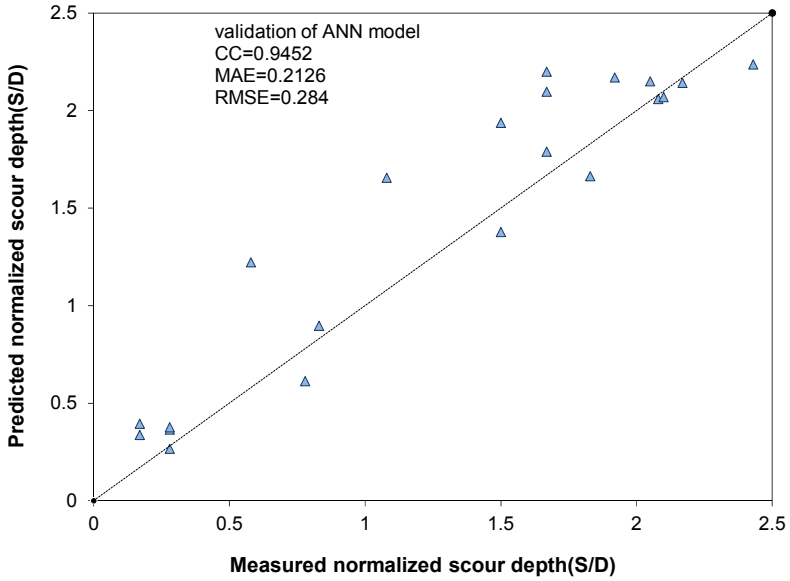

Figure 4-7. Comparison between the observed and predicted normalized scour depths by ANN for the testing phase

In Figure 4-6 and Figure 4-7 the results of the trained SVM and ANN models for other sets of testing data were shown to compare and assess the validation of these models. Displayed error measures on the figures show that SVM can provide more reliable error statistics compared to ANN; However, the differences between Correlation Coefficients of both models as well as those of MAE and $RMSE$ are not significant. For instance, the difference between the correlation coefficient of the models is about 0.97 percent.

4.4.2 Verification by the experimental data presented in this study

Figure 4-8 displays the prediction amounts of SVM models for the large-scale experimental data introduced in this dissertation. In this figure, measured normalized scour depth values of the experiment plotted against the predicted normalized scour depth by the SVM model. The statistical measures of the SVM predictions were shown at the bottom right corner of the figure. It can be seen that predictions have acceptable correlation coefficient measure of $CC = 0.9673$ with reliable error measures of $RMSE$ and MAE. Figure 4-9 also illustrates the result of ANN for the large-scale experimental data addressed in this study. Error measures of ANN were also shown on Figure 4-9. Compared to SVM, Correlation Coefficient of ANN is about 16.67% less than the CC of SVM.

The comparison of both figures related to SVM and ANN , clearly shows that non-dimensional ratios of scour which is about 0.75 in case of 9 piles was not predicted satisfyingly compared to those of other arrangements. The number of data for 9 piles arrangements as the most complicated configuration, were only two points (9 piles experiment addressed in Chapter 2) and was not enough to train both for this pile group. Less accurate results for the pile group with less number of data, highlights the

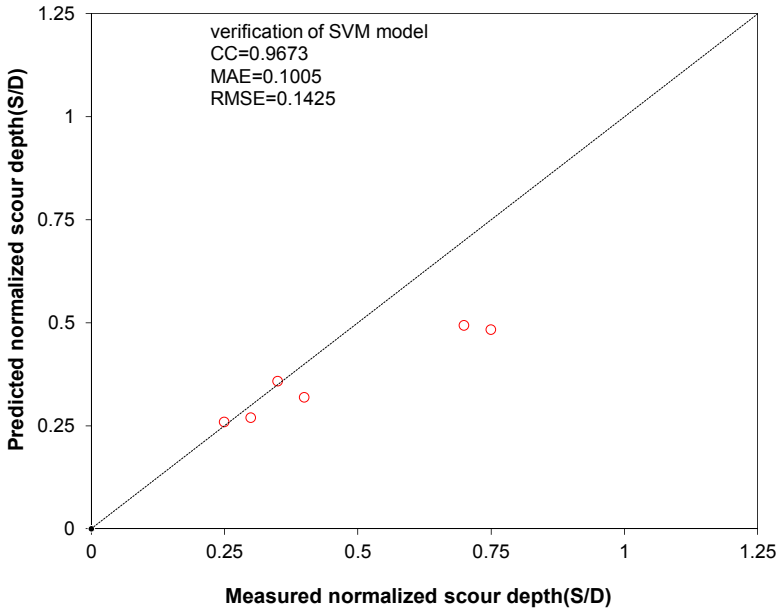

Figure 4-8. Comparison between the observed and predicted normalized scour depths by SVM for the experimental data of this study

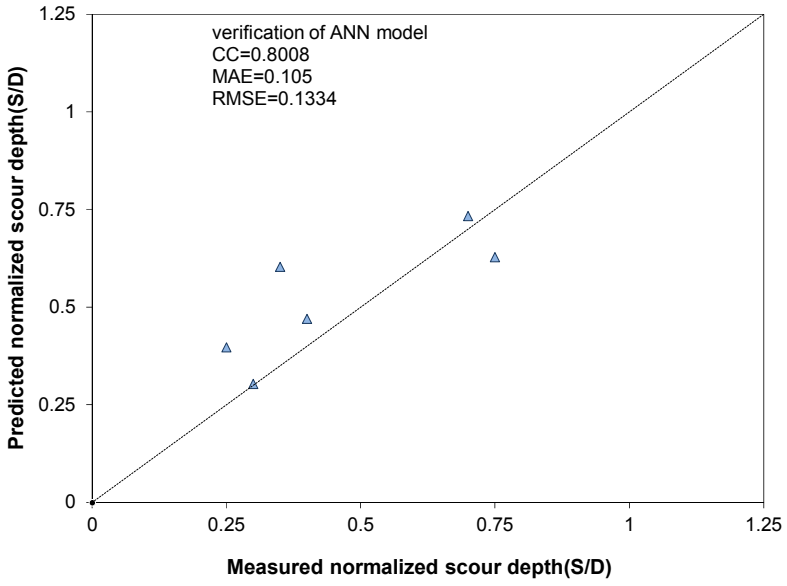

Figure 4-9. Comparison between the observed and predicted normalized scour depths by ANN for the experimental data of this study

importance of enough number of data to train the data mining to receive satisfying results in the testing phase.

4.4.3 Summary of the results

Table 4-19 shows the summary of the results of all stages of modelling by soft computing approaches. In this table error statistics of training phase, validation of the models and verification by the experimental data addressed in Chapter 2 were given.

The comparison of the results of SVM and ANN models, displayed in Table 4-19 denotes that in all steps of modelling error parameters of SVM are more satisfying compared to ANN. Specifically in case of validation by the large-scale experimental data, SVM is about 13% more reliable in terms of accuracy compared to ANN.

4.5 Comparisons of the computation times

To have better understanding about the time taken to apply soft computing models, times taken to build a model as well as the time taken to run the model and receiving the result form the model are displayed for both soft computing models of ANN and SCM that were applied in this study were reported in Table 4-20.

Note that the computation times are based on using a PC with an intel i5-2410M processor of 2.4 GHz and 4.0 GB RAM for both SVM and ANN models.

Table 4-19. Summary of the results of all steps for both SVM and ANN

Approach	**Training phase**		**Validation phase**		**Verification by the experimental data**	
	CC	***RMSE***	***CC***	***RMSE***	***CC***	***RMSE***
SVM	0.893	0.3526	0.9513	0.2576	0.9673	0.1425
ANN	0.8513	0.4494	0.9452	0.284	0.8008	0.1334

Table 4-20 Required times for both SVM and ANN

Approach	Times taken for Training phase (s)		Times taken for testing phase (s)		Times taken for verification for experimental data	
	Building the model	**Running the model**	**Building the model**	**Running the model**	**Building the model**	**Running the model**
SVM	0.04	0.05	0.06	0.02	0.03	0.01
ANN	0.27	0.06	0.07	0.02	0.06	0.01

As shown, SVM is a less time-consuming model in comparison with ANN. Specifically, time taken to build a model at the training phase for ANN is 4 times the SVM model. In addition, less required setting parameters is another advantage of SVM in comparison with ANN (see also Lin, Chen et al. (2009) Lin, Chen et al. (2009)) and it can be concluded that SVM is more time-efficient model in compared to ANN.

4.6 Sensitivity analysis

To extend the outcomes of the study, sensitivity tests were also conducted to determine the relative significance of each input variable on the normalized scour depth (S/D) which is the output for the SVM model. Table 4-21 demonstrates each model performance in the absence of each input parameter .

The results in Table 4-21 show that G/D, KC and m/n have the most significant effect on equilibrium scour depth since, by ignoring each of them, the CC and $RMSE$ values increase significantly. The results about the importance of G/D and KC are also in line with those of Sumer and Fredsøe (1998), Bayram and Larson (2000) about the relative importance of the input parameters on equilibrium scour depth around pile groups due to waves. Bateni and Jeng (2007) also noted the strong dependence of S/D on KC.

Table 4-21. Sensitivity analysis of the governing parameters for the SVM model

Error statistics of the SVM model in the absence of	CC	$RMSE$
KC	0.8745	0.3827
G/D	0.8444	0.4291
m/n	0.8928	0.3592
$m \times n$	0.904	0.3333
N_s	0.9041	0.3394
N_{RE}	0.901	0.3373
θ	0.904	0.3311

In their work, only a 2×2 pile arrangement was studied; hence, geometric parameters were not considered in their investigations.

The error measures in Table 4-21 also show that the arrangement parameters, i.e. G/D and m/n are more important than other parameters (except KC). In fact, as seen by excluding N_s, N_{RE} and, they do not change the accuracy of the model significantly. Table 4-21 shows that sensitivity analysis of the SVM model is in line with previous studies and the nature of scouring.

4.7 Comparison of all approaches

To evaluate the accuracy and capability of the developed models in predicting the scour depth around pile groups due to wave, a set of data of the three groups applied in this study were selected randomly and their results were compared with those of three existing semi empirical methods.

Figure 4-10 shows scour depth values using two data mining models and the existing formulae for the same data set. As illustrated, the methods proposed by Myrhaug and

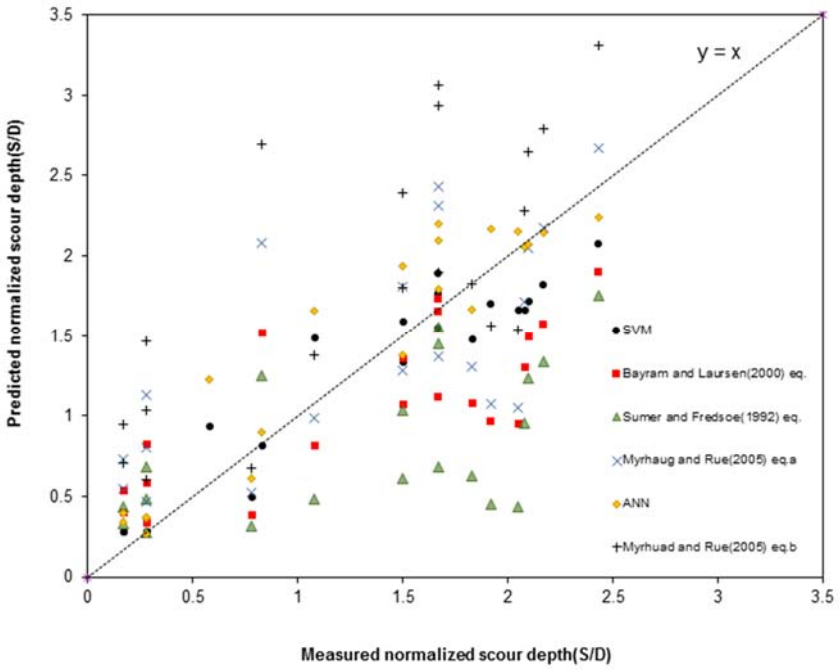

Figure 4-10. Comparison with empirical models

Rue (2005), Bayram and Larson (2000) and ANN model overestimate the scour depth, while other approaches underestimate it.

Table 4-22 illustrates the error statistics of all models. Note that the same data set was used for all of them. As seen, both data mining models provide better results compared to the empirical methods. In addition, for the best existing method (Bayram and Larson 2000), $RMSE$ is 1.2526 and CC is 0.1176 compared to respectively 0.2582 and 0.951 for the SVM model. This shows a 3 fold decrease in error measures when using the developed SVM model. To sum up, comparison between the results of SVM and ANN models with those of empirical methods, which are based on simple regressions, shows that complex problems like scouring around pile groups can be modelled more accurately using soft computing methods.

Table 4-22. Performance indices of various approaches to predict the scour depth

Approach	Error statistics	
	CC	$RMSE$
Myrhaug and Rue (2005)	0.2333	1.6776
Bayram and Larson (2000)	0.1176	1.2526
Sumer, Fredsøe et al. (1992)}	0.04516	1.2914
SVM (current study)	0.9513	0.2576
ANN (current study)	0.9452	0.284

4.8 Summary

The development and application of a multi-layer perceptron neural network with a 7-1-1 architecture, learning rate=0.3, error per epoch=0.08 and number of iterations=1500 and support vector machine with a polynominal kernel, value of $C = 1$ and $\varepsilon = 10^{-4}$ were outlined for estimation of the wave-induced scour depth around pile groups.

Two sets of laboratory and field data, including various arrangements of piles in a group, were used to train and test both data-driven models. Then, using statistical error parameters, the results were compared with those of previous empirical approaches. It was shown that ANN and support vector machines can predict scour depth more accurately than the existing empirical methods. The data-mining results were generally more satisfactory than those of empirical methods because of low errors and higher correlation coefficients and it is concluded that SVM outperforms ANN.

The developed SVM and ANN models also were used to estimate the amounts of scour depths for the large-scale experimental cases addressed in Chapter 2 of this dissertation. To evaluate the capability of the soft computing models, experimental measurements were compared with the predicted results by SVM and ANN. Results

showed that SVM can provide better estimations of the scour depth with about 13% in terms of accuracy. Moreover; the comparison of the times required for computation indicated that SVM is a less-time consuming model compared to ANN.

A sensitivity analysis was also conducted to investigate the effect of different input parameters on the equilibrium scour depth. The sensitivity analysis showed that the scour depth was mainly governed by the Keulegan– Carpenter (KC) number and the gap to diameter ratio.

5 CONCLUSIONS AND RECOMMENDATIONS

5.1 Conclusions

In this study, several sets of large-scale experiments were carried out for 3×3 , 2×3 , 2×2 and 1×2 arrangements of piles and scoured bed was surveyed to record the wave-induced scour depths.

Two soft computing models of Support Vector Machines (SVM) and Artificial Neural Networks (ANN) were also developed and applied to investigate the applicability of soft computing approaches to predict wave-induced scour depths.

For the laboratory experiments, time determination tests were done and results confirmed that one hour is enough to reach the equilibrium scour depths. Piles were exposed to waves with KC numbers of $KC = 3.9$ and $KC = 5.9$ for one hour and equilibrium scour depth around them were measured.

In a single-pile experiment, it was mainly observed that by the increase of $KC = 3.9$ to $KC = 5.9$, the symmetrical bed profile along X section was changed to an asymmetrical one. Results were in line with previous studies about scouring around pile groups.

In the two piles tests it was noticed that in larger KC number along X section, the scoured bed profile of the back pile was above the front pile at all recorded points. The scour trends were almost same along X section for smaller KC. Comparison of the results of this set of experiment with the findings of Sumer and Fredsøe (1998) about the tandem arrangement of pile groups, confirmed the importance of considering the configuration parameter in addition to KC number in the study of scouring around pile groups.

In case of 2×2 configuration, it was seen that for smaller KC number, the maximum scour depth recorded for both rows along X section was 4 cm and occurred at the piles front to the wave direction. In case of larger KC number, the maximum sour depth was 3.5 cm and similar to the case with smaller KC number was observed at the front piles. The trends of the scoured bed profiles for both KC numbers were almost same in this arrangement.

For 2×3 arrangements of piles, it was mainly observed that for both KC numbers along X sections, the scoured bed profiles have the same trends in all three rows of piles. The third row of piles had the least scour along that row of piles and the first row facing to the wave had the lowest bed profile showing the most scour along front piles. Furthermore, the 75% larger maximum scour than the maximum recorded scour for 2×2 arrangements with less number of piles, highlighted the effect of arrangement of the piles in the researches about the wave-induced scour of pile groups.

In nine piles tests, same as the 6 piles cases, for both KC numbers along X sections the first and third row of piles had the most and least amounts of scour along X sections in this set of experiment. Moreover, the amounts of scour along the gaps remained constant for most of the sections either vertical or parallel to the wave direction. The maximum scour depth that was recorded for smaller KC number was less than this

amount for larger one, denoting the effect of both KC number and configuration parameter factor for experimental studies and modelling of scouring phenomena around groups of piles.

Overall, the comparison of the bed profiles along each section for each arrangement indicates that in most of the cases sections along the first row of piles, facing to the wave directions have higher scour values compared to other sections and directions. It is concluded that using an arrangement parameter, which is defined based on the wave direction to consider the configuration of the pile group, is an important controlling factor. On the other hand, variations of observed scour values by the number of piles as well as the type of their arrangements in a pile group also highlights the importance of considering the configuration parameter in addition to the fundamentally considered parameter of KC number.

To assess the applicability of data mining approaches in prediction of pile group scouring due to waves, first, the development of a multi-layer perceptron neural network with a 7-1-1 architecture, learning rate=0.3, error per epoch=0.08 and number of iterations=1500 and support vector machine with a polynominal kernel, value of $C = 1$ and $\varepsilon = 10^{-4}$ were described. Then, the applicability of the developed models was studied by comparison of the results of the experiment and the amounts predicted by the data mining models. The outputs of the soft computing models were plotted against observed amounts in case of each experimental case and statistical parameters and error measures were used for assessment and comparison. Comparison between the outputs of data mining models and the surveyed amounts confirmed the reliable applicability of data mining approaches as an alternative approach that provides better predictions of scouring properties due to waves compared to current available empirical formulae.

A sensitivity analysis was also conducted to investigate the effect of different input parameters on the equilibrium scour depth. The sensitivity analysis showed that the scour depth was mainly governed by the Keulegan– Carpenter (KC) number and the gap to diameter ratio. Results of the application of data mining models mainly indicated that SVM is a more reliable model with better generalization error, independent from the variations of the training data in addition to its robustness and less-required time to be trained which are the main advantages of SVM over ANN (MLP/BP).

5.2 Recommendations for future researchers

Future studies are necessary to improve the laboratory findings about the process of pile group scour due to waves. The below are a few suggestion in order to extend the future work on this topic:

a) This study focused on specified number of configurations. The study of other arrangements of piles and other numbers of piles in the arrangements also seems necessary.

b) Regarding the large scale of the experiments of this study, only gap over diameter ratio of 1 was considered. Considering the importance of this parameter, study of other ratios is of significance as well.

c) In current study, waves with two KC numbers of 3.9 and 5.9 were generated. Assessment of other KC numbers, as the most important characteristic of wave, is also recommended.

d) In this study the applicability of SVM and ANN were assessed. The study of other data mining models such as Adaptive Neuro-fuzzy Inference System (ANFIS) is also recommended for future works.

e) This study attempted to develop a multi-layer preceptor with BP training algorithm and the SVM with a polynomial kernel. The Assessment of other algorithms of ANN and comparing their results with those of SVM with various kernels and training algorithms can also be another research topic.

REFERENCES

Angus, N. M. and R. L. Moore (1982). *Scour repair methods in the Southern North Sea*. Offshore Technology Conference, Offshore Technology Conference.

Bateni, S. and D.-S. Jeng (2007). "*Estimation of pile group scour using adaptive neuro-fuzzy approach*." Ocean Engineering 34(8): 1344-1354.

Bayram, A. and M. Larson (2000). "*Analysis of scour around a group of vertical piles in the field*." Journal of waterway, port, coastal, and ocean engineering 126(4): 215-220.

Bennett, K. P. and C. Campbell (2000). "*Support vector machines: hype or hallelujah?*" ACM SIGKDD Explorations Newsletter 2(2): 1-13.

Bray, M. and D. Han (2004). "*Identification of support vector machines for runoff modelling*." Journal of Hydroinformatics 6: 265-280.

Breusers, H. and A. J. Raudkivi (1991). *Scouring*, Balkema Rotterdam, The Netherlands.

Campbell, C. (2000). "*Kernel methods: A survey of current techniques.*" Neurocomputing 48: 63-84.

Chow, W.-Y. and J. B. Herbich (1978). *Scour around a group of piles*. Offshore Technology Conference, Offshore Technology Conference.

Dey, S., B. M. Sumer and J. Fredsøe (2006). "*Control of scour at vertical circular piles under waves and current*." Journal of hydraulic engineering 132(3): 270-279.

Eadie, R. W. and J. B. Herbich (1986). "*Scour about a single, cylindrical pile due to combined random waves and a current*." Coastal Engineering Proceedings 1(20).

Gershenson, C. (2003). "*Artificial neural networks for beginners*." arXiv preprint cs/0308031.

Ghazanfari-Hashemi, S., A. Etemad-Shahidi, M. H. Kazeminezhad and A. R. Mansoori (2011). "*Prediction of pile group scour in waves using support vector machines and ANN*." Journal of Hydroinformatics 13(4).

Herbich, J. B., R. Schiller, W. Dunlap and R. Watanabe (1984). "*Seafloor scour: Design guidelines for ocean-founded structures*."

Isaacson, M. (1979). "*Wave-induced forces in the diffraction regime*." Mechanics of wave-induced forces on cylinders: 68-89.

Islam, S. and R. Kothari (2000). "*Artificial neural networks in remote sensing of hydrologic processes*." Journal of Hydrologic Engineering 5(2): 138-144.

Jain, A. K., J. Mao and K. M. Mohiuddin (1996). "*Artificial neural networks: A tutorial*." IEEE computer 29(3): 31-44.

Jain, P. and M. Deo (2006). "*Neural networks in ocean engineering*." Ships and Offshore Structures 1(1): 25-35.

Kambekar, A. and M. Deo (2003). "*Estimation of pile group scour using neural networks*." Applied Ocean Research 25(4): 225-234.

Kazeminezhad, M. and A. Etemad-Shahidi (2010). "*An alternative approach for investigation of the wave-induced scour around pipelines*." Journal of Hydroinformatics 12(1): 51-65.

Khosronejad, A., G. Montazer and M. Ghodsian (2003). "*Estimation of Scour Hole Properties around Vertical Pile Using ANNs*." International Journal of Sediment Research 18(4): 290-300.

Kobayashi, T. and K. Oda (1994). "*Experimental study on developing process of local scour around a vertical cylinder*." Coastal Engineering Proceedings 1(24).

Lin, G.-F., G.-R. Chen, P.-Y. Huang and Y.-C. Chou (2009). "*Support vector machine-based models for hourly reservoir inflow forecasting during typhoon-warning periods*." Journal of Hydrology 372(1): 17-29.

Lin, G. F., G. R. Chen, M. C. Wu and Y. C. Chou (2009). "*Effective forecasting of hourly typhoon rainfall using support vector machines*." Water resources research 45(8).

Lippmann, R. P. (1987). "*An introduction to computing with neural nets*." ASSP Magazine, IEEE 4(2): 4-22.

Liriano, S. and R. Day (2001). "*Prediction of scour depth at culvert outlets using neural networks*." Journal of hydroinformatics 3: 231-238.

Mahjoobi, J. and E. Adeli Mosabbeb (2009). "*Prediction of significant wave height using regressive support vector machines*." Ocean Engineering 36(5): 339-347.

Mathworks. (2014). "*Analyze Neural Network Performance After Training*." from http://www.mathworks.co.jp/jp/help/nnet/ug/analyze-neural-network-performance-after-training.html

Mathworks. (2014). "*Improve Neural Network Generalization and Avoid Overfitting*." from http://www.mathworks.co.jp/jp/help/nnet/ug/improve-neural-network-generalization-and-avoid-overfitting.html.

Melville, B. W. and Y.-M. Chiew (1999). "*Time scale for local scour at bridge piers*." Journal of Hydraulic Engineering 125(1): 59-65.

Mohandes, M., T. Halawani, S. Rehman and A. A. Hussain (2004). "*Support vector machines for wind speed prediction*." Renewable Energy 29(6): 939-947.

Myrhaug, D. and H. Rue (2005). "*Scour around group of slender vertical piles in random waves*." Applied Ocean Research 27(1): 56-63.

Palmer, H. D. (1969). *Wave-induced scour on the sea floor*. Civil Engineering in the Oceans II, ASCE.

Rajasekaran, S., S. Gayathri and T.-L. Lee (2008). "*Support vector regression methodology for storm surge predictions*." Ocean Engineering 35(16): 1578-1587.

Singh, K., M. Pal, C. Ojha and V. Singh (2008). "*Estimation of removal efficiency for settling basins using neural networks and support vector machines*." Journal of Hydrologic Engineering 13(3): 146-155.

Smola, A. J. and B. Schölkopf (2004). "*A tutorial on support vector regression*." Statistics and computing 14(3): 199-222.

Sumer, B., N. Christiansen and J. Fredsøe (1993). "*Influence of cross section on wave scour around piles*." Journal of waterway, port, coastal, and ocean engineering 119(5): 477-495.

Sumer, B. M., N. Christiansen and J. Fredsøe (1997). "*The horseshoe vortex and vortex shedding around a vertical wall-mounted cylinder exposed to waves*." Journal of Fluid Mechanics 332: 41-70.

Sumer, B. M. and J. Fredsøe (1997). *Hydrodynamics around cylindrical structures*, World Scientific.

Sumer, B. M. and J. Fredsøe (1998). "*Wave scour around group of vertical piles*." Journal of waterway, port, coastal, and ocean engineering 124(5): 248-256.

Sumer, B. M. and J. Fredsøe (2002). *The mechanics of scour in the marine environment*, World Scientific.

Sumer, B. M., J. Fredsøe and K. Bundgaard (2005). *Global and local scour at pile groups*. The Fifteenth International Offshore and Polar Engineering Conference, International Society of Offshore and Polar Engineers.

Sumer, B. M., J. Fredsøe and N. Christiansen (1992). "*Scour around vertical pile in waves*." Journal of waterway, port, coastal, and ocean engineering 118(1): 15-31.

Vapnik, V. N. (1995). "*The nature of statistical learning theory*."

Wang, R.-K. and J. B. Herbich (1983). *Combined current and wave-produced scour around a single pile*, Department of Civil Engineering, Texas Engineering Experiment Station.

Zounemat-Kermani, M., A.-A. Beheshti, B. Ataie-Ashtiani and S.-R. Sabbagh-Yazdi (2009). "*Estimation of current-induced scour depth around pile groups using neural network and adaptive neuro-fuzzy inference system*." Applied Soft Computing 9(2): 746-755.

LIST OF FIGURES

FIGURE 1-1. THE CHANGE IN THE FLOW PATTERN AND THE BOUNDARY LAYER AFTER BEING EXPOSED TO CURRENT (SUMER AND FREDSØE 2002) 3

FIGURE 1-2. PRESENCE OF HORSESHOE VORTICES BY KC AND ωt VARIATIONS (SUMER, CHRISTIANSEN ET AL. 1997) 6

FIGURE 1-3. THE DEVELOPMENT OF HORSESHOE VORTICES IN KC =10.3 (SUMER, CHRISTIANSEN ET AL. 1997) 7

FIGURE 1-4. THE FORMATION OF LEE-WAKE VORTEX AT VARIOUS KC AND ωt (SUMER, CHRISTIANSEN ET AL. 1997) 9

FIGURE 1-5. DISPLAY OF BED SHEAR STRESS COUNTERS (SUMER, CHRISTIANSEN ET AL. 1997, SUMER AND FREDSØE 2002) 10

FIGURE 1-6. VARIATIONS OF SD AGAINST KC FOR A CIRCULAR PILE $\theta < \theta cr$ SUMER, FREDSØE ET AL. (1992) 11

FIGURE 1-7. A CONCEPTUAL DISPLAY OF LOCAL AND GLOBAL SCOUR AROUND A PILED STEEL PLATFORM (ANGUS AND MOORE 1982) 13

FIGURE 1-8 GLOBAL AND LOCAL SCOUR AROUND A 9 PILES-ARRANGEMENT AT THE EXPERIMENT (SUMER, FREDSØE ET AL. 2005) 14

FIGURE 1-9. SD AGAINST GD FOR 2-PILE ARRANGEMENTS (SUMER AND FREDSØE 1998) 15

FIGURE 2-1. WAVE BASIN OF COASTAL SEDIMENTARY LABORATORY 21

FIGURE 2-2. THE PRIMARY DESIGN OF THE EXPERIMENTAL MODEL.....22

FIGURE 2-3. THE AS-BUILT PHOTO OF THE EXPERIMENTAL MODEL 23

FIGURE 2-4. THE ILLUSTRATION OF THE CONCEPTUAL SCOURING ZONE AROUND EACH PILE.....24

FIGURE 2-5. THE PLAN VIEW OF THE EXPERIMENTAL MODEL 25

FIGURE 2-6. THE INSTALLATION OF THE EXPERIMENTAL MODEL IN THE WAVE BASIN 25

FIGURE 2-7 . THE INSTALMENT OF THE EXPERIMENTAL MODEL IN THE WAVE BASIN.....26

FIGURE 2-8.THE AMOUNTS OF SD AGAINST GD FOR 2-PILE ARRANGEMENTS (SUMER AND FREDSØE 1998) 26

FIGURE 2-9. PILE GROUP CONFIGURATIONS STUDIED BY SUMER AND FREDSØE (1998).....27

FIGURE 2-10. THE ARRANGEMENT OF PILE GROUPS USED IN EXPERIMENTS 28

FIGURE 2-11. X-Y COORDINATES AND SECTIONS USED FOR BED SURVEY 29

FIGURE 2-12. PHOTO OF THE SINGLE PILE EXPERIMENTAL MODEL.....30

FIGURE 2-13. SCOUR DEVELOPMENT OVER TIME FOR SINGLE PILE 31

FIGURE 2-14. BED PROFILE OF SINGLE PILE ALONG X SECTION FOR $KC = 3.9$.....33

FIGURE 2-15. BED PROFILE OF SINGLE PILE ALONG Y SECTION FOR $KC = 3.9$.....33

FIGURE 2-16. BED PROFILE OF SINGLE PILE ALONG X SECTION FOR $KC = 5.9$.....34

FIGURE 2-17. BED PROFILE OF SINGLE PILE ALONG Y SECTION FOR $KC = 5.9$.....34

FIGURE 2-18. PHOTO OF THE TWO PILES EXPERIMENTAL MODEL.....35

FIGURE 2-19. BED PROFILE OF TWO PILES ALONG X SECTION FOR $KC = 3.9$.....36

FIGURE 2-20. BED PROFILE OF TWO PILES ALONG Y SECTION FOR $KC = 3.9$.....36

FIGURE 2-21. BED PROFILE OF TWO PILES ALONG X SECTION FOR $KC = 5.9$.....38

FIGURE 2-22. BED PROFILE OF TWO PILES ALONG THE Y-SECTION FOR $KC = 5.9$.....38

FIGURE 2-23. PHOTO OF THE FOUR PILES EXPERIMENTAL MODEL.....39

FIGURE 2-24. BED PROFILE OF 4 PILES ALONG X SECTION FOR $KC = 3.9$ 40

FIGURE 2-25. BED PROFILE OF 4 PILES ALONG Y SECTION FOR $KC = 3.9$ 40

FIGURE 2-26. BED PROFILE OF 4 PILES ALONG X SECTION FOR $KC = 5.9$ 41

FIGURE 2-27. BED PROFILE OF 4 PILES ALONG Y SECTION FOR $KC = 5.9$ 41

FIGURE 2-28. PHOTO OF THE SIX PILES EXPERIMENTAL MODEL 43

FIGURE 2-29. BED PROFILE OF 6 PILES ALONG X SECTION FOR $KC = 3.9$ 44

FIGURE 2-30. BED PROFILE OF 6 PILES ALONG Y SECTION FOR $KC = 3.9$ 44

FIGURE 2-31. BED PROFILE OF 6 PILES ALONG X SECTION FOR KC $= 5.9$ 45

FIGURE 2-32. BED PROFILE OF 6 PILES ALONG Y SECTION FOR KC $= 5.9$ 45

FIGURE 2-33. PHOTO OF THE 9 PILES EXPERIMENTAL MODEL 46

FIGURE 2-34. BED PROFILE OF 9 PILES ALONG X SECTION FOR $KC = 3.9$ 47

FIGURE 2-35. BED PROFILE OF 9 PILES ALONG Y SECTION FOR $KC = 3.9$ 47

FIGURE 2-36. BED PROFILE OF 9 PILES ALONG X SECTION FOR $KC = 5.9$ 48

FIGURE 2-37. BED PROFILE OF 9 PILES ALONG Y SECTION FOR $KC = 5.9$ 48

FIGURE 3-1. CONCEPTUAL BIOLOGICAL NEURON (GERSHENSON 2003) 53

FIGURE 3-2. A BACK PROPAGATION NEURAL NETWORK (SINGH, PAL ET AL. 2008) 54

FIGURE 3-3. ROLE OF AN ACTIVATION FUNCTION IN A BACK PROPAGATION NETWORK (GERSHENSON 2003) 55

FIGURE 3-4. A GEOMETRIC INTERPRETATION OF THE ROLE OF THE HIDDEN UNIT IN A TWO-DIMENSIONAL INPUT SPACE (JAIN, MAO ET AL. 1996) 58

FIGURE 3-5. TWO POSSIBLE LINEAR DISCRIMINANT PLANES (BENNETT AND CAMPBELL 2000) 60

FIGURE 3-6. EXAMPLE OF NON-SEPARABLE CASES BY SIMPLE LINEAR DISCRIMINANT FUNCTIONS (CAMPBELL 2000) 62

FIGURE 3-7. SCHEME OF THE SUPPORT VECTOR REGRESSION BY STANDARD DEVIATION OF ε 65

FIGURE 3-8. THE SOFT MARGIN LOSS SETTING FOR A LINEAR SVM (SMOLA AND SCHÖLKOPF 2004) 67

FIGURE 3-9. COMPARISON BETWEEN THE OBSERVED AND PREDICTED SD BY ANN FOR THE TRAINING PHASE.....71

FIGURE 3-10. COMPARISON BETWEEN THE OBSERVED AND PREDICTED SD BY SVM FOR THE TRAINING PHASE.....71

FIGURE 3-11. COMPARISON BETWEEN THE OBSERVED AND PREDICTED SD BY ANN FOR THE TESTING PHASE.....72

FIGURE 3-12. COMPARISON BETWEEN THE OBSERVED AND PREDICTED SD BY SVM FOR THE TESTING PHASE.....72

FIGURE 4-1. CONFIGURATIONS OF THE USED PILE GROUPS IN THE LABORATORY (SUMER AND FREDSØE 1998) 78

FIGURE 4-2. CONFIGURATION OF THE PILE GROUP IN THE FIELD (BAYRAM AND LARSON 2000).....81

FIGURE 4-3. SCHEME OF THE MLP NETWORK USED IN CURRENT STUDY 88

FIGURE 4-4. COMPARISON BETWEEN THE OBSERVED AND PREDICTED NORMALIZED SCOUR DEPTHS BY SVM FOR THE TRAINING PHASE.....97

FIGURE 4-5. COMPARISON BETWEEN THE OBSERVED AND PREDICTED NORMALIZED SCOUR DEPTHS BY ANN FOR THE TRAINING PHASE 97

FIGURE 4-6. COMPARISON BETWEEN THE OBSERVED AND PREDICTED NORMALIZED SCOUR DEPTHS BY SVM FOR THE TESTING PHASE.....98

FIGURE 4-7. COMPARISON BETWEEN THE OBSERVED AND PREDICTED NORMALIZED SCOUR DEPTHS BY ANN FOR THE TESTING PHASE.....98

FIGURE 4-8. COMPARISON BETWEEN THE OBSERVED AND PREDICTED NORMALIZED SCOUR DEPTHS BY SVM FOR THE EXPERIMENTAL DATA OF THIS STUDY.....100

FIGURE 4-9. COMPARISON BETWEEN THE OBSERVED AND PREDICTED NORMALIZED SCOUR DEPTHS BY ANN FOR THE EXPERIMENTAL DATA OF THIS STUDY 100

FIGURE 4-10. COMPARISON WITH EMPIRICAL MODELS 104

LIST OF TABLES

TABLE 2-1. WAVE PROPERTIES IN CASE OF 4 PILES FOR T=1.2S.....31

TABLE 3-1. SOME COMMONLY USED ACTIVATION FUNCTIONS.....56

TABLE 3-2. EXAMPLES OF SOME KERNEL FUNCTIONS.....63

TABLE 4-1. SELECTED DATA OF SUMER AND FREDSØE (1998) APPLIED IN THIS STUDY.....79

TABLE 4-2. RANGES OF THE EXPERIMENTAL DATA PRESENTED BY SUMER AND FREDSØE (1998)..80

TABLE 4-3. DATA OF THE FILED SURVEY PUBLISHED BY (BAYRAM AND LARSON).....82

TABLE 4-4. RANGES OF THE FIELD DATA PRESENTED BY (BAYRAM AND LARSON).....84

TABLE 4-5. DATA OF THE BED SURVEY PRESENTED IN THIS STUDY.....85

TABLE 4-6. RANGES OF THE EXPERIMENTAL DATA PRESENTED IN THIS STUDY.....85

TABLE 4-7. RESULTS OF THE NETWORK WITH ONE HIDDEN LAYER FOR DIFFERENT NUMBERS OF ITERATION.....89

TABLE 4-8. RESULTS OF THE NETWORK WITH 2 HIDDEN LAYERS FOR DIFFERENT NUMBERS OF ITERATION.....89

TABLE 4-9. RESULTS OF THE NETWORK WITH 3 HIDDEN LAYERS FOR DIFFERENT NUMBERS OF ITERATION.....90

TABLE 4-10. RESULTS OF THE NETWORK WITH 4 HIDDEN LAYERS FOR DIFFERENT NUMBERS OF ITERATION 90

TABLE 4-11. RESULTS OF THE NETWORK WITH 5 HIDDEN LAYERS FOR DIFFERENT NUMBERS OF ITERATION 91

TABLE 4-12. RESULTS OF THE NETWORK WITH 6 HIDDEN LAYERS FOR DIFFERENT NUMBERS OF ITERATION 91

TABLE 4-13. RESULTS OF THE NETWORK WITH 7 HIDDEN FOR DIFFERENT NUMBERS OF ITERATION 92

TABLE 4-14. RESULTS OF THE NETWORK WITH 8 HIDDEN FOR DIFFERENT NUMBERS OF ITERATION 92

TABLE 4-15. RESULTS OF THE NETWORKS WITH DIFFERENT TOPOLOGIES 93

TABLE 4-16. RESULTS OF THE NETWORKS WITH LARGE NUMBERS OF HIDDEN LAYERS 94

TABLE 4-17. ERROR VARIATION AS A FUNCTION OF C 95

TABLE 4-18. ERROR VARIATION AS A FUNCTION OF ε 95

TABLE 4-19. SUMMARY OF THE RESULTS OF ALL STEPS FOR BOTH SVM AND ANN 101

TABLE 4-20 REQUIRED TIMES FOR BOTH SVM AND ANN 102

TABLE 4-21. SENSITIVITY ANALYSIS OF THE GOVERNING PARAMETERS FOR THE SVM MODEL 103

TABLE 4-22. PERFORMANCE INDICES OF VARIOUS APPROACHES TO PREDICT THE SCOUR DEPTH . 105

CURRICULUM VITAE

Name: Samaneh Ghazanfari Hashemi

Nationality: Iranian

Birth: August 7, 1981, Tehran, Iran

2011 - 2014

PhD in Coastal Engineering

Disaster Prevention Research Institute (DPRI), Kyoto University, Japan

2006 - 2009

Master of Science in Water Resources Engineering

Iran University of Science and Technology, Iran

2000 - 2005

Bachelor of Science in Civil Engineering

Department of Civil Engineering, Iran University of Science and Technology, Iran